Acta Materialia 107 (2016) 508–544

Contents lists available at ScienceDirect

Acta Materialia

journal homepage: www.elsevier.com/locate/actamat

By invitation only: overview article

Failure of metals III: Fracture and fatigue of nanostructured metallic materials

André Pineau [a, *], A. Amine Benzerga [b, c], Thomas Pardoen [d, *]

[a] Mines ParisTech, Centre des Matériaux, CNRS UMR 7633, BP 87, 91003 Evry, France
[b] Department of Aerospace Engineering, Texas A&M University, College Station, TX 77843, USA
[c] Department of Materials Science and Engineering, Texas A&M University, College Station, TX 77843, USA
[d] Institute of Mechanics, Materials and Civil Engineering, Université catholique de Louvain, B-1348 Louvain-la-Neuve, Belgium

ARTICLE INFO

Article history:
Received 20 March 2015
Received in revised form
18 July 2015
Accepted 18 July 2015
Available online 11 August 2015

Keywords:
Ductility
Fracture
Fatigue
Metals
Nanocrystalline
Thin films
Necking
Damage

ABSTRACT

Pushing the internal or external dimensions of metallic alloys down to the nanometer scale gives rise to strong materials, though most often at the expense of a low ductility and a low resistance to cracking, with negative impact on the transfer to engineering applications. These characteristics are observed, with some exceptions, in bulk ultra-fine grained and nanocrystalline metals, nano-twinned metals, thin metallic coatings on substrates and freestanding thin metallic films and nanowires. This overview encompasses all these systems to reveal commonalities in the origins of the lack of ductility and fracture resistance, in factors governing fatigue resistance, and in ways to improve properties. After surveying the various processing methods and key deformation mechanisms, we systematically address the current state of the art in terms of plastic localization, damage, static and fatigue cracking, for three classes of systems: (1) bulk ultra-fine grained and nanocrystalline metals, (2) thin metallic films on substrates, and (3) 1D and 2D freestanding micro and nanoscale systems. In doing so, we aim to favour cross-fertilization between progress made in the fields of mechanics of thin films, nanomechanics, fundamental researches in bulk nanocrystalline metals and metallurgy to impart enhanced resistance to fracture and fatigue in high-strength nanostructured systems. This involves exploiting intrinsic mechanisms, e.g. to enhance hardening and rate-sensitivity so as to delay necking, or improve grain-boundary cohesion to resist intergranular cracks or voids. Extrinsic methods can also be utilized such as by hybridizing the metal with another material to delocalize the deformation - as practiced in stretchable electronics. Fatigue crack initiation is in principle improved by a fine structure, but at the expense of larger fatigue crack growth rates. Extrinsic toughening through hybridization allows arresting or bridging cracks. The content and discussions are based on experimental, theoretical and simulation results from the recent literature, and focus is laid on linking microstructure and physical mechanisms to the overall mechanical behavior.

1. Introduction

While the companion overviews [1,2] deal with recent research advances in the fracture of industrial metallic alloys involving typical microstructure dimensions within the tens of microns range as used in traditional macroscopic components, the present overview addresses the state of the art and future perspectives regarding the physics and mechanics of fracture in metallic materials with nano-scale internal or external dimensions. Several reviews have been dealing in recent years with the mechanical behavior of these systems, e.g. [3–8], with a focus on the deformation mechanisms controlling the extreme strengths that can be attained, but often with limited attention to fracture. The resistance to fracture is usually reported to be weak, as quantified by a limited ductility and/or low fracture toughness. This is a key issue that must be solved in order to open the range of possible viable applications of nanostructured metallic materials. Fig. 1 describes the coverage of the paper; it deals with bulk "3D" macroscopic metals involving submicron characteristic internal microstructure features as well as metallic structures involving at least one submicron dimension, i.e. both "2D" films or coatings and "1D" wires, rods and beams which involve submicron characteristic internal microstructure sizes as well. The fracture of 1D and 2D structures is more complex in a

* Corresponding authors.
E-mail addresses: andre.pineau@mines-paristech.fr (A. Pineau), thomas.pardoen@uclouvain.be (T. Pardoen).

http://dx.doi.org/10.1016/j.actamat.2015.07.049
1359-6454/

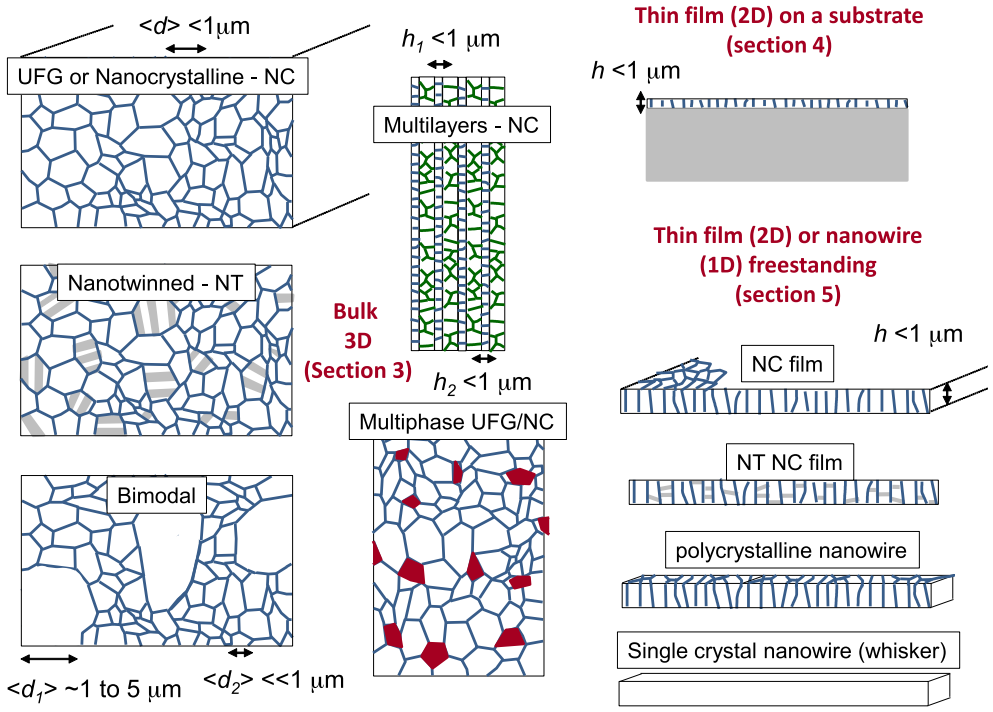

Fig. 1. Description of the different UFG and nanocrystalline metallic materials, single phase or hybrids, addressed in the paper from the viewpoint or their failure behavior, involving bulk systems (Section 3), thin films and coatings on substrate (Section 4) and freestanding thin film and nanowires (Section 5).

sense, as both the microstructural and component characteristic lengths generally affect it. Incidentally, covering all three types of material systems enables links to be made between the community that develops bulk nanostructured alloys for potential structural applications and that working on nano- and thin-film mechanics for electronics, coatings and nanotechnology. In order to limit the scope, only room temperature static fracture and fatigue of crystalline metals will be addressed with no consideration for other important issues related to environment, high or low temperature effects or to metallic glasses. Fracture is addressed from the general perspective of failure analysis in the presence or not of a pre-crack, under static or cyclic conditions. The ductility is set either by the onset of plastic localization or by the onset of cracking. Fatigue and fracture are treated in terms of the resistance to crack initiation and propagation from a pre-existing crack.

Before entering into the topic of fracture, Section 2 sets a series of basic elements on processing and deformation mechanisms. The processing methods are briefly covered while presenting the specific materials and systems addressed in this overview. The second part of Section 2 provides a survey of the mechanisms that control the strength in metals with nanoscale dimensions. These aspects are needed and must be understood as they dictate the ensuing mechanisms of localization, damage and fracture. Indeed, the essence of the "local approach" to fracture that traverses the three overviews is to address failure mechanisms in their connection with the microstructure and the physical phenomena. Damage and cracking are the results of the specific deformation mechanisms developing in this class of materials.

The fracture and fatigue behavior of bulk 3D nanostructured metals is treated in Section 3. The research in this field has been intense over the last two decades, opening applications to a variety of engineering fields where a high strength is the main performance of interest. One of the key issues with these materials, in addition to the difficulty to transfer the processing routes to industrial structural applications, is the usually low ductility both in terms of uniform elongation and fracture strain which negatively impact the forming capabilities and resistance to cracking when used in structural components. The low strain hardening capacity is the main reason for the limited resistance to plastic localization and for the low uniform elongation. Regarding damage and cracking, the key issue is the predominance of intergranular decohesion mechanisms because of the extreme stress build-up on grain-boundaries (GBs) and the presence of processing defects. Work-arounds recently found to recover ductility by introducing heterogeneities at multiple scales and by favouring rate sensitivity will be analysed, for instance the nano-twinned (NT) metals [9] or hybrid nano-structuring strategies involving bimodal or multimodal grain size distributions, multi-phase alloys, graded single or multiphase systems, multi-layered metallic composites, generation of controlled internal stress distributions, and combination of these solutions.

The fracture of 2D and 1D materials is addressed in Sections 4 and 5. Fracture in thin metallic layers on substrate has probably been more studied than in bulk nanostructured metals, partly because these systems have been available for a long time owing to well-controlled deposition/coating methods. A seminal example is found in galvanization layers (although usually not exhibiting submicron thickness). The mechanics of fracture of coatings on substrates has been rigorously established more than 20 years ago, as reviewed in [10]. Thin metallic layers are used in a wide range of applications involving microelectronics, protective and/or functional coatings, and membranes. The ductility and fracture resistance of the films is often a key property needed in applications. In flexible electronic devices, stretchability is essential for preserving electrical conductivity even under large distortions. In thin functional coatings, the ductility of the thin layer or multilayer must be large enough to sustain forming operations performed on the substrate or to resist scratching or impact conditions, as well as

thermal loadings. Micro- or nano-electromechanical systems (MEMS/NEMS) devices and other microsystems sometimes involve thin metallic films either freestanding or lying on a substrate, and which can undergo significant straining under operation or manufacturing. In microelectronic devices, large strains in thin interconnects result from thermal cycling and associated internal stress evolution. In all these applications, permanent plastic deformation is not necessarily prohibited, but should develop without or with limited micro-cracking to preserve the expected function. The same problem as for bulk nanostructured systems of Section 3 emerges: most metallic films exhibit limited ductility [11], even though recent counterexamples have been described in the literature with thin freestanding metallic films deforming by more than 10%, e.g. [12,13]. For the sake of clarity, the fracture of metallic coatings while lying on a substrate is addressed in Section 4, and the fracture of freestanding films or wires in Section 5. Even though the intrinsic failure mechanisms are usually similar, the experimental challenges and failure scenarios can be quite different. In particular, the flexible electronics community has developed a series of innovative extrinsic ductilization strategies, involving similarities with the hybrid approaches applied to bulk nanostructured metals. In the case of freestanding films, we review recent progress about *in situ* characterization of failure mechanisms with a realm of new observations and improved understanding.

In these three core Sections 3–5, we will address failure in terms of the properties that are used to quantify the resistance to fracture:

(1) the *uniform elongation*, in terms of the engineering strain A_g (%) or true strain ε_u (/), which is the strain at the onset of diffuse necking;
(2) the *true fracture strain* ε_f (/) which is the effective plastic strain attained in the broken region as measured from the area reduction of section;
(3) the *total elongation* ε_{engf} (/) which is extracted from a uniaxial tensile test as the total displacement at fracture divided by initial length. This quantity is often reported in the literature but can lead to confusion as it is gauge length dependent and very much dominated by the magnitude of A_g;
(4) the *true fracture stress* σ_f (MPa) which may be more meaningful than the true fracture strain when the behavior is brittle or quasi-brittle;
(5) the *fracture toughness* expressed by the critical stress intensity factor K_{Ic} (MPa m), critical energy release rate G_{Ic} (J/m^2), critical value of the J integral J_{Ic} (J/m^2), or the critical Crack Tip Opening Displacement (CTOD) δ_{Ic} (μm) (limited here to mode I crack opening conditions) which requires, to be valid, samples with a sharp pre-crack and sufficiently large dimensions to represent an intrinsic, geometry-independent material fracture resistance index. These values are usually defined at cracking initiation except if indicated otherwise. The meaning and relevance of these concepts in the context of submicron components will be critically discussed;
(6) the *resistance to fatigue* expressed by the *endurance limit* σ_{end} (MPa) which is the stress amplitude above which fracture by fatigue does not occur below a given high number of cycles (usually 10^6–10^7 cycles), or by the $\Delta a/\Delta N$ (μm) versus ΔK (MPa m) response which gives the increment of crack growth Δa per loading cycle ΔN under a given amplitude of stress intensity factor ΔK.

Even though a material is not physically broken when plastic localization occurs (as quantified with A_g or ε_u), the integrity of the structure is compromised and, from an engineering viewpoint, one may consider that failure has been attained. The prediction of the integrity of a structural component or the formability of a material part must be based on a series of failure criteria involving both fracture from preexisting defect or not and plastic localization (and buckling, though not discussed here). We will discuss how these properties play out in the systems described above, how they connect with the microstructure and with the various characteristic lengths involved. On the one hand, the small size makes the testing and characterization more complicated for some aspects, such as for quantitative load measurement, manipulation and alignment, but, on the other hand, direct observation with TEM on the full scale specimen can be performed and volumes similar to those analysed experimentally can be treated with atomistic simulations or dislocation dynamics codes. For this, relevant recent literature on experimental, computational and theoretical researches will be reviewed involving open questions. Even though the literature on fracture and fatigue of these systems is much less extensive than the literature dealing with deformation and strength aspects, it is still wide enough and we do not claim a comprehensive treatment. Instead, we propose some possible lines of articulation for the underlying questions and recent findings.

2. Basics on processing, microstructures and deformation mechanisms

2.1. Processing of nanostructured metals

This sub-section involves information both on the processing methods and main characteristics of the micro- and nanostructures, with an emphasis on the elements that are needed to understand the different topics addressed in the paper. The term nano-crystalline (NC) will be reserved for grain sizes below ~100 nm and ultra-fine grained (UFG) for grain sizes between ~100 nm and ~1 μm. Classical metallic polycrystals will be referred as coarse grained (CG). A film is considered as "thin" when the thickness is below 1 μm and a nanowire is defined as having a more or less equiaxed section with a characteristic dimension below 1 μm.

2.1.1. Bulk ultrafine grained and nanocrystalline metals

The most common method to produce UFG and NC metallic alloys is through *Severe Plastic Deformation* (SPD), under high hydrostatic pressure to avoid failure problems, sometimes at high strain rates. Many reviews have been dedicated to this topic, e.g. [14–16]. There is a large number of possible routes to apply ultra deformation involving [16] equal-channel angular pressing (ECAP), high pressure torsion (HPT), accumulative roll bonding (ARB), multi-axial forging, twist extrusion, swaging and all sorts of derivatives of these processes. Depending on the details of the process, the grain size can be refined to a mean dimension below 1 μm, and sometimes below 100 nm by a mechanism of grain fragmentation through dislocation cells formation, see an example in Fig. 2a of a very fine grained Cu microstructure obtained by ECAP [17]. SPD methods have been successfully applied on most pure and alloyed metals.

In terms of hybrid nanostructured metals, if the initial grain size obtained by SPD is sufficiently small as in Fig. 2a, a bimodal structure can be produced by heat treatments with the size of the large grains in the micron range, see the example of Cu in Fig. 2b [17]. The ARB process has been successfully applied to produce laminates of alternating Cu and Nb layers owing to repeated roll bonding, cutting, stacking and further rolling, e.g. [18,19]. The layer thicknesses range from ~10 to ~1000 nm with up to meter scale in-plane dimensions. A variant of the ARB process named "repeated press and rolling" has been used to process nano-layered composites with alternating Cu/Fe, Cu/Ag, Fe/Ag and Cu/Nb

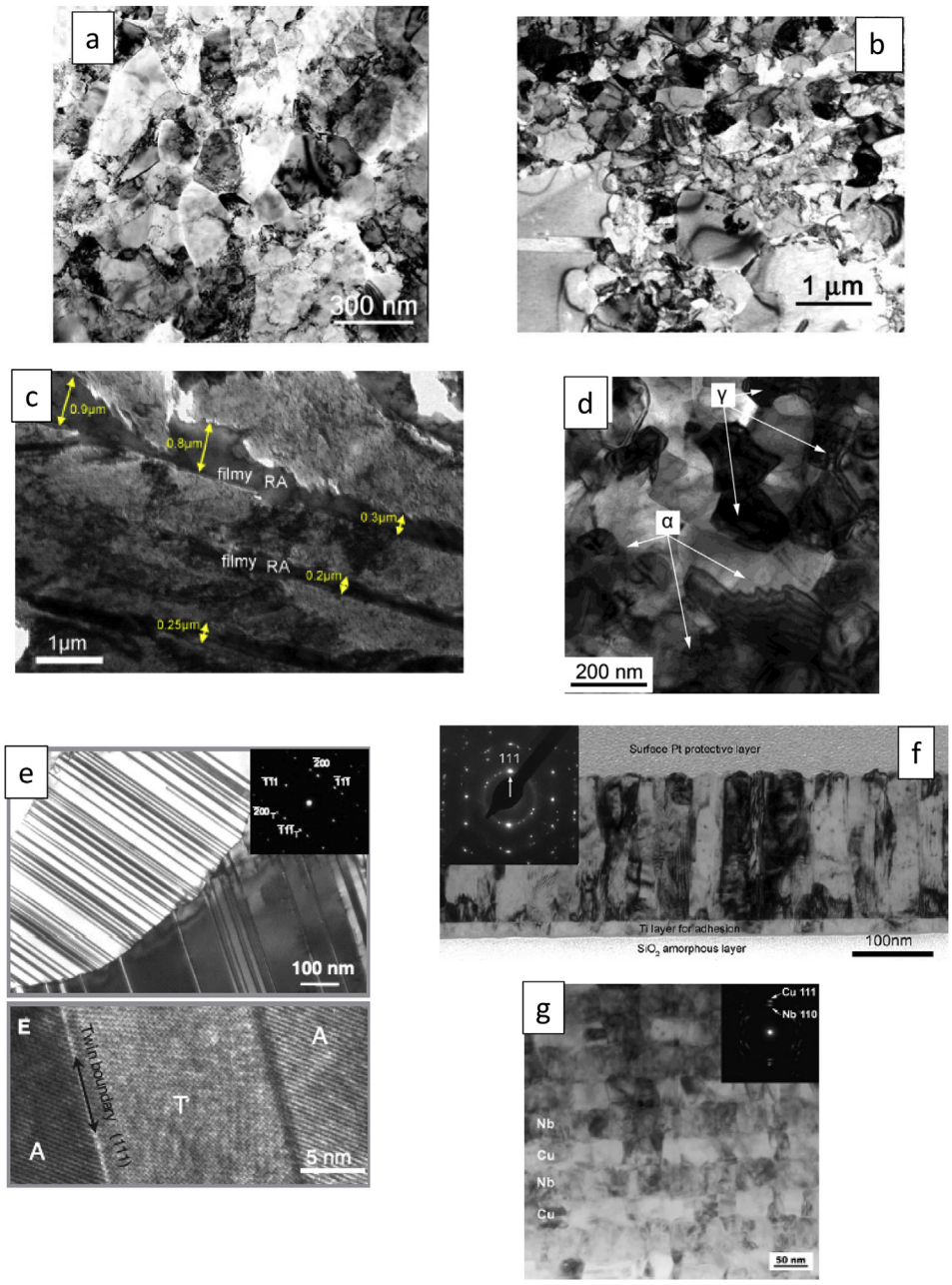

Fig. 2. Set of UFG, NC and thin film metallic microstructures; (a) NC Cu produced by ECAP [17]; (b) bimodal structure produced after heat treatment from the microstructure shown in (a); (c) TEM micrographs of the submicron thick film type retained austenite in BAT (see definition on the text) from [29]; (d) High Mn steel with very fine-grained austenite-ferrite (<400 nm) duplex microstructure obtained by combining rolling and intercritical annealing, from [30]; (e) nanotwinned Cu produced by electrodeposition, from [42]; (f) TEM bright field micrograph of a FIB cross section of a 300 nm thick Pd film with 30 nm elongated columnar grains exhibiting a ⟨111⟩ texture parallel to the normal of the film [51]; (g) TEM bright field micrograph of a 40 nm Cu/40 nm Nb multilayer showing {111}Cu||{110}Nb fiber texture [228].

compositions, e.g. [20–22]. Accumulative "extrusion, drawing and bundling" can generate nano-filaments of Nb within a channeling, highly textured Cu matrix with a controlled hierarchical structure see e.g. [23]. Shot peening can be also considered as a SPD process as it heavily deforms under high strain rates the near surface regions of metals, leading to a hybrid structure with very fine grain sizes at the surface and a gradient towards to core with larger grains [24,25].

Recently, new routes involving *advanced thermo-mechanical treatments* have been proposed to produce nanostructured metals, especially steels, with processing routes compatible with industrial practice. In particular, there is a growing interest in the development of new advanced high strength steels (AHSS) with enhanced combination of strength and ductility. UFG dual phase (UFG DP) steels can be produced using two types of concept: the Q&P and the inter-critical heat treatments. In both cases, metastable retained austenite (RA) can transform into martensites ε (hcp) and α/or α' (bcc or BCT) leading to a transformation induced plasticity (TRIP) effect. The RA phase may also remain stable and give rise to mechanical twinning due to its low stacking fault energy (SFE), especially in high Mn (~10%wt) steel. The UFG steels are thus complex hybrid multiscale systems. The UFG DP steels are known for a long time (see e.g. Jin et al. [26]). Their microstructure may also be met in inter-critically heat-affected zones of multi-pass

welds [27]. The process named Q&P, in which Q stands for "Quench" and P for "Partitioning", involves an initial cooling step to a quenching temperature, T_q, such as $M_f < T_q < M_S$ (M_S and M_f mean the "start" and the "end" of martensitic transformation, respectively), followed by an isothermal holding at T_q or at higher temperature with the purpose of promoting C (and other Γ stabilizing elements, such as Ni and Mn) transfer from martensite into the austenite. This austenite is thus stabilized and retained at room temperature. The RA phase is often under the form of very thin films (<0.1 μm) located along the martensite lath boundaries [28]. The second concept involves only a quenching followed by inter-critical tempering. Gao and co-workers [29] studied three heat treatment routes incorporating bainite formation during quenching, namely bainite-based quenching plus tempering (BQ&T), bainite austempering (BAT) and bainite-based quenching plus partitioning (BQ&P). These heat-treatments were applied to a medium C–Mn–Si–Cr alloyed steel. Enhanced mechanical properties with BQ&P heat treatment were attributed to an increased amount of refined filmy RA (22 vol.%, width < 100 nm and length around 100–500 nm), as shown in Fig. 2c taken from Ref. [29]. The same concept can be applied to martensitic steels to produce duplex microstructures. In these materials, an inter-critical heat treatment can be applied at relatively low temperature provided that the material contains enough Γ stabilizer elements. This is the method recently applied to a high Mn steel [30]. The alloy exhibits a very fine-grained austenite-ferrite (<400 nm) duplex microstructure, shown in Fig. 2d, achieved by a combination of cold rolling and inter-critical annealing at 550 °C for 6000 s (B550) or at 610 °C for 370 s (B610). The enrichment (partitioning) in Mn of the reverted austenite is such that during tensile testing at room temperature the austenite deforms by mechanical twinning (TWIP effect), ε and α' martensite phase transformation (TRIP effect) in succession, producing a TWIP/TRIP effect.

Nanostructured metals and alloys can also be produced by *powder metallurgy routes*. A fine powder, produced for instance by spray atomization, is heavily deformed, involving sometimes cracking and re-welding mechanisms, in dry high-energy ball mills under protective environmental conditions. The heavy deformation involves shear banding and dynamic recrystallization of the metal constituting the powder, similar to a SPD process but performed in a random way. Cryo-milling is particularly efficient to produce very fine grain structures [31]. The powder is then compacted and finally consolidated to full or nearly full density by hot pressing, and further mechanical compression methods. Mixing powders having undergone different intensity of milling allows the generation of controlled multimodal grain size distributions, e.g. [32]. Applications to Al, Cu and Ni alloys have been particularly successful, e.g. [33–35], while more complex materials like the nanostructured Oxide Dispersion Steels (ODS) strengthened by adding about 0.3 wt % Y_2O_3 particles to steel [36] are intensively studied.

Electro-deposition is an electrochemical process requiring high current densities to produce nanostructured materials. High current densities avoid the growth of the nuclei created on the electrode surface. High current density requires the use of short pulses at low voltage. The use of additives in the electrolytes promotes grain size reduction as well, by a continuous heterogeneous nucleation process and a control of the grain growth process. A low temperature is also favourable for maintaining a small grain size. Electro-deposition allows the processing of mm thick specimens with grain sizes below 50 nm, and even below 20 nm under pulsed current control. The literature contains many examples of studies on electrodeposited Ni foils for instance, e.g. [37–39]. Electro-deposition has been used to produce NT metals, in particular NT Cu [40–42], shown in Fig. 2e, widely studied in recent years for the excellent strength-ductility compromise (see in further sections). Alloys, like NiCu [43] and NiW [44], can also be processed by electro-deposition.

Other methods involve for instance the crystallization of a metallic glass, e.g. [45,46], inert gas condensation, e.g. [47,48], or friction stir processing, e.g. [49], but with more limited success or coverage in the literature. Most of the results discussed in the present overview deal with the failure of bulk NC metals produced from SPD, advanced thermomechanical treatments, mechanical milling or electro-deposition.

2.1.2. Metallic thin films, beams, ribbons and nanowires

Metallic films are commonly deposited using chemical or physical methods such as low pressure chemical vapor deposition, plasma enhanced chemical vapor deposition, electron beam evaporation, magnetron sputtering or atomic layer deposition, and many variants of these. Each method has advantages regarding the degrees of freedom in the deposition temperatures, the control of the final composition, the time required for deposition, allowing significant variations of the microstructure characteristics. Nevertheless, the typical microstructure of a thin metallic film is often, as shown in Fig. 1, made of columnar grains (with a specific morphology and shape dependent on deposition temperature and pressure), one over the thickness, see Fig. 2f, and exhibiting a sharp texture. The grain size is submicron due to the dimensional connection with the thickness. Conditions with several grains over the thickness can be favoured by repeated interruptions of the deposition process. As for bulk metals, different alloying compositions are possible leading to solid solution, often with segregation at GBs. Twinned structures can be easily produced as a result of annealing, deformation (internal stress driven) or growth twinning mechanisms, see e.g. [50] for Cu and stainless steels films or [51,52] for Pd films. Compared to bulk NC specimens, the presence of internal stress and the state of the surface in terms of oxides, roughness, GB grooving or depletion layers, must be carefully accounted for when addressing deformation and fracture behavior. Multilayered thin coating structures can be easily processed by deposition methods more easily than for bulk systems with the main condition that the elements are not miscible, see e.g. example of Cu/Ag thin multilayers [53] or Cu/V and Al/Nb systems [54]. Probably the most widely studied multi-layered metallic coating material is the Cu/Nb system [55], see example Fig. 2g, which can be produced by sputtering with thicknesses of the alternating layers varying typically between a few nm and 100 nm with total thickness around a micrometer or more. Compared to the ARB Cu/Nb macroscopic materials, the nano-laminate films tend to exhibit a wavy pattern due to the transfer and accumulation from one layer to the other of the roughness. More sophisticated Cu/Nb laminated hybrids involve stacks of series of alternating layers with a change of the thickness among the different series [56].

Micro- or nano-scale structures can be produced out of bulk materials or thin films specimens relying on micro- or nano-machining. A widely used method is Focused Ion Beam (FIB), often with Ga ions, which allows machining pillar, beam or ribbon structures with micron sizes down to typically 100 nm. This method is now routinely available in many experimental laboratories and does not necessitate clean room environment. The key issue is the production of defects in terms of near surface defects, e.g. [57–59], that artificially modify the microstructure and thus the mechanical behavior of the materials. Lithography methods combined with etching can be less aggressive than FIB if the etchants are properly selected. The question of etching selectivity is delicate. These methods borrowed from microelectronics often require clean room facilities. They allow producing freestanding structures in the form of membranes, ribbons, beams or nanowires. Wires or beams with sizes down to 10 nm can be produced

by e-beam lithography. The freestanding structures produced by FIB or lithography can then be directly tested using the adapted instrument (see Section 5) or cut and manipulated to position them in the test frame. As explained in Sections 4 and 5, the properties of freestanding structures can be different than when resting on the substrate due to the different constraint acting on one of the sides of the material. As an alternative to these top down approaches to produce nano-scale structures, nano-wires or nano-ribbons can be directly grown using bottom up processing methods. For instance metallic nanowires can be produced by physical vapor deposition, often at elevated temperature and under ultra-high vacuum conditions, e.g. [60,61]. These nano-whiskers can be tens of micrometers long with diameters ranging from tens to hundreds of nanometers, involving a very clean and defect free single crystal structure. They offer model system to address plasticity in ideal defect free conditions. Nano-manipulation is needed to transport these structures to the test apparatus (see Section 5).

2.2. Basics on deformation mechanisms in metals with nano-scale dimensions

Prior to failing, most metals deform plastically and nanostructured metals are no exception. However, compared with conventional metallic systems in which plasticity is essentially dominated by forest type dislocation activity, nanostructured metals exhibit a variety of deformation mechanisms involving thermally activated dislocation nucleation from GBs, grain growth with GB migration, room temperature diffusion and exhaustion hardening (or dislocation starvation). These mechanisms either cooperate or compete with one another leading to complicated physical *scenarii* which set the magnitude of the stress levels that are attained, the rate sensitivity and the stability of the microstructure. Sub-divided into the various types of systems addressed subsequently, this section surveys the minimum needed to appreciate the role of plasticity in fracture. Comprehensive review papers on nanostructured materials develop these topics in more detail, e.g. [3–8].

The two key parameters that quantify the connection between strength and plastic deformation are the strain hardening exponent n and strain rate sensitivity m defined in general terms as $n = \partial \ln \sigma_y / \partial \ln \varepsilon^p$ and $m = \partial \ln \sigma_y / \partial \ln \dot{\varepsilon}^p$, respectively, where σ_y is the current yield stress, ε^p is the accumulated plastic strain, and $\dot{\varepsilon}^p$ is the effective plastic strain rate.

The reference for further comparisons and discussions is provided by *Conventional CG polycrystals* whose main characteristics regarding plastic deformation are reminded hereafter. *CG polycrystals* deform at room temperature by dislocation-mediated mechanisms, involving sometimes deformation twins. Dislocations are produced from different types of sources, glide, interact with other dislocations and with other microstructure features (solute atoms, precipitates, grain and phase boundaries), get pinned and depinned, which may require the generation of additional dislocations to pursue the deformation, leading to the forest hardening behavior. At moderate strains, more dislocations are produced than recovered, leading to the stage III strain hardening mechanism [62]. Depending on the recovery capacity, hence on the stacking fault energy, CG metals exhibit a value of n varying between 0.05 and 0.5. Dislocations tend to organize into cells with high dislocation density into cell walls. At very large strains, the so-called stage IV strain hardening regime sets in with a constant, low hardening rate. The strength σ_y is a combination of the initial resistance to dislocation glide in the original microstructure σ_0 plus the strain hardening contribution. When refining the microstructure by decreasing the grain size d, σ_0 varies as K_{HP}/d^{α} (see later for more details) with α often around 0.5 as expressed by the Hall–Petch law [63,64] and K_{HP} a constant, see Fig. 3a. Usually, the rate sensitivity m is low in CG fcc (below 0.01) and moderately low in bcc and hcp materials at room temperature (not more than 0.03–0.05 except for very low melting point metals).

2.2.1. Deformation mechanisms in single phase UFG and NC metals

In UFG metals, qualitatively the same mechanisms as in CG metals occur except that no dislocation cells are observed. Furthermore, Geometrically Necessary Dislocations (GNDs) accumulate near GBs to accommodate possible deformation incompatibility among neighboring grains. Presumably, accumulation takes place in boundary layers whose width is comparable with the grain size. The so-called “core and mantle” [4] description of the deformation of grains with a wide central part (the core) and a thin boundary layer (the mantle) involving a high dislocation density loses its significance. Hence, the increase of strength with decreasing grain size still follows a K_{HP}/d^{α} trend but with a value α or a proportionality constant K_{HP} that can differ, see Fig. 3b with an example for IF steels [65], while other examples can be found for Al [66] or Ti [67]. Sinclair et al. [68] followed by [69], developed a closed form description of the dislocation accumulation near GBs. With the introduction of a saturation of the GB dislocation density, involving the relaxation of the impenetrable character of the GB, as well as a back stress evolution law invoking a progressive shielding by the dislocations on the opposite side of the GB, these authors captured not only the evolution of the yield stress but also the decrease of strain hardening capacity for small grain size. The high density of GNDs compared to statistically stored dislocations (SSDs) leads to high kinematic hardening levels.

All these effects can be described using advanced continuum plasticity models that take into account barriers to plastic flow and the impact of GNDs on hardening usually through higher order boundary conditions and higher order stress quantities - the so-called strain gradient plasticity (SGP) theories -, e.g. [70] or through back stress based formulations related to the plastic slip incompatibility [71], both theories being mathematically equivalent under some prescriptions [72]. In these theories, the accumulation of GNDs at GBs is accounted for in a smeared way, leading to the introduction of one or several phenomenological internal lengths qualitatively connected to dislocation mechanisms, see e.g. discussion in [73,74]. Recently, these strain gradient plasticity theories have been enhanced to better represent the behavior of GBs involving the partial or full transparency to dislocation motion under stress, e.g. [65,74–77], which allowed, for instance, better capturing experimental trends at the smallest grain size in IF steels, see Fig. 3b [65]. Discrete dislocation dynamics (DDD) simulations of polycrystals have also allowed looking at this range of grain sizes in 2D [78]. The Hall-Petch relationship is fairly well captured by these simulations but the drop of strain hardening with decreasing grain size is not, because specific rules for the GB response are missing. In [78], the authors explicitly indicated the need for transmission rules at GBs to better reflect the physics, which was included in recent SGP theories as explained above. Interestingly, incorporating enhanced physics that accounts for dislocation junctions and forest hardening following [79,80] does not affect the macroscopic response, including Hall-Petch scaling and hardening rates, although it does affect the dislocation density evolution [81] with possible consequences on energy storage that could eventually drive recrystallization and grain refinement. Thus, a better understanding of relaxation mechanisms at GBs is still needed.

The deformation mechanisms in NC metals are even more complex. In this range of sizes, dislocation mechanisms compete or cooperate with other deformation mechanisms associated with the mobility of GBs. Internal dislocation sources are scarce as the grain size decreases. Several authors have suggested, based on molecular

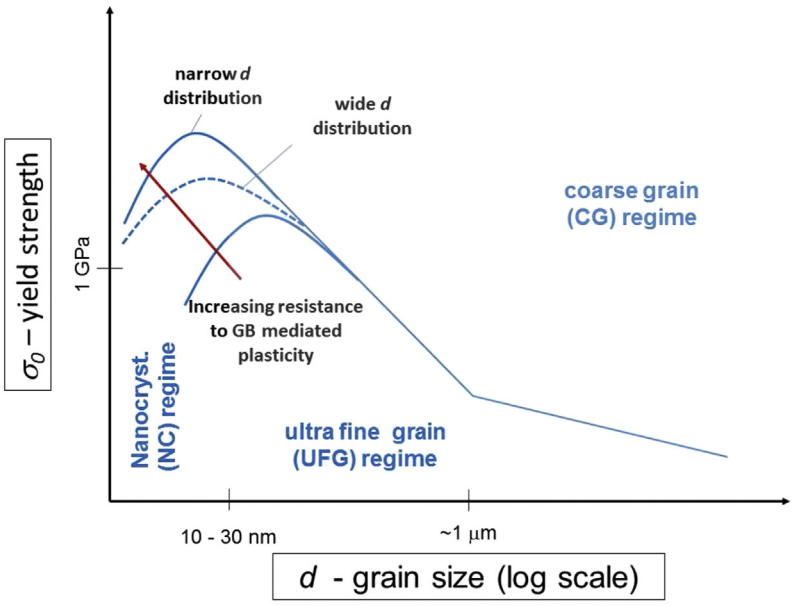

(a)

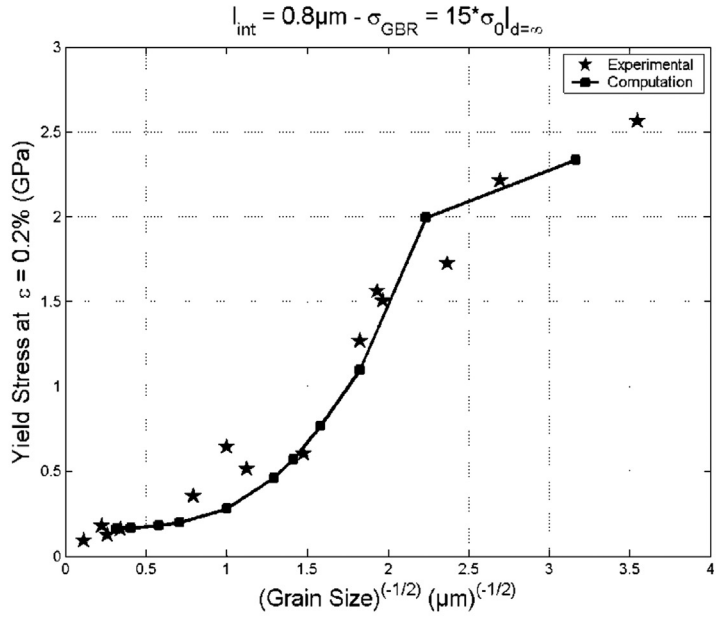

(b)

Fig. 3. (a) Schematic representation of the variation of the yield strength as a function of grain size, with several possible *scenarii*; (b) example for IF steels with comparison between experimental data and FE simulations based on an advanced strain gradient plasticity formulation, reproduced from [65].

dynamics simulations, that GB dislocation sources are activated in nano-grains [82] from ledges or other local stress concentration owing to the very large strength levels. The GBs act as dislocations sinks in which their stress field can spread [83]. But dislocations, owing to the high stress levels, can also traverse the GBs while leaving some debris. This transition from regular dislocation activity from pre-existing intra-granular dislocation sources to GB dislocation nucleation dominated plasticity is not abrupt. It depends on the magnitude and distribution of the initial dislocation density from grains to grains and on the distribution of grain size. Now, as the grain size decreases, GB mediated deformation mechanisms involving GB sliding [84], GB rotation [85] and GB migration [86] start competing with dislocation-mediated plasticity. A number of studies have indeed reported stress-assisted grain growth as an efficient mechanism in small-grained materials [87–91]. The detailed mechanisms of GB sliding or shear coupled GB migration, by atom shuffling or GB dislocations, depend on the misorientation, on the orientation of the GB plane with respect to the tensile axis and on the presence or not of GB solute elements.

In real NC polycrystals, the grain size distribution is such that the smallest grains can be extremely resistant to plasticity while

other grains, better oriented or larger, can deform by more classical dislocation mechanisms or relax the stress by GB sliding or migration, leading to huge levels of internal stress and long elastoplastic transitions, see e.g. [92,93]. The concept of yield stress is thus not well defined anymore and must be given at a representative level of plastic strain [93]. The extreme strengths are attained for conditions of grain sizes and GB nature such that dislocation nucleation dominated deformation is pushed to the upper stress limit at which the GB mediated mechanisms start relaxing the load. This typically occurs at average grain sizes around 10–50 nm with σ_0 sometimes equal to several GPa. In [94], it was shown that the yield stress could peak at 10 nm grain size in NC Cu. In the meantime, the difficulty to store dislocations increases the difficulty for further plastic flow and leads to very limited strain hardening capacity n near 0. All mechanisms described above involve the cooperative activity of only a small number of atoms which can be triggered by thermal activation owing to a small activation area. An essential characteristics of NC metals is thus to exhibit a high rate sensitivity m as depicted in Fig. 4 which has been constructed based on a wide compilation of data provided in [95]. In fcc, m monotonously increases with decreasing grain size; but for bcc, m first decreases with decreasing grain size while it re-increases only at sizes around 30–50 nm. Furthermore, the long elastoplastic transition resulting from the heterogeneities in the microstructure and the different natures of the deformation mechanisms lead to *very large back stress levels*. The combination of high back stress and high rate sensitivity can result in the surprising observation of reverse (creep-)plasticity under small load levels, e.g. [96]. In summary, single phase NC metals involve high strengths, high rate sensitivity, high levels of back stress and low isotropic strain hardening capacity. Finally, in NC metals with grain size below 10–20 nm, GB deformation mechanisms dominate. Aspects of the behavior bear resemblance to that of amorphous materials and this goes beyond the scope of the present review.

2.2.2. Deformation mechanisms in NT metals

The twinning tendency of a Face-Centered-Cubic (fcc) metal is largely determined by its stacking fault energy (SFE). For example coarse-grained (CG) fcc metals with high SFE such as Al and Ni normally deform by slip of perfect dislocations, while fcc metals with low SFE such as Ag primarily deform by twinning which is produced by the propagation of partial dislocations. High strain rates and low deformation temperatures also promote deformation twinning: see [99] for a review on deformation twinning in CG metals. An essential element for further discussion in this paper is that the formation of mechanical twins produces an increase of the work-hardening rate quantified here by n through a progressive Hall-Petch type mechanism, e.g. [100,101]. The focus in this section is on deformation twinning in NC fcc metals or on the plasticity mechanisms in NT fcc metals (in which the grain size is not necessarily very small). Three main issues are addressed: (i) the condition to nucleate mechanical twins in NC metals, (ii) the effect of twins on the mechanical behavior of NT metals or, otherwise stated, the interaction between twins, and (iii) the stability of these twins during deformation. These issues are also addressed in the review by Zhu et al. [102].

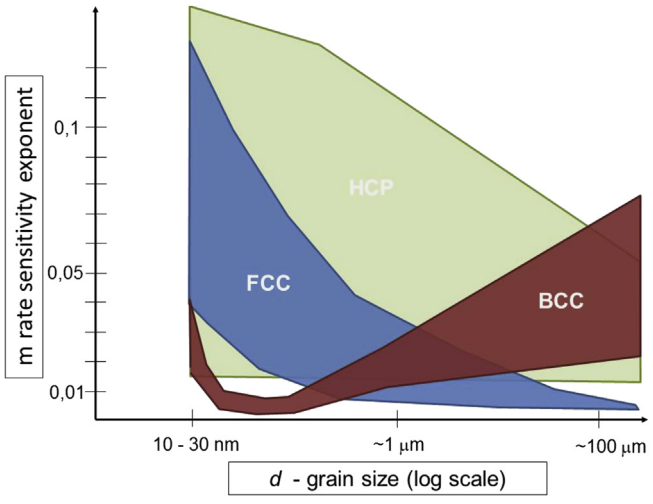

Fig. 4. Schematic variation of the rate sensitivity exponent m as a function of grain size for fcc, bcc and hcp metals inspired from the compilation of data provided in [95].

Contrary to CG metals which become more difficult to twin with decreasing grain size, NC (fcc) metals twin more easily with decreasing grain size, reaching a maximum twinning probability, and then become more difficult to twin when the grain size decreases further, i.e. exhibiting an inverse grain-size effect on twinning [102–104]. Molecular dynamics simulations (MD) have revealed several important deformation mechanisms of NC materials, see [102]. Emission of Shockley partials from GBs has been extensively observed. Three mechanisms for twin nucleation and growth were suggested by Yamakov et al. [105] and discussed by Zhu et al. [102] (see in their Fig. 11). In UFG Cu (with grain size in the range 400–600 nm), pronounced enhancement of the strain hardening rate occurs when the twin spacing is smaller than 15 nm. It has been suggested that at larger twin spacing, the strength of such NT Cu is dominated by the twin boundary (TB) resistance to dislocation slip activities, e.g. [103]. As the twin spacing is reduced to less than 15 nm, nucleation of twinning partials at TB-GB intersections could lead to a reduction of yield strength and a modification of strain hardening capacity [9,103]. Moreover, the presence of dense nanoscale twins significantly influences the evolution of the activation volume for plastic flow which is three orders of magnitude smaller than the one known in CG Cu [106]. This explains why a large number of experimental studies and modelling has been devoted to NC metals and alloys containing a large fraction (20–50%) of NT (twin spacing, $\lambda < 100$ nm). At the twin spacing transition, the yield strength is almost 10 times the yield strength of pure Cu. Moreover the critical twin spacing varies linearly with grain size [102]. The transition in twinning behavior from CG to NC metals is caused by the change in deformation mechanism as indicated earlier. An analytical model based on observed deformation micro-mechanisms in NC metals, i.e. emission of dislocations from twins in NC fcc metals has been proposed [102,107,108]. The interactions between pre-existing twins and partial dislocations have also been studied using molecular dynamics simulation [109,110] and by high resolution TEM [52,111]. These studies have confirmed that these interactions tend to promote a strengthening effect related to slip arrest in the form of Lomer-Cottrell locks [112].

The NTs are not always stable. De-twinning effect is often observed. This phenomenon is not specific to NC metals since de-twinning can also occur in CG metals. This process is caused by the interaction between matrix perfect and partial dislocations (PDs) and TBs, see e.g. [113–115] for recent reviews. De-twinning can be partly responsible for the deformation of NC metals, in particular for their work softening. *In-situ* TEM experiments on NT Cu revealed systematic activation of Shockley twin PDs from TB-GB triple junctions and their motion parallel to TBs causing TB migration [116]. This migration may annihilate entirely thin twin lamellae producing de-twinning, especially when the twin thickness λ is very small ($\lambda <$ ~30 nm) [117]. Wang et al. [115] described a mechanism operating in incoherent TB (ITB). These ITBs propagate

as a disconnection or a step (see [118] for a description of disconnections) that is a multiple {111} atomic planes thick resulting from the collective glide of multiple TPs which may possess identical or different Burger vectors, satisfying the mechanism needed for de-twinning. Wang et al. [115] have suggested when modelling the migration of ITBs that de-twinning becomes the dominant deformation mechanism for growth twins of the order of a few nanometers thick. De-twinning explains also the annihilation of TBs in rolled, highly textured NT Cu films and the softening effect observed in UFG NT Cu. It can also be noted that the motion of TBs controlled by a local shear stress generating the displacement of twin partial dislocations produces an elongation in a direction perpendicular to the plane of the TB, as described in [119], and modelled in [120,121].

2.2.3. Deformation mechanisms in NC and UFG multiphased metals

In bimodal grain distribution structures, the deformation is heterogeneous with the continuous network of small grains providing the high strength while the large grains bring about an isotropic strain hardening contribution. Furthermore, a large kinematic hardening contribution results from the strength mismatch between small and large grains [122]. The importance of the back stress generated by a bimodal distribution has been captured by FE cell simulations of representative grain aggregate using SGP type models allowing the introduction of higher order boundary conditions that mimic the constraint of GBs on plastic flow [65,123].

Deformation mechanisms in multi-phase microstructures imply strong obstacles to dislocation motion due to the interfaces between different phases. These interfaces are often stronger than GBs regarding dislocation transmission. Strong back stress is generated due to the different strength of the different phases, leading to the accumulation of high densities of GNDs. Another size effect, in addition to the grain size of the first matrix phase, comes from the dimension of the second phase. Recently developed hybrid systems exhibit even more complex mechanisms. For instance, the effect of thin films of austenite located along lath or grain boundaries in ferrous lath martensite (Fig 2c) must be distinguished from the dual phase effect observed in duplex UFG steels. The recent studies by Mine et al. [124] and Maresca et al. [28] provide a detailed analysis of the deformation modes of the tiny austenite films. Slip transfer from one phase to the other one depends on the crystallography and the orientation relationship. In dual phase materials the effect of the second phase is more "massive", in particular when this phase can be deformed by mechanical twinning or by martensitic phase transformations (ε (hcp); α' (bcc)), see [30]. Quantitative study of these phase transformations would require the knowledge of the local stresses and the local composition which controls in particular the stacking fault energy, SFE. Some observations [30] indicate that the α' transformation is "stress-induced", contrarily to what is observed in many coarse grain low SFE steels. In these steels, α' preferentially nucleates at the intersection of twins and/or ε platelets while in the high Mn steel with a duplex UFG microstructure α' is preferentially nucleated at grain boundaries leading to the assumption that α' was "stress induced". If this was the case, one should expect that this effect and its consequences like the TRIP effect should be amplified when the test temperature is decreased. The nature of work-hardening in multi-phased materials due to a TRIP effect is very much dictated by SGP effects connected to the submicron size of the transforming domains [125,126].

In thick multilayer metallic systems, the resistance to slip transmission across the interphase boundaries constitutes the dominant factor that dictates the maximum strength of the multilayer. In Cu/Nb laminates produced by magnetron sputtering, semi coherent energetically favourable interfaces form respecting the Kurdjumov-Sachs orientation relationship typical of fcc-bcc systems. The strength increases with decreasing layer thickness through a Hall-Petch type mechanism down typically to 50 nm, e.g. [56,127]. Below 50 nm thickness, the strength keeps increasing with decreasing layer thickness through the so-called confined layer slip. When the thickness gets about a few nm, the dislocations are then able to glide across the interfaces and the peak strength is attained [127,128]. The overall picture is thus not much different than in Fig. 3a, although the relaxation mechanism that dictates the position of the peak is different. The shear strength of the semi coherent interfaces in Cu/Nb multilayers is not very large [129]. In general, the isotropic strain hardening of Cu/Nb multilayers is very small in the small layer thickness regime. The Cu/Nb produced by ARB exhibit deformation twins when the individual layer thickness is below 50 nm while Cu/Nb produced by PVD does not. This intriguing result has been recently explained by a detailed analysis of the crystallography of the interfaces: the faceted {112}Cu||{112}Nb type interfaces in ARB multilayers favour the production of deformation twins in Cu while the {111}Cu||{110}Nb atomistically flat interfaces of PVD multilayers favour symmetric slip [18,130,131]. The control of the crystallographic texture is another key issue texture [132]. Cu/Ni/Nb trilayer based systems processed by PVD can provide more strain hardening capacity by favouring the operation of so-called super threaded dislocations, which leave some dislocation content at the fcc-bcc interfaces [133]. Note finally that metallic multilayers with alternating crystalline and amorphous layers reveal interesting properties [134,135] but these systems go out of the scope of this review.

2.2.4. Deformation mechanisms in metallic films, pillars and nanowires

Systems with at least one submicron external dimension involve a very fine microstructure dictated by the outer dimensions but also by the typical deposition processes which are often far from equilibrium and which lead to a high density of defects in terms of twins, GBs, vacancies, stacking faults etc (nanowhiskers constitute one notable exception). The main mechanical characteristic of these nano-objects is that the flow strength increases with decreasing dimensions. This is illustrated by the data compiled in [6] and schematically reproduced in Fig. 5. The data has essentially

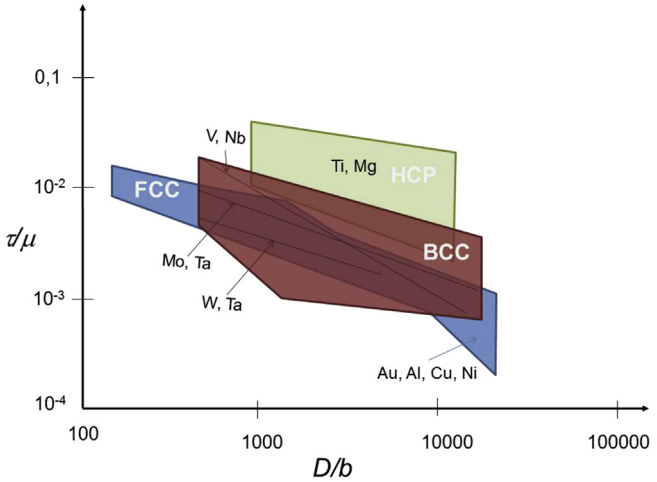

Fig. 5. Schematic variation of the shear flow stress on relevant slip or twinning system normalized by the elastic shear modulus as a function of pillar diameter normalized by the norm of Burger's vector for fcc, bcc, and hcp systems, inspired from the large set of data compiled in [6].

been obtained using pillar compression. Note that the behavior in pillars exhibits stochastic aspects so that the increase in strength is accompanied with an increase in scatter. The same trends are obtained when pulling thin metallic films in tension, e.g. see [136]. This "smaller is stronger" effect parallels the Hall-Petch behavior described in Section 2.2.1. The origin of this effect is partly similar as the grain size usually scales down with the dimensions of the film, see Section 2.1.2, but not entirely. Indeed, the plasticity mechanisms discussed in Section 2.2.1 are still valid for thin films and nanowires but with at least five important points of attention:

(1) Dislocations in thin films constrained by an underlying substrate often move through a mechanism of channeling: so called "threading dislocations" advance or recede by gliding on well oriented planes, with the dislocation line extending from the free surface to the interface [137,138]. This mechanism gets more and more difficult to operate with the decrease of the configurational force as the thickness decreases [137], providing one origin of the increasing strength at small thicknesses.

(2) When there are only one or a few grains over the thickness/diameter, which is the usual configuration in thin films/nanowires, the presence of free surfaces can significantly impact plasticity by allowing dislocations to escape, preventing their accumulation inside the metal. The imbalance between the rates of escape and generation of fresh dislocations leads to exhaustion hardening [139,140]. This phenomenon is also sometimes referred to as "dislocation starvation". In addition, the behavior in small volumes is often source limited. When dimensions are small (i) the probability of finding dislocation sources is low and they are harder to operate because of reduced activation lengths [141], and (ii) the operation of the few available ones is hindered by the proximity of free surfaces leading to hardening by source truncation [142]. Dislocations can also nucleate from GBs and then escape the grain with no capacity of storage. This explains the very low strain hardening capacity beyond a transient of extreme hardening. This and related phenomenology have recently been addressed by El-Awady [143] through a comprehensive set of DDD simulations on single micro- and nano-crystals. One key parameter is the product $D\rho$ with D the crystal size and ρ the initial dislocation density. El-Awady identifies four mechanisms: (i) if $D\rho$ is very small, pure dislocation starvation is active with no capacity for storing dislocations; (ii) at larger $D\rho$, the so-called "single source strengthening" dominates, as governed by a single source or a few sparse sources that hardly interact with other dislocations - again a very small strain hardening capacity is expected; (iii) the third mechanism is identified as the "exhaustion hardening" with a relatively high number of dislocation sources, but the mobile dislocations exhaust from mutual interaction and the corresponding density is insufficient to sustain flow with increasing the applied stress - a larger (albeit transient) strain hardening capacity is expected here; also see [144]; (iv) the fourth mechanism is the classical forest hardening. All simulation results for different conditions merge into a single master evolution when plotted as $\tau_y\sqrt{D}/\mu$ versus $D\rho$, where τ_y is the yield stress in shear and μ is the shear modulus. The overall behavior of a real thin film or nanowire is the collective response of micro- or nanocrystals involving GB and free surface and falling in one of these categories depending on the distribution of sizes and initial dislocation density. Factors such as the grain shape, the presence of oxide at the surface and the resistance of this oxide will also play a role in the dislocation starvation capacity, see e.g. [145,146].

(3) When the structure is columnar for thin films and bamboo-types for nanowires with a single grain in the small dimension, the lack of constraint in one or two of the dimensions facilitates the operation of GB sliding and migration mechanisms. The grain rotation or GB sliding can be easily accommodated in the transverse direction. Many examples have indeed been provided in studies on thin metallic films, e.g. [86,147,148]. This has been confirmed by MD simulations of tensile tests on Ni nanowires with 10 nm grain size [149]: the contribution to the overall deformation from GB mediated mechanisms is dominant in wires with diameter on the order of the grain size, while larger wires with several grains in the diameter exhibit also GB activity initially but with the development of high internal constraints at triple junctions that further lead to dislocation activity. The predominance of GB mediated plasticity mechanisms which are thermally activated with small associated activation volumes often leads to very large rate sensitivity exponents, see e.g. $m = 0.05–0.15$ for Al [12,150], 0.03–0.15 for Au [151], 0.02–0.1 for Pd films depending on ageing time and on the presence or not of a thin protective surface layer [152–154].

(4) The free surface can have other indirect consequences. In particular, the presence of GB grooves or a significant roughness acts as stress concentrators for initiating the plasticity mechanisms. Mompiou et al. [147] have recently shown that the GB grooves in 200 nm thick Al films initiate a process of GB dislocation glide, leading to GB sliding and grain rotation. Only after a few % of deformation, intragranular dislocation activity is observed, probably due to the generation of local stress concentration, with evidences of grain growth mechanisms as well (see also [148]). Furthermore, the free surfaces constitute a preferential region for atomic diffusion, which favours creep mechanisms in thin films, e.g. [155].

(5) Strain gradient plasticity can play an additional role in setting the resistance to deformation of small objects if the deformation mechanism is dominated by dislocation glide and storage, i.e. if the product of grain size or specimen size with dislocation density ($d\rho$ or $D\rho$) is not too small. When thin films are bent [156], or micro- or nanowires are subjected to torsion [157], the gradient of plastic strain over the thickness or diameter can be extreme and must be accommodated by a high density of GNDs. This leads to an extra source of strengthening, similar to the effects discussed in Section 2.2.1. It is emphasized that the notion of GNDs is scale-dependent and that more complex interactions between SSDs and GNDs occur inevitably. In particular, GNDs are not only induced by externally imposed gradients, as in bending [158,159] or indentation [160], but also result from deformation-induced strain gradients [161]. A plasticity size effect can thus emerge in microcrystals in the absence of macroscopic gradients. Such behavior may not be ubiquitous but has been reported experimentally [162].

Note finally that extremely large Bauschinger effects have been observed in thin metallic films upon unloading, e.g. [163], giving rise to significant recovery mechanisms. Saif and coworkers have found that thin Al and Au films with grain sizes around 50 nm deformed in the plastic domain and unloaded can recover a large fraction (50–100%) of the plastic strain under zero applied stress [164,165].

3. Fracture of bulk UFG and nanostructured metals

The significant increase in strength σ_y with decreasing microstructure size shown in Fig. 3a is usually accompanied by a drop in ductility. Fig. 6a shows the schematic variation of σ_y versus elongation to failure (or total elongation) ε_{engf} reported in the literature with the so-called "banana curve", e.g. [7,35,166]. The schematic Fig. 6a is supplemented by Fig. 6b and c compiling real data from the literature. Fig. 6b provides an example for Ni systems prepared by different methods [35]. Fig. 6c is a compilation by Speer et al. [166] of a wide range of data for steels. We have added in Fig. 6c the results on UFG-DP steels obtained in [30] for two annealing temperatures and the results on medium C steel [29], see descriptions in Section 2.1.1 The BQ&P treatment applied to the medium C steel and the short anneal applied at 610 °C on the low C steel lead to extremely attractive properties. Fig. 6d provides a recent compilation by Sharon et al. [167] of elongation at fracture versus microstructure length scale showing the same expected trend for a range of metals. It is essential to realize that the use of the elongation to failure ε_{engf} as a ductility index mixes both the resistance to necking, ε_u, and the resistance to damage accumulation, which is better quantified by the true fracture strain ε_f, see Section 1. A low value of ε_{engf} in a material capable of necking always implies a low ε_u, but not necessarily a low ε_f. This is why we separate the two aspects. Section 3.1 deals with the resistance to plastic localization in bulk nanostructured metals addressing possible ways to improve it. Section 3.2 focuses on the resistance to damage and fracture.

The intricate mechanisms of plasticity in nanostructured metals ultimately impart a rate-dependent hardening behavior. Models of damage and fracture that are rooted in a bottom-up approach based on explicit rendering of dislocation slip and twinning are not mature enough to enable a broad interpretation of available experiments. In the local approach to fracture, a phenomenological hardening law is typically introduced which will allow discussing among others the resistance to necking with quantitative parameters:

$$\sigma_y = \sigma_0 + k_1(\varepsilon^p)^n(1 + k_2\dot{\varepsilon}^{\,p})^m \tag{1}$$

where σ_y and σ_0 are current and initial yield stress, respectively, ε^p is the accumulated plastic strain, $\dot{\varepsilon}^{\,p}$ is the effective plastic strain rate, n and m are, respectively, the constant strain hardening and strain rate sensitivity exponents associated with this specific form of hardening law, and k_1 and k_2 are two hardening parameters. More physical hardening laws are available, e.g. [62], but Eq. (1) is sufficient for the present context.

3.1. Plastic localization in UFG and bulk NC metals

The essentials regarding plastic localization are summarized in Fig. 7 assuming the following phenomenological hardening law (1). Fig. 7 contains eight curves:

(1) Represented by *curve 1* is the engineering stress σ_{eng} versus engineering strain ε_{eng} response of a reference CG metal with yield stress σ_{0a}, strain hardening capacity $n_1 = 0.1$ and strain

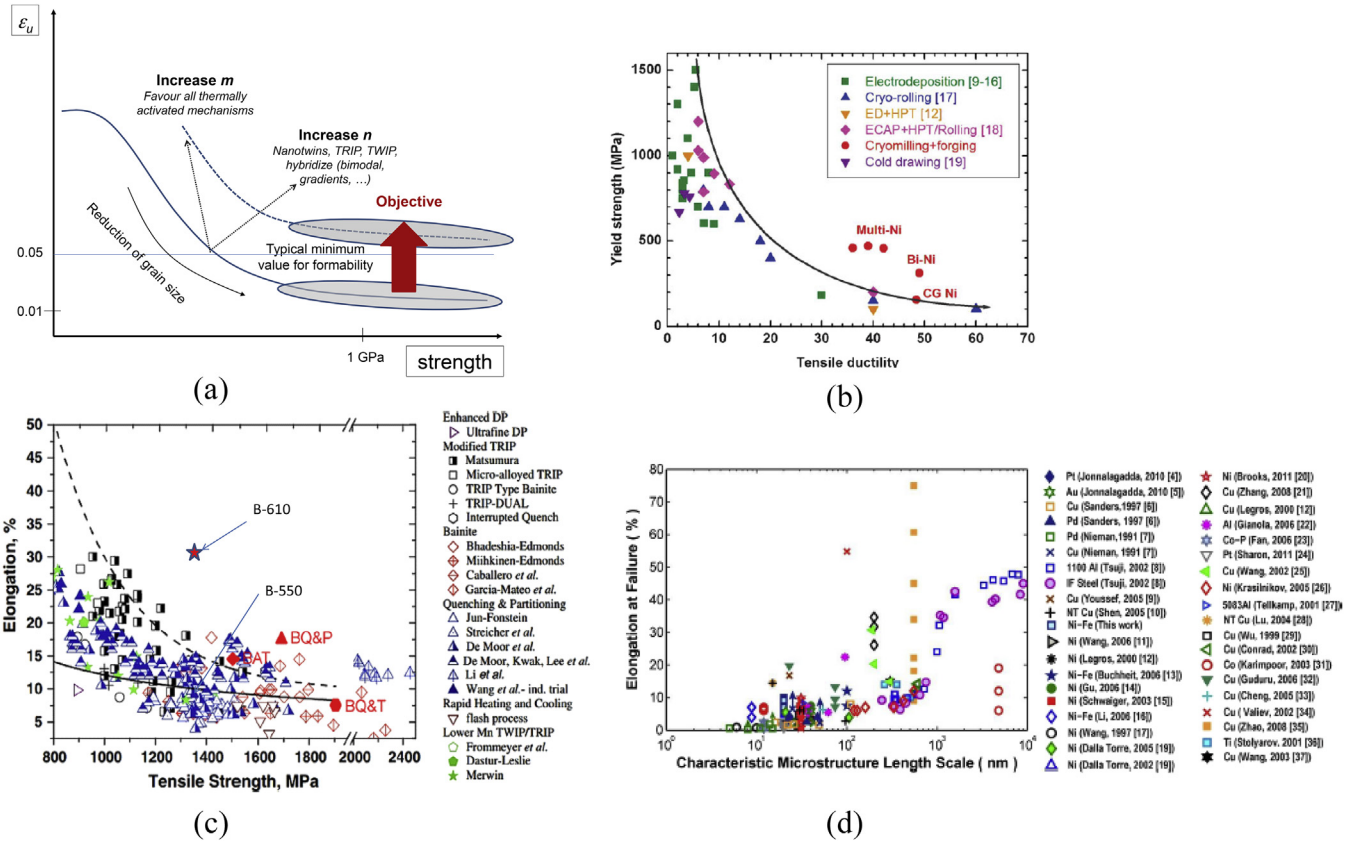

Fig. 6. Variation of the ductility as a function of strength (or characteristics microstructure length scale); (a) schematic evolution of uniform elongation/strain at necking with yield stress, showing the possible options to move out of the "banana syndrome"; (b) collection of data for a variety of bulk Ni systems produced by different methods [35]; (c) compilation of elongation versus tensile strength data for high strength steels produced by many different techniques, see [166] – see text for the notations BQ&P, BQ&T, B-550 and B-610; (d) compiled variations of elongation versus characteristic microstructural length scale taken from published quasi-static (~10^{-6}–10^{-3} s^{-1}) tensile experiments and reported by Sharon et al. [167]. The references for (b), (c) and (d) are given in the reference cited in this caption, and the numbering system appearing in these figures pertain to these papers.

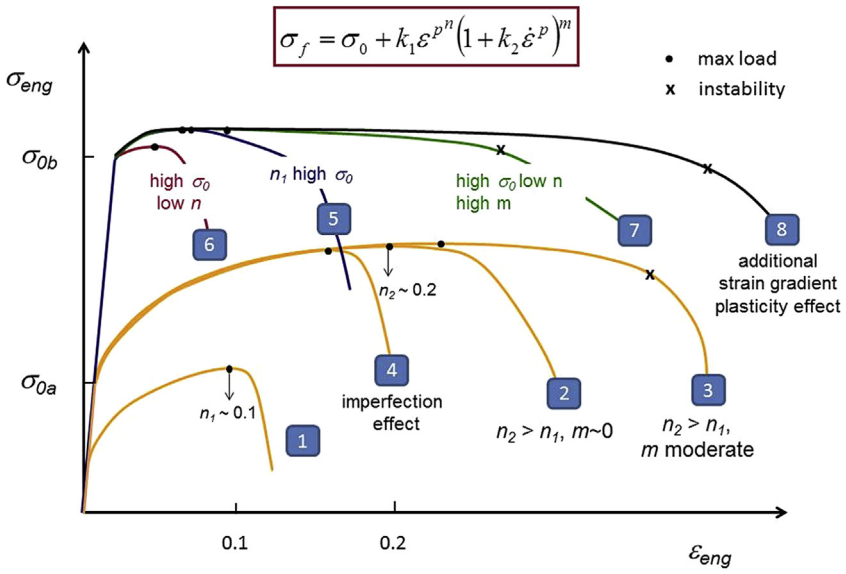

Fig. 7. Schematic engineering stress/engineering strain uniaxial tension curves of metallic materials involving different levels of yield stress, strain hardening capacity, rate sensitivity and imperfection - see text for a description of each curve.

rate sensitivity $m \to 0$. The onset of necking occurs at the maximum load with strain $\varepsilon_{Fmax} = \varepsilon_u \approx n_1 = 0.1$ as predicted by applying the Considère criterion $d\sigma/d\varepsilon = \sigma$ on Eq. (1) (assuming that σ_0 is sufficiently small compared to the strain hardening term in Eq. (1)).

(2) If the strain hardening capacity of the material is, by any possible means (e.g. lower stacking fault energy), increased to $n_2 = 0.2$ such as in *curve 2* the resistance to necking increases proportionally.

(3) Usually, m is lower than 0.01 in fcc materials (Fig. 4) and does not play any significant role in plastic localization. But, if m is not negligible as for *curve 3* because of higher homologous temperature or intrinsic rate sensitivity, such as in several bcc and hcp alloys (Fig. 4) a significant improvement in the resistance to necking is observed. The instability does not occur at the peak load anymore but later. The rate sensitivity stabilizes the incipient necking process. This effect can be quantitatively modelled by an imperfection type analysis (e.g. [168–170]) and not anymore by a simple Considère type analysis.

(4) If the material contains imperfections in the form of small machining defects (e.g. small reduction of section) or an aggregate of grains with soft orientation, the impact on the resistance to necking can be significant as exhibited with *curve 4* again for $n = 0.2$. A 1% section reduction typically leads to a 20% decrease of ε_u [170].

(5) *Curve 5* corresponds to a hypothetical UFG or NC metal with exactly the same characteristics as the reference material in terms of strain hardening and no rate sensitivity, but a much higher yield strength $\sigma_{0b} \gg \sigma_{0a}$. The corresponding ε_u is now much lower than 0.1. It is often not sufficiently realized that application of the Considère criterion leads to a decrease of ε_u with strength even at constant strain hardening capacity.

(6) In reality, the strain hardening capacity n of NC or UFG metals is, as explained in Section 2.2.1, lower than the reference CG case, see *curve 6*, [5]. The main reason for this lack of strain hardening capacity results from the impossibility to activate forest hardening mechanisms (involving dislocation dipoles, locks and pinning) during which obstacles multiply due to an increasing dislocation density.

(7) As explained in Section 2.2.1, fcc NC metals exhibit m values higher than in their CG counterpart, see [95,34,7] and Fig. 4, while, bcc metals do not show a monotonic increase of m with decreasing grain size, but still high m values at very small grain dimensions. If m increases, the resistance to necking can be significantly improved as shown with *curve 7*. The improvement of the ductility, while maintaining a high strength, has been demonstrated in several studies as in [17] in the case of Cu deformed at low strain rates. Detailed theoretical calculations have recently been performed by Pardoen [171] using an imperfection-based analysis for finite length specimens. There, it was assumed that the yield stress and strain rate sensitivity were related to grain size through, respectively, the following phenomenological laws

$$\sigma_0 = \sigma_{00} + K_{HP1} \Big/ \sqrt{d}, \tag{2}$$

$$m = \left(\frac{\frac{\tan^{-1}(a_1(d_c - d))}{\pi/2} + 1}{\frac{\tan^{-1}(a_1)}{\pi/2} + 1} \right) (m_1 - m_\infty) + m_\infty, \tag{3}$$

where σ_{00} is the contribution to yield stress independent of grain size (friction stress and other sources of hardening through solid solution or precipitates), K_{HP1} is the Hall-Petch constant, the limit m_∞ corresponds to the large grain size limit, m_1 corresponds to the small grain size limit, and a_1 is a tuning parameter controlling the spread of the transition region. A temperature effect could be taken into account by changing the values of m_1 and m_∞. Values reported in Section 2.2 motivate the following possible choice of parameters for typical fcc metals: $m_1 = 0.009$, $m_\infty = 0.1$, $d_c = 250$ and $a_1 = 10$ (this last parameter allowing a smooth transition at $d \approx d_c$) which match experimental data for Pd, [172] and are reasonable for Al as well [173]. Fig. 8 shows the predicted strain at plastic instability against grain size [171]. If m is constant, the ductility drops continuously just because of the increase of strength as discussed for *curve 5* in Fig. 7. But, if m varies with grain size following (3), the drop can be suppressed with even a possible improvement of the strain at necking.

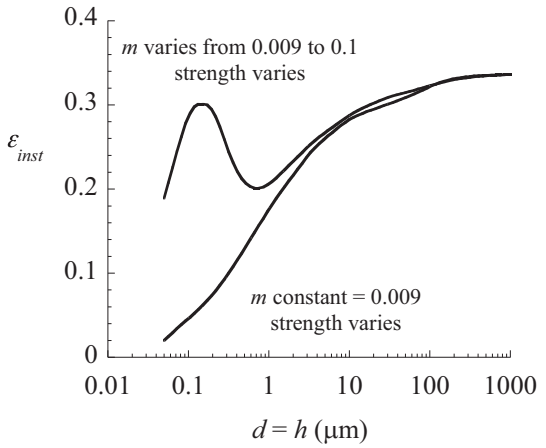

Fig. 8. Variation of the strain at necking as a function of the grain size *d* showing the effect of the increase of rate sensitivity with decreasing grain size compared to no change of rate sensitivity.

(8) *Curve 8* is described in the context of Section 5 as it only applies to micro- or nano-scale specimens.

The plastic localization mechanism discussed up to now refers essentially to diffuse necking under uniaxial tension. But, plastic localization also occurs under more general loading conditions. Furthermore, diffuse necking only develops if the deformation field is sufficiently homogeneous, otherwise, only localized necking can form. Localized necking develops at larger strains compared with diffuse necking (except under plane strain tension conditions where they coincide), sometimes inside diffuse necks [170]. Forming limit diagrams are used to represent the locus of localization strains under biaxial loading conditions (both for localized and diffuse necking). The prediction of localized necking is more complicated and typically requires the use of bifurcation theory, see the seminal papers [174,175], as well as to account for complex issues related to corners on the yield surface, softening mechanisms, crystal plasticity and texture effects. This goes beyond the scope of the present review, in particular because the literature is still very limited regarding in depth studies on this topic for NC materials. Nevertheless, all messages carried away from Fig. 7 remain qualitatively valid when dealing with localized bands. Based on the above discussion, we can synthetize the different means available to improve the resistance to necking, see Fig. 6a, by distinguishing the increase of the strain hardening and the increase of the rate sensitivity.

Increase the strain hardening capacity:

(1) Accumulation of dislocations in metals with grains as small as 10–30 nm has been recently demonstrated in different fcc alloys [176–178]. These data were obtained on thin films (see Section 5) but there is no reason that this should not be observed in bulk NC. One possible reason for this accumulation of dislocations is because of a pre-existing population of defects inside the grains, as a result of the processing, providing obstacles to pin the dislocations nucleated from the GBs and avoiding thus that all dislocations sink in the opposite GBs. This goes along with the importance of considering the initial dislocation density ρ through the product $D\rho$ as explained in Section 2.2.4.
(2) The processing of a bimodal grain size distribution is highly beneficial to resist necking as a source of strain hardening by dislocation storage in the large grains and as a source of back stress. Nevertheless, a necklace structure of nanograins in which isolated larger grains are embedded must be maintained in order to preserve the high strength [122].
(3) As explained in Section 2.2.2, nanotwins, whatever their origin (growth, annealing or deformation), constitute a source of strain hardening [38,179,180] with a work hardening capacity increasing with decreasing twin spacing down to an optimum size. First, TBs constitute regions for dislocation storage leading to an isotropic hardening contribution. Also, a TB probably gets more and more impenetrable with deformation due to an increasing incoherency [111,181,182]. Pre-existing twins constitute also a source of back stress, leading to a kinematic contribution to strain hardening. Now, de-twinning is a source of softening with a negative impact on the resistance to plastic localization motion [183].
(4) Deformation twins or so-called TWIP effect [184] is a very strong source of strain hardening if properly mobilized. The introduction of new TBs brings new obstacles to dislocations during the deformation which adds to the other sources of strain hardening mentioned just before associated to TBs present before deformation. This continuous source of new interfaces leads to a continuous increase of the back stress.
(5) A TRIP effect very significantly enhances strain hardening. A TRIP effect acts positively on the resistance to necking only if it occurs sufficiently late to bring the extra hardening at strains approaching the localization condition [185–187]. A too fast or too slow TRIP effect is not interesting, as proved on coarse grain TRIP steels [187]. The explanation is similar to the aforementioned TWIP effect and related to the introduction of new interfaces in the course of deformation (as well as of a new hard phase). Many recent studies devoted to Q&P steels described in Section 2 with very fine grains, see [188–193], have shown that it is possible to significantly improve both the strength and the ductility of UFG steels owing to a TRIP effect [194,195].
(6) Composite effect can also be engineered such as to bring a source of strain hardening, essentially through a back stress contribution that can significantly delay necking. Good examples can be found in the literature. In multi-phased hybrid steels, the austenite plays a predominant role in blocking the slip transfer from the ferrite phase and in increasing the work hardening rate. This largely contributes to the excellent ductility measured in these high strength steels, also found in earlier works on DP-UFG steels [196]. In multilayers, the capacity to generate super threading dislocations which deposit dislocation debris along the interfaces in tri-layers Cu/Nb/Ni show superior strain hardening capacity compared to Cu/Nb [130]. A final sophisticated example is given by nanostructured high strength Mo alloy to which significant ductility was conferred through a hierarchical structure made of submicron grains and nanometric oxide particles [197].
(7) Deforming metals at low temperatures limits the action of recovery mechanisms, maintains the work hardening to higher values and positively contributes to plastic localization (except if the lower temperature significantly decreases the rate sensitivity capacity - see next paragraph)

Increase the rate sensitivity:

The importance of increasing the rate sensitivity has been explained above. The rate sensitivity can be increased by triggering all possible sources of thermally activated mechanisms: dislocation

nucleation dominated plasticity regime or GB mediated deformation all involve the activation of a limited number of atoms to generate a local configuration change with an associated discrete strain events. Now, the balance between the generation of thermally activated mechanisms and the possible lack of strain hardening associated with these mechanisms must be carefully evaluated to find the optimum condition. For NT systems, the problem is simple: NTs not only act positively on strain hardening but also bring enhanced rate sensitivity due to the thermally activated nature of the dislocation/TB reactions [106,108]. But, in other cases, the fact that GB mediated mechanisms can take the lead over intra-granular dislocation activity can generate a drop of n that is not compensated, in terms of ductility, by the increase in m; and, in some circumstances, can possibly lead to softening and dramatic local structural instabilities. These aspects regarding the control of the rate sensitivity will be discussed in more details in Section 5.2 when dealing with thin films, for which there are many data available and where the mechanisms leading to rate sensitive effects are often amplified.

Obviously, many combinations of the different mechanisms discussed above, involving bimodal grain size distribution, NT, TWIP and TRIP effects should cooperate to bring even higher resistance to plastic localization. A good example is given by 316L austenitic stainless steel microstructures produced first by a dynamic plastic deformation under high strain rate (10^2–10^3 s^{-1}) at ambient temperature followed by an annealing at 730–800 °C. The microstructure made of micron size grains, nano-size grains and NT bundles of micron size involves different sources of strain hardening that can operate at different steps of the deformation and probably some amount of rate sensitivity, leading to an excellent strength-ductility balance [198]. The competition between raising m at the expense of n is certainly an important point of analysis that has not been systematically identified for NC systems, and certainly not addressed from the viewpoint of optimizing the strength-ductility compromise. On this topic, it would be interesting to follow ideas similar to the one recently developed for macroscopic metal matrix composites [199]. Another key aspect that has not received systematic attention is the controlled engineering of multiscale micro- and nanostructure with the target of maintaining enough kinematic hardening effects even at large strains. Finally, graded structures, like NC graded Cu, can lead also to excellent strength ductility performances through a capacity of forcing plasticity to be heterogeneous and gradual, which leads to strain delocalization [24]. This process allows deforming, without early failure, the surface outer nano-grains, which then undergo GB migration mechanisms. In addition to strain hardening and rate sensitivity effect, this millimetre scale architecturing leads to a delocalization process which resembles the approach followed in flexible electronics described in Section 4. All these unconventional approaches to increasing ductility suffer from a lack of models to help guide microstructure optimization in problems involving numerous parameters.

3.2. Static damage and fracture in UFG and NC metallic systems

In the review by Kumar et al. [5], it was stated that "... *the damage tolerance of these materials does not meet certain minimum acceptable levels for particular application. Despite such need, very little published information is presently available on the damage tolerance characteristics of NC metals and alloys*". This state of affairs is still true 10 years later. If a much better understanding of the resistance to plastic localization has been attained, as summarized in the former section, studies regarding the damage mechanisms controlling the fracture resistance, under various loading conditions, remain scarce for bulk nanostructured materials. One of the main reasons is probably that the methods used for CG metals, based on classical polishing cross-sections of the deformed samples [200] or more modern X-ray microtomography [1,201,202], are not applicable to NC bulk samples due to the small nature of the damage. Another reason is the limited size of the samples that can be processed in order to perform conventional mechanical tests, such as on notched cylindrical specimens. A lot of progress in the understanding has been made from testing thin metallic films *in situ* and characterizing the damage mechanisms. This will be covered in Section 5.3 but the question of the transfer of these observations obtained on small scale systems to bulk nanostructured metals, although qualitatively valid, might not be always direct.

3.2.1. Single phase

Considering materials with no pre-crack and no marked processing defects, one of the most convincing study of damage evolution in bulk nanostructured metal is the one by Kumar et al. [38] on electro-deposited Ni with grain size around 30 nm, which dates back to 2003, and was already summarized in Ref. [7]. The main conclusion of this work was that the dimple size on the fracture surface was significantly larger that the grain size, in agreement with other results [67,203]. The observed damage process is schematized in Fig. 9 (from [5]). Void nucleation occurs at GB and more preferentially at triple junction, but not necessarily along all GBs. The selected triple junctions that give rise to voids are probably the one that must accommodate the largest GB sliding mismatch from the connected grains. The mechanism of void nucleation at triple junctions associated to GB sliding has been theoretically investigated by Ovid'ko et al. [204] using a GB disclination type configuration. Some voids might also result from pre-existing nano-voids due to hydrogen loading during the process. When a void nucleates, relaxation takes place on neighboring GBs. The voids grow until final impingement with the plastic flow localized in the intervoid ligament, reminiscent of the void coalescence process observed in CG metals, but here at the scale of a single crystalline ligament. The true fracture strain resulting from this mechanism can be quite large as recently shown by Sharon et al. [167] for thick electrodeposited NiFe alloy layers exhibiting 75% area reduction at fracture and clear dimples. These films can be considered as being bulk NC systems as the grain size was around 30 nm involving thus hundreds of grains over the thickness.

This mechanism of failure related to intergranular voids competes with a brittle mode of rupture, either inter- or trans-granular. This cleavage type mechanism is triggered when the local stresses, set by the flow strength, exceeds the fracture stress, see e.g. [205]. Most investigations show that this brittle failure mechanism is intergranular. We will come back in Section 5.3 to these mechanisms, on the competition of failure modes as well as on the issue of modelling damage.

Regarding now the resistance to crack initiation and propagation from a pre-existing crack, ideally one would analyze it in the context of fracture mechanics. The fracture test methods are similar to those used for CG bulk macroscopic samples. However, a wide range of nanostructured materials produced by SPD, electrodeposition or mechanical alloying exhibit relatively small dimensions. The small scale yielding assumption, which requires the plastic zone size to be a very small fraction of the crack length, is often not verified meaning that the concepts of non-linear fracture mechanics theory, such the J integral or the CTOD, δ, must be used. Even with these non-linear concepts, the loss of constraint due to the small dimension of the sample, [1], might be such that the extracted fracture toughness J_{Ic} or δ_c will be specimen-size dependent, which is not sufficiently realized in the literature.

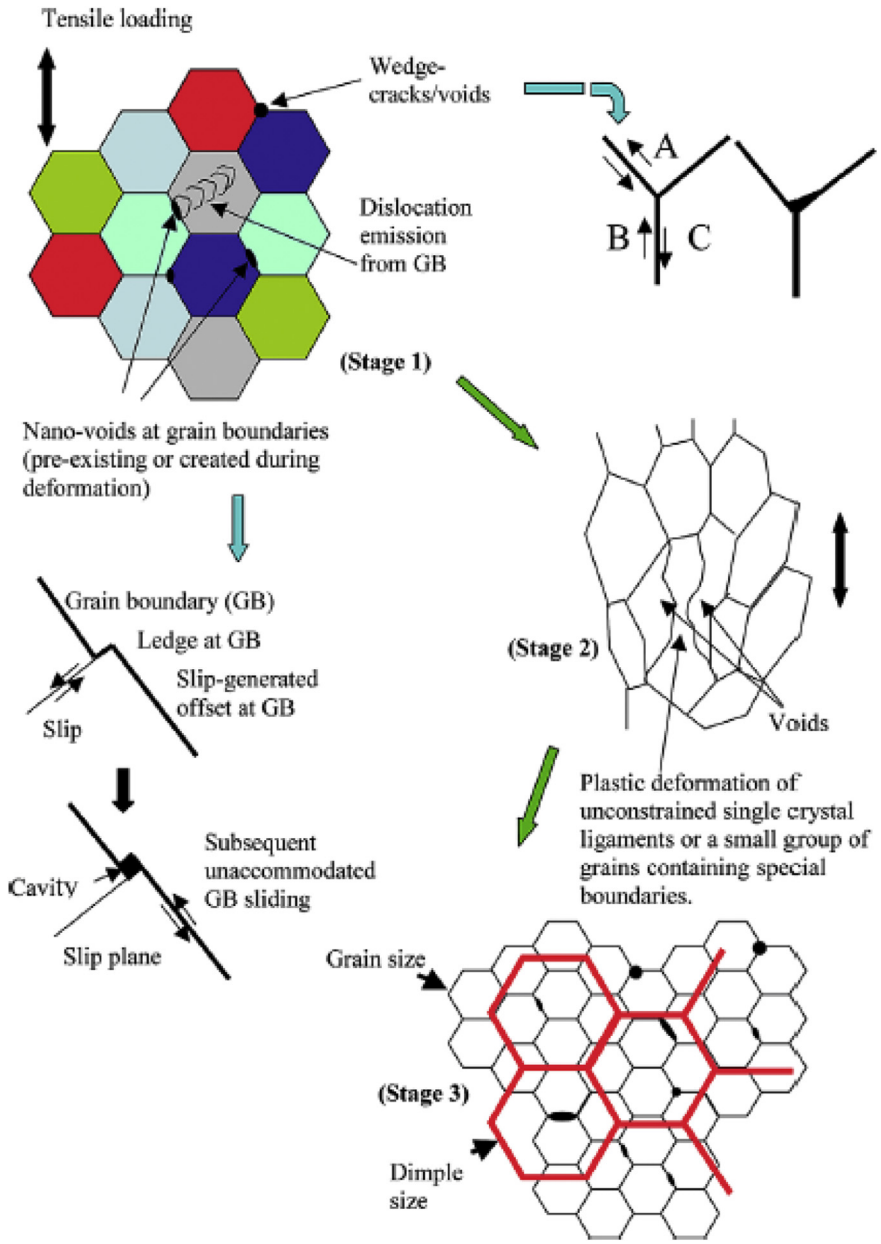

Fig. 9. Schematic illustration of the damage evolution mechanisms in NC bulk metals by void nucleation at GBs and triple junctions and subsequent void growth, indicating that the void spacing has been observed to be significantly larger than the grain size, reproduced from [5].

Furthermore, the plastic zone size can often be larger than the thickness. For instance, Mirshams et al. [208] measured on electro-deposited 20 nm grain size NC Ni foils $K_{Ic} = 120$ and 20 MPa$\sqrt{m}$ for 0.22 and 0.35 mm foils, respectively. These values can hardly be compared to CG Ni ($K_{Ic} = 60$ MPa$\sqrt{m}$) due to the plane stress/plane strain conditions. The fracture toughness depends then on the thickness in a complex way with a regime of toughness increasing with thickness due to crack tip necking effects [206,207], followed by a decrease towards the plane strain regime. Even at the same thickness, we claim that the fracture toughness of two different foil materials cannot necessarily be compared due to the change of regime between plane stress and plane strain occurring at different loads, as a function of the strength of the foil (which affects the plastic zone extension). This issue of thickness dependence will come back in Section 5.3.

Now, there have been a few recent reports of fracture tests performed on the thickest possible SPD samples that can be made, from the group of Pippan, see review [209]. Specimens of Cu, Ni, Fe and pearlitic steels with a diameter of 30 mm and thickness around 7.5 mm have been processed by HPT [210–212]. These authors carefully looked at the validity of the measurements and worked with elasto-plastic fracture mechanics concepts. Their main conclusion is that, even though the failure mechanism is clearly ductile, the critical CTOD δ_c is always relatively small and the higher yield strength does not compensate for attaining J_{Ic} values typical of the CG corresponding materials [210]. Our opinion is that the lower fracture toughness of UFG-NC metals compared to bulk counterparts is not surprizing based on the basic rationale for the mechanisms setting the resistance to ductile tearing, see e.g. [1,213,214]. Indeed, dimensional analysis shows that, see [215] for more details,

$$\frac{J_{Ic}}{\sigma_0 X_0} = F\left(\frac{\sigma_0}{E}, n, f_0, \frac{\sigma_n}{\sigma_0}, \text{other microstructural features}\right) \quad (4)$$

where X_0 is the mean void spacing, E is the Young's modulus, f_0 is the initial void volume fraction (pre-existing voids added to the voids nucleated during deformation), σ_n is an average critical stress for void nucleation and F is a function that typically varies between 1 and 10. The fracture toughness is thus directly proportional to the distance X_0 that separate cavities. Assuming that $\sigma_0 = K_{HP1}/\sqrt{d}$ and that X_0 scales proportional to d, then J_{Ic} should decrease proportional to $\sqrt{d}$ if all other parameters are kept constant. Furthermore, as explained in [1,215], the strain hardening exponent n has a large influence on the function F with F significantly decreasing when n decreases, which is the rule in UFG-NC metals. In addition, due to the large stress levels developing in UFG-NC metals, void nucleation ahead of the crack tip starts at smaller strains. All these aspects go also in the direction of a lower J_{Ic}. Now, the assumption that X_0 scales with grain size is based on the idea that the nucleation sites are located at GBs (e.g. particles sitting on GBs or triple junctions) and that they are all activated. As explained above [38,67,203], the fact that X_0 has been repetitively found to be significantly larger than d, see Fig. 9, is favourable for J_{Ic}, even though not yet fundamentally understood. It is often not sufficiently realized that, if the nucleation results from second phase particles, coarser particles are, at constant volume fraction of nucleation sites, preferable because it allows for larger fracture process zones to develop (larger X_0) hence larger energy spent per unit area. Another point is that Eq. (4) applies to metals exhibiting rate independent conventional plasticity. To what extent rate sensitivity can impact the magnitude of F remains to be systematically investigated. Finally, if the voids are in the submicron range, the void growth rate can be much smaller than with micron sizes and this could also lead to an increase of F. We will come back to this final question in Section 5.3.

In terms of mechanisms, atomistic simulations of crack propagation in Ni with ~10 nm grain sizes [216,217] have also demonstrated that fracture is intergranular as a result of the coalescence of voids nucleated along well oriented grain boundaries, in agreement with the mechanisms discussed for un-cracked specimens. MD simulations by Xu and Demkowicz [218] have recently demonstrated that migrating GBs tend, on average, to heal nano-cracks by decreasing the local stress intensity factor, hence providing an interesting toughening mechanism that remains to be demonstrated experimentally. The competition between a brittle and ductile mode of cracking has been addressed in a series of theoretical analyses by Ovid'ko and Sheinerman, e.g. [219,220].

3.2.2. Multiphase/hybrids/nanotwinned bulk metals

The effect of twin density on the crack initiation fracture toughness of NT Cu has been investigated by Qin et al. [221] and by Singh et al. [222]. The fracture toughness values determined on 40 μm thick specimens were found to be larger in high density NT Cu (17.2 MPa $m^{1/2}$) than in lower density NT Cu (14.8 MPa $m^{1/2}$). However, these results obtained on thin specimens which do not satisfy the plane strain conditions cannot be considered as true indicators of an intrinsic fracture toughness.

The beneficial effect of “dual-phase” microstructures (here: matrix + twins) on the ductility and fracture toughness seems to be a general property. This has been illustrated by some recent work on Zr [223]. An excellent combination of yield strength (~600 MPa) and fracture toughness (~120 MPa $m^{1/2}$) was obtained on thin (~0.5 mm) cryo-rolled ($\varepsilon \sim 2.87$) sheets of Zr which were subsequently annealed at 450 °C for 1 h. This thermo-mechanical heat-treatment produced a nanostructure composed of ~22% nano-scale sub-grains and grains (<100 nm), 55% UFGs (100 nm-1 μm) and 23% CGs (>1 μm) embedded in a nano-scale and UFG matrix. The fracture surface of the tested specimens was covered with ductile dimples with a size much larger than the size of the nanograins, as already observed in single phase materials. The formation of these deep dimples requires large deformations which contribute to the increase of the dissipated energy at fracture.

Nanostructures have been recently produced from real multiphase materials, such as bainitic steels by Haddad et al. [224]. These authors modified from ferritic-pearlitic to an UFG bainitic the initial microstructure of a 0.45% C steel using HPT (5 rotations under 6 GPa pressure) at 350 °C. A unique NC microstructure consisting of equiaxed and elongated ferrite grains with a mean size < 150 nm was generated. *In situ* tensile tests in a SEM showed very high tensile strength of the order of 2100 MPa with a total elongation of 4.5%. These characteristics are comparable to those obtained on high strength, high alloyed steels [225]. The failure consists in the initiation of small localization bands at the edges of the specimens before any observable diffuse necking. These small localization bands give rise to micro-cracks that propagate from the edges through the entire specimen. The mechanism is fully ductile with submicron dimples involving two classes of sizes.

UFG DP steels consisting of austenite (fcc) along martensite (bcc) laths is one of the best illustration of the interest of nanostructures. The thin films of the fcc phase have two beneficial effects: (i) they can act as cleavage crack arrestors when the material is tested at sufficiently low temperature below the DBTT, (ii) they strongly modify the conditions of slip transfer at the interface. Recent studies by Mine [124] and Maresca and Geers [28] have started to throw some light on the relative role of each effect.

It can be added that the ballistic fracture performances of NC and NT stainless steels have also been studied using gas gun firing of projectiles on 2 mm thick sheets [226]. The comparison with CG counterparts shows lower energy absorption and lower ballistic limit related to a shear plugging mechanism. Cu/Nb has also been studied under ballistic conditions [227] showing a ductile damage mechanism by void nucleation and growth in the middle of the Cu layers and not by interface decohesion. Nevertheless, at low deformation rates the few studies reporting fracture data on Cu/Nb show only limited ductility around 3% due to the limited strain hardening capacity [228]. In [22], ductility near 10% was attained for samples rolled multiple times and with a low fraction of Nb. The ductility of Cu/Ni/Nb trilayer based systems [133] is expected to be higher owing to the increased strain hardening capacity as mentioned in Section 2.

The graded NC material [24] already mentioned in Section 3.1 for its extremely good capacity to delay necking, also exhibits remarkable post necking elongation with fracture strains over 100%. Quite surprisingly, damage nucleates first in the highly deformed CG areas. A bimodal grain distribution is also effective in retarding damage propagation with coarse grains playing the role of ductile patches that can bridge the cracks originating from the more brittle nanostructured areas [32]. This proves that a ductile core interacting with hard NC regions, either in terms of gradient or bimodal structures leads to synergetic effects on the damage and crack shielding. Other sorts of synergetic effects that can retard cracking or make it non-percolating will be addressed in Section 4.

3.3. Fatigue in NC and UFG metallic systems

The cyclic behavior of NC and UFG metals is examined in a first sub-section before considering the fatigue life. Since NC metals are usually not available as readily in bulk form suitable for conventional fatigue tests as the UFG materials, most of the studies to date have been performed on UFG materials prepared by various SPD

methods (see Section 2.1). UFG Cu and Ni have been investigated in more detail than other metals. Some of the results obtained so far apply also to NC materials.

3.3.1. Cyclic behavior of NC and UFG metals

The cyclic deformation and fatigue properties of UFG metals and alloys have been reviewed in some detail by Mughrabi [229], Mughrabi and Höppel [230] and more recently by Höppel and Göken [231], Kunz [232], and Padilla and Boyce [233], see also [234–236]. From these reviews, it arises that the cyclic and fatigue behavior strongly depend on parameters of the SPD procedure, on the purity of the material and on the type of fatigue loading. This is the reason why special care must be taken when comparing results from various sources. All these studies have shown that UFG materials exhibit, as already mentioned in Section 2.2, significant Bauschinger effect as compared to conventional polycrystals, see e.g. Fig. 10a and b for Cu taken from [237] and from [238]. A Bauschinger parameter β_E can be defined as

$$\beta_E = \frac{2\sigma_p \Delta\varepsilon_p - \int \sigma d\varepsilon}{\int \sigma d\varepsilon} \tag{5}$$

where σ_p is the maximum tensile stress in the loop of width $\Delta\varepsilon_p$. In Fig. 10a, two tests were run on as prepared material (1 and 2). The Bauschinger effect is much larger in specimens 1 and 2 when compared to two other specimens annealed at 473 K (3) and 773 K (4). This behavior is also observed in NT Cu, see Fig. 10b. The Bauschinger effect is due to the presence of intense internal stresses which are directly related to the microstructure. A simple calculation by Mughrabi and Höppel [230] showed that the stabilized dislocation cell size in polycrystalline metals at the stress saturation stage (or at mid-life) was larger than the grain size of UFG metals. The dislocations thus move inside the small grains without the formation of cells, as illustrated in Fig. 11 [239], and GBs directly participate to the mechanical response of these UFG materials. A strong grain size effect on the cyclic behavior is observed contrarily to CG counterparts where the cyclic behavior is almost independent of grain size: the cyclic stress response of UFG metals exhibits a grain-size dependence of a form similar to the Hall-Petch relationship, as found for instance in Ni by Mughrabi [229].

UFG metals exhibit more or less severe cyclic softening in particular when tested under strain controlled conditions, corresponding to the low cycle fatigue (LCF) regime, see Fig 12 for the definitions of the two regimes and the relative position of CG and UFG metals, whereas there is almost no cyclic softening in stress - controlled tests corresponding to HCF conditions for which the plastic deformation is extremely small.

Evidences showing that SPD metals are intrinsically unstable

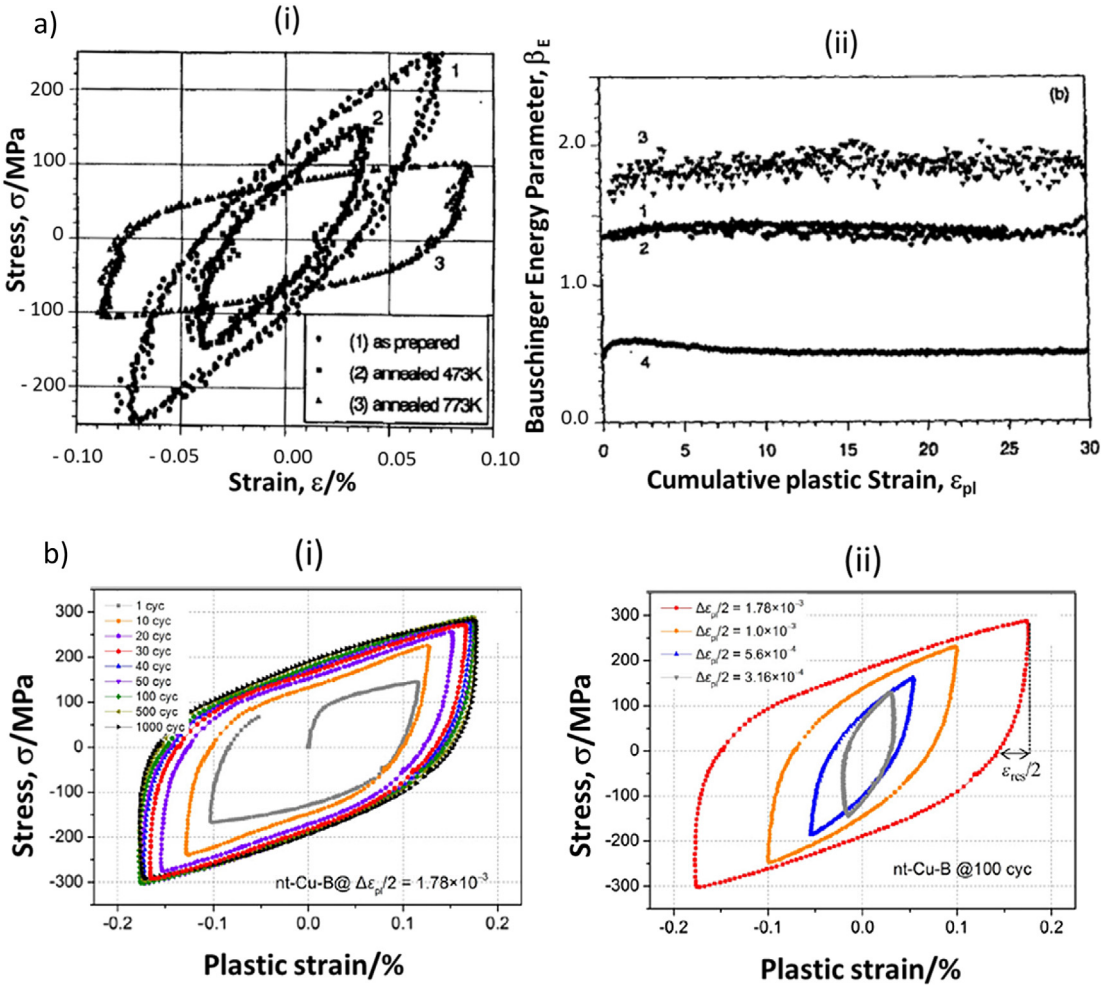

Fig. 10. (a) UFG copper in the as-prepared and after heat treatment; (i) hysteresis loops in the stabilized stage (cumulative plastic strain = 500%); (ii) Bauschinger energy parameter as a function of cumulative plastic strain [237]; (b) UFG nano-twinned copper; (i) Hysteresis loops under strain-controlled pull-push conditions with $\Delta\varepsilon_p/2 = 1.78 \times 10^{-3}$; (ii) Changes of steady-state hysteresis loops of NT-Cu fatigued at different constant plastic strain amplitudes [238].

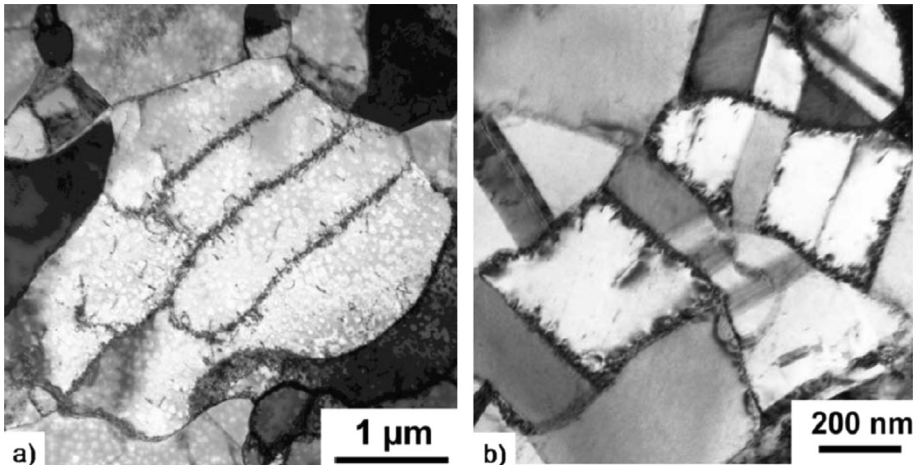

Fig. 11. TEM micrographs of dislocation microstructure in fatigued nickel specimens of different grain sizes; (a) Dislocation substructure inside the grains of a specimen with larger grain size; (b) Lack of fatigue-induced dislocation structure inside the grains in specimen with very small grains. Original micrographs by Klemm [239], after Mughrabi [229].

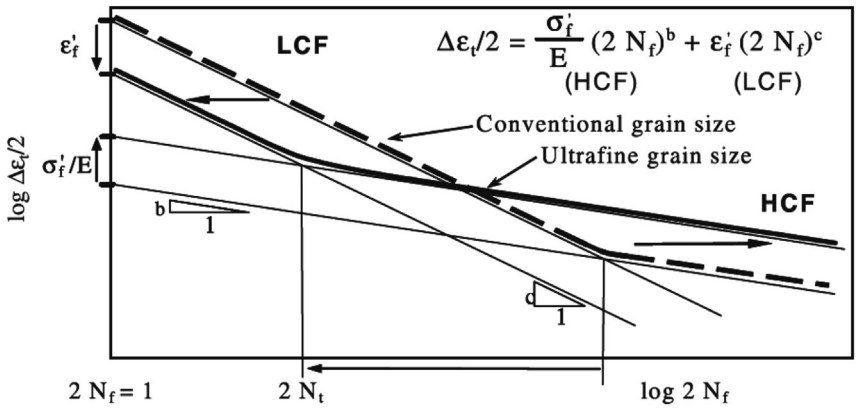

Fig. 12. Illustration of fatigue lives of strong UFG and more ductile and softer CG materials in a total fatigue life diagram (After Mughrabi [229]).

upon cyclic conditions do exist. This instability associated with a more or less pronounced softening effect may also be related to the formation of macroscopic shear bands extending over distances much larger than the grain size. Since UFG materials produced by SPD are heavily pre-deformed, the occurrence of microstructural instabilities which lead to grain coarsening and shear banding is not too surprising. Fatigue cracks are initiated from these shear bands (see e.g. [112]). In the case of UFG copper, it should be noted that grain coarsening was observed at room temperature (RT), i.e. at a homologous temperature as low as 0.2 T_m (where T_m is the melting temperature) after mild cyclic strain-controlled deformation conditions ($2 \times 10^{-4} < \Delta\varepsilon_p/2 < 1.0 \times 10^{-3}$) and was attributed to dynamic recrystallization [240]. In spite of this softening effect, the stabilized cyclic stress in strain-controlled tests (most often measured at mid-life) is about 2 or 4 times larger than in similar tests on CG Cu.

3.3.2. Fatigue life of some NC and UFG metals

The fatigue life of UFG metals is generally much larger than that in CG counterparts when a Wöhler representation is terms of stress is adopted (see e.g. Fig. 13 for Ti [236]). The opposite is often observed in the LCF regime as schematically represented in Fig. 12. This conclusion applies to various materials including NC Cu which has been investigated in particular by the Brno group, see [232]. The fatigue response of electro-deposited NC Ni and cryo-milled UFG Al-Mg alloy has been studied by Hanlon et al. [241,242]. The stress life fatigue behavior and fatigue crack growth characteristics of pure Ni were studied as a function of grain size, spanning a wide range from tens of nm to tens of μm. It was found that grain refinement in the true NC regime generally leads to a significant increase in total life under stress controlled fatigue conditions (see Fig. 14a for Ni [242]).

The studies discussed above relate mainly to basic investigations

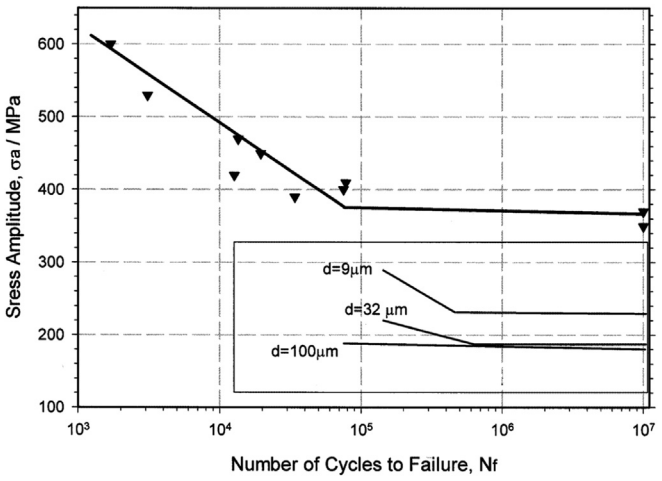

Fig. 13. Wöhler plot of fatigue lives of UFG titanium and comparison with titanium involving conventional grain size. (After Vinogradov et al. [236]).

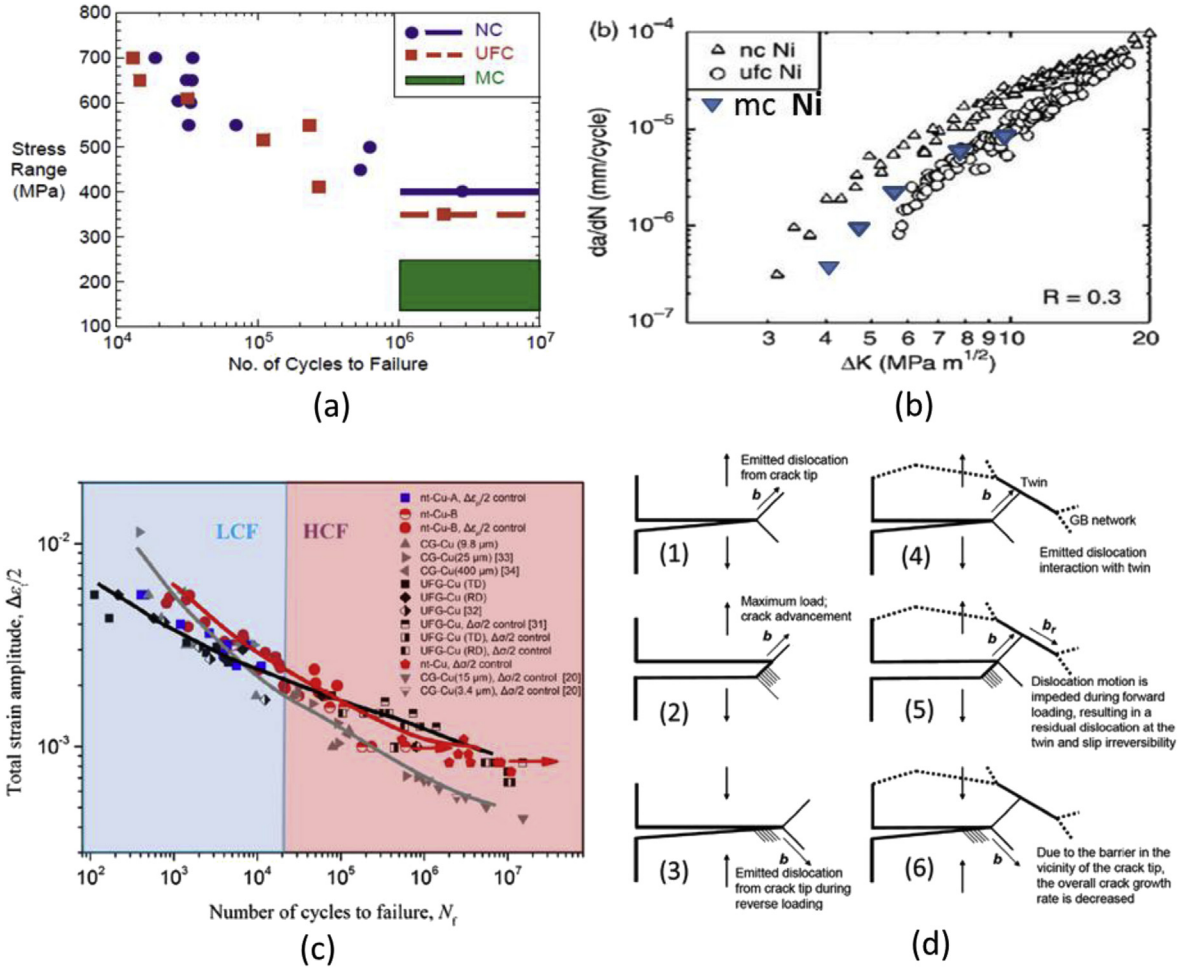

Fig. 14. Effect of grain size from the micro to the nano-regime in pure Ni; (a) Cyclic stress versus number of cycles to failure; (b) Fatigue crack growth rate as a function of ΔK (taken from [242]); (c) Fatigue lives of NT-, CG- and UFG-Cu samples in a total strain amplitude-fatigue life diagram showing that superior fatigue performances in both LCF and HCF regimes are obtained in NT-Cu [238]; (d) Interaction between dislocations emitted from a fatigue crack tip and mechanical twins. See text for the comments. Taken from Sangid et al. [250–252].

on simple pure metals. Attention has been recently focused also on structural alloys, in particular UFG Al, Ti and Mg alloys and on NT metals. In an Al-Mg alloy, the microstructural stability was enhanced by increasing the Mg content and the number of ECAP passes. In all cases, the total strain fatigue life curves of UFG and CG Al-Mg alloys intersected as expected from Fig. 12 (for more details, see Mughrabi [229]). Earlier works dealt with the fatigue of UFG Ti [236] as indicated previously. More recent work has been devoted to the alloy Ti-6Al-4V ELI (extra low interstitial) [234] exhibiting strong improvement of the fatigue properties by grain refinement. On the other hand, and as expected, the Coffin-Manson plot of the NC material shows shorter fatigue lives than the CG counterpart.

It should be noted that there is almost no data on the fatigue lives over a large range from LCF to HCF of UFG steels. The work by Furuya et al. [243] on carbon steels showed that the fatigue strength of the UFG ferrite-cementite steel matched that of the tempered martensite steel, see Fig. 3 in [243].

NT metals require special attention. Very recently Pan and Lu [41] have conducted strain-controlled fatigue tests on NC Cu with NT oriented parallel to the free surface. Their results are reproduced in Fig. 14c where the comparison with results obtained under various conditions and on various materials, including UFG and CG Cu, clearly shows that NT Cu exhibits superior fatigue performance in both the LCF and HCF regimes. The effect of deformation twins on the fatigue life of NC materials is not yet completely clarified (This is not surprising since this effect in CG materials is still largely debated). In CG fcc materials, the presence of twins and their influence on fatigue crack initiation and crack growth has been addressed by a number of authors, see e.g. [244–246]. The mechanisms of formation of deformation, annealing and growth twins in fcc metals and alloys is still largely discussed [99,247,248]. The correlation between sites of strain localization and twin boundaries (TB) during cyclic loading has been made by a number of investigators; see in particular Man et al. [249] for 316 stainless steel and Sangid et al. [250–252] and Castellucio and Mc Dowell [253] in a Ni base superalloy. To date, only a small number of attempts have been made to model the effect of TBs on fatigue crack nucleation, with a few notable exceptions [250–253]. In the model developed by these authors, the presence of twins was found to be detrimental to fatigue life in comparison with microstructures without twins. We are still very far from a full understanding of the influence of existing and deformation twins in NT metals on their fatigue life.

A limited number of observations suggest that the fatigue life of NC metals can be improved with a bimodal grain size distribution. This has been shown in a recent work by Fintova and Kunz [254] on an UFG AZ91 Mg alloy. The microstructure consisted of very fine grained areas involving a higher density of second phase particles $Mg_{17}Al_{12}$ coexisting with areas exhibiting somewhat larger grains

and lower density of second phase particles. The fatigue cracks initiating in areas of larger grains were related to the cyclic slip bands. This initiation mechanism is similar to the one observed in cast alloy. The second initiation mechanism is related to GB cracking which takes place predominantly in the fine grained areas.

3.3.3. Fatigue life modelling of single-phase UFG materials

Modelling fatigue life of metals is the topic of overview II [2]. The complexity and the extremely small scale of UFG materials constitute real challenges for modelling the fatigue behavior.

Based on the present-day state of knowledge, local grain coarsening and, more specifically shear banding over distances much larger than the grain size plays an important role in the fatigue crack initiation of UFG metals. In Cu, the slip bands, their shape and mean features resemble the slip bands formed in CG Cu. As stated by Kunz [232] "*The role of the coarsened structure in the crack initiation process and the specific mechanism of initiation are not sufficiently understood. Contrary to the CG Cu, where the specific dislocation structures associated with cyclic slip bands are described thoroughly, there are no similar and conclusive observations on UFG Cu*". The fatigue initiation mechanism of UFG Cu might be dominated by the voids formed by grain boundary sliding, which leaves wedges at triple junctions of GBs, as observed in NC Ni under tensile loading conditions [38].

It is worth mentioning the life prediction model developed by Mughrabi and Höppel mainly based on crack propagation for UFC metals [230] in terms of the following Manson-Coffin relationship

$$\frac{\Delta\varepsilon_p}{2} = \left[\frac{192C^2}{\lambda\pi^2F^2}\left(\frac{n'}{n'+1}\right)\left(\frac{R_{pUFG}}{K'}\right)\ln\left(\frac{a_f}{a_i}\right)\right]^{\frac{1}{3n'+1}}(2N_f)^{-\frac{1}{3n'+1}} \quad (6)$$

where R_{pUFG} is the cyclic yield strength, λ (taken as 0.05) is a cyclic plastic zone correction factor, the numerical factors $F = R_{pUFG}/R_p$ and C take into account the grain boundary strengthening and the plastic constraint caused by the grain boundaries, respectively. The initial fatigue crack length, a_i, which is, to some extent, an adjustable parameter, is taken as equal to the grain size and a value of 2 mm is assumed for the final crack length a_c. The choice of the exact value for the final crack size is not critical in these calculations because of the strong non-linearity of the crack growth law. Using the cyclic stress strain curve expressed as

$$\frac{\Delta\sigma_s}{2} = K'\left(\frac{\Delta\varepsilon_p}{2}\right)^{n'}, \quad (7)$$

the fatigue life can alternatively be expressed in the form of the Basquin relationship in a stress representation.

3.3.4. Fatigue crack growth in UFG, NC and NT metals

A number of studies have been conducted on the fatigue properties of NC metals, in particular Cu, but up to now very limited data on the Fatigue Crack Growth Rate (FCGR) behavior of these materials are available. This is mainly due to the difficulty in obtaining large bulk volumes of material to be machined in standard specimens for crack propagation tests. We start this review by examining the FCGR behavior of various materials with emphasis on the Cu system and then we will concentrate on NT metals.

Experimental FCGR curves for the UFG Cu can be found in the literature [255–257]. These studies show that UFG metals exhibit the same crack propagation behavior as conventional polycrystals, i.e. a threshold regime at low crack growth rate (~10^{-7} mm/cycle), an intermediate stable growth regime well described by the Paris-Erdogan "law", and an unstable regime at high FCGR. In UFG Ni the growth in the threshold is higher than in CG counterpart, as shown in Fig. 14b [241,242,258]. A similar behavior was noted in Cu. However, Collini [259,260] found that the threshold in UFG Cu was higher than in the CG counterpart, (see Table 3 in [259]). These differences are likely due to the procedures used to prepare the UFG materials. The threshold behavior has been attributed to the crack path which generates a larger fracture surface roughness and favours crack closure when the grain size is enlarged. However, there are a few exceptions to this rule. NC Ni-Co alloys show superior resistance to fatigue crack growth [261]. The addition of Co to Ni increases the strength of the material by refining the grain size and by reducing the SFE, thereby increasing the prevalence of mechanical twinning.

UFG Cu produced by SPD typically exhibits a grain size of about 300 nm. This is comparable to the smallest cells observed at the tip of a fatigue crack propagating at $K \sim 10$ MPa $m^{1/2}$ in a polycrystal [262]. From this point of view the crack propagation resistance of UFG and CG copper in this intermediate regime of crack growth should be similar. This is what is indeed observed within a first approximation. Strong differences, however, can be expected in the threshold region. Here, the stability of the UFG microstructure would play a decisive role. Horsky et al. [257] studied the crack propagation in UFG Cu prepared by high pressure torsion. They observed very extensive grain coarsening in the vicinity of the fatigue cracks in high purity Cu. Moreover they noted also a retardation of the crack growth. This clearly indicates that the stability of the microstructure of UFG metals plays a key role in affecting the FCGR behavior when the GBs are not strongly pinned by impurities or particles.

Only a few studies have been devoted to steels as indicated previously. However, the study by Kim et al. [263] on UFG low C steel should be mentioned. The FCG resistance and ΔK_{th} of the UFG steel was slightly lower than in the as-received coarse grained conditions. This behavior was attributed to a less tortuous crack path and a reduced crack closure effect. Chapetti et al. [264] have shown that in a carbon steel (0.15 C, 1.80 Mn, wt%) the fatigue threshold ΔK_{th} was a decreasing function of grain size, in the range between 1 μm and 60 μm. Similarly, Niendorf et al. [265] have shown that the FCGR in an IF (interstitial free) steel were higher in the threshold regime as compared to conventional CG steels.

The fatigue response of electro-deposited NC Ni and cryo-milled UFG Mg alloys has been studied by Hanlon et al. [241,242]. The stress life behavior and FCGR characteristics of pure Ni have also been characterized as a function of grain size [242]. Yan et al. [258] investigated the FCGR in Ni micro-beams.

Al alloys have been investigated in more detail. The behavior of Al alloys (pure Al, Al-Mg, Al-Mg-Sc, Al-Mg-Sc-Zr) and Ti alloys (pure Ti and Ti-6Al-4V) has been reported by Estrin and Vinagradov [266]. Avtokratova et al. [267] have also compared the FCG behavior of a UFG Al-6% Mg-0.3% Sc alloy with that of a polycrystalline material. All these studies show that, as a general rule, the FCGR of UFG metals and alloys is higher than in CG metal only in the threshold regime. In the intermediate regime in which the Paris-Erdogan "law" applies, the effect of grain size is very much reduced.

The determination of the fatigue threshold in NC and NT metals is challenging, as indicated previously. Recently, a model has been proposed by Chowdhury et al. [121,268] to evaluate this parameter in the presence of NT for Cu, Ni, and Al. Their model utilizes the concept of irreversibility of the glide of dislocations emitted from the crack tip. Predicted ΔK_{th} for relatively short cracks is found to be enhanced by a refinement in twin lamellar thickness and twin spacing, as observed experimentally.

The fatigue crack growth behavior of NC metals can be qualitatively explained by considering the plastic zone size, r_p, under plane stress condition compared to grain size. The reverse plastic zone size is given by [269]:

$$r_p \sim \pi/10\,(\Delta K/\sigma_0)^2 \tag{8}$$

where ΔK is the stress intensity factor range. In UFG/NC metals, r_p is much larger than the grain size. This allows for the simultaneous formation of slip bands in several grains, thereby resulting in a macroscopically flat fracture surface. Assuming that the crack growth per cycle is proportional to the change in crack tip opening displacement $\Delta\delta$, which is a model valid for the intermediate FCGR regime, the Paris relationship can be expressed as:

$$da/dN \sim \Delta\delta = \Delta K^2 \Big/ 4\sigma_0 E. \tag{9}$$

Higher yield stress due to grain size reduction causes smaller $\Delta\delta$ under the same stress intensity factor conditions. This should in turn lead to an increase of the resistance to crack growth in NC and UFG materials. Even though it is difficult to quantitatively evaluate all factors mentioned previously, the beneficial effect of the reduction in $\Delta\delta$ due to a higher yield strength seems to be comparable to the detrimental effect of a less tortuous crack path and a large plastic zone size compared to grain size on the FCGR of UFG materials like Cu, Al, Ti and steel.

The role of mechanical twins on crack propagation has been investigated by several authors, in particular by Sangid et al. [250–252,261] in their study on the FCG behavior of NC Ni-Co alloys, and Kamaya [244], Blochwitz [245], Dunne [246], Christian [99], Gray [247], Man et al. [249]. The mechanisms proposed by Sangid et al. [261] to explain the beneficial role of mechanical twins on the FCG are schematically depicted in Fig 14d. This figure shows the emission of dislocations from the crack tip during the loading of the material. These dislocations interact with a twin present in the near crack tip region and the motion of these dislocations is impeded during forward loading resulting in residual dislocations incorporated within the TB producing either a thickening of the twin or a de-twinning effect (Fig 14d4 and d5). A recent review about these dislocation-twin reactions can be found in Sangid et al. [261] and in Pineau [113]. Fig 14d6 illustrates the situation which can take place during the reverse loading where dislocations are also emitted but contrarily to Fig 14d3 the crack tip does not advance during the half cycle. These mechanisms are still speculative and much more detailed observations are necessary to better understand the interaction between a propagating crack and a mechanical twin.

3.3.5. Fatigue modelling of hybrid UFG metals and alloys

The data on FCGR measurements on hybrid UFG metals are still very limited. The presence of a second phase adds another important parameter. In this section an attempt is made to use experimental and theoretical results on macroscopically heterogeneous materials to throw some light on the fatigue behavior of microscopically hybrid UFG metals and alloys. In DP alloys the difference in strength of the two materials may strongly affect the local driving force for propagating fatigue cracks as in macroscopically heterogeneous materials.

The mismatch effect is particularly important in welded joints, see e.g. [270,271] and is similar to the situation met with UFG DP steels. This effect is related to the difference in strength between the base and weld metals or in the UFG DP steels between α and Γ phase. Undermatching corresponds to the situation where the strength of the first metal, σ_{01}, is lower than that of the second material, σ_{02}, while overmatching corresponds to the opposite. A crack located in the GB separating the two materials undergoes asymmetrical crack opening. For instance the overmatching effect produces an elevation of the local stress which promotes fracture initiation at a lower crack tip opening displacement, CTOD, level than in homogeneous material.

Fracture perpendicular to the interface of elastic-plastic bi-materials has been studied by a number of researchers; see e.g. [272–274]. The local approach to fracture [1] has been applied to this situation in the presence of cleavage fracture [275]. It has been shown that this bi-material situation can be beneficial or detrimental, depending on the applied load (quantified by J integral).

These developments were made for two semi-infinite media. Multi-layered structures have been recently studied, in particular by Kolednik and his coworkers [276]. Their theory allows in essentially elastic materials to account for the geometry and the difference in Young's modulus (and yield strength to some extent) of the two materials forming a layered microstructure with a crack perpendicular to the interface and the crack tip located in one of the two materials. Kolednik has applied his theory to the experimental results on duplex specimens published by Pippan et al. [277]. These authors have investigated the behavior of a fatigue crack located in the soft material (Armco iron) and hitting the interface with a much harder material (SAE 4340 steel overmatching). They have also studied the undermatching situation. It was shown that in overmatching situation, the crack decelerates when approaching the interface and eventually arrests before reinitiating in the hard material. The Kolednik's theoretical results could explain the observed behavior showing that the stress intensity factor reaches a minimum value right at the interface.

All the above approaches remain too macroscopic to be applied to NC materials. They do not include a number of details, such as the crystallography, the orientation relationship between both phases, the slip systems of each phase. All these details are known to play a key role in the deformation and fracture mechanisms of DP materials. However, it is worth mentioning the recent works in Ref. [124,28]. Mine and his co-workers [124] performed mechanical tensile tests on extremely small specimens with a gage length of about 50 μm. They investigated the different components of the lath martensite which possesses a hierarchical structure (former Γ grains, packets, blocks, lath, and dislocation cells) with pronounced crystallographic aspects involving the 24 variants associated with the martensitic transformation. These microstructures have been simulated recently using a polycrystalline model [28] with fine austenite laths along the martensite laths. These authors have shown that the presence of even a small volume fraction of inter-lath retained austenite (5%) strongly affects the tensile behavior of the material. The presence of inter-lath retained austenite can be a plausible explanation for the observed large ductility of these bcc-fcc mixtures. These results must be considered as preliminary and further work along the lines followed in Ref. [28] should be pursued to understand in much better detail and at a much smaller scale the behavior of these UFG DP materials with the emphasis laid on cyclic loading.

To sum up, UFG and NC materials exhibit an improved resistance to crack initiation as compared to CG metals. Their fatigue strength at 10^6–10^8 cycles can be largely improved provided that the UFG microstructure remains stable. This depends both on the material, i.e. the details of microstructure related to processing and also on the type of cyclic loading. These results must be kept in mind for future possible applications.

3.3.6. Guidelines for improving the fatigue properties of UFG and NC metals and alloys

There are several strategies for improving the fatigue properties of UFG materials, as suggested by Höppel and Göken [231]. Some of them can be listed as follows:

(1) Increasing the ductility of UFG/NC metals to improve the fatigue properties, especially in the LCF regime. The ductility can be enhanced by an appropriate heat treatment applied after SPD processing. This returns to the discussions made in Sections 3.1 and 3.2.
(2) Introducing a bimodal grain structure where larger grains of a few μm are embedded in a matrix of ultrafine grains. Bimodal grains structure has been shown to improve the fatigue properties of a magnesium alloy [254] tested in the LCF regime. This bimodal structure should also lead to an increase of the threshold stress intensity in FCGR measurements. In conclusion, bimodal structures if properly designed are beneficial to the resistance to plastic localization, to static cracking and to fatigue.
(3) Varying the grain size as the limiting factor for the slip length of dislocations. The grain size can be adjusted either by a post SPD heat treatment or by selecting appropriate SPD processing conditions.
(4) The fatigue limit, which is the most important quantity for the design of engineering components subject to fatigue loading, is significantly higher in NC and UFG metals and alloys. Thus UFG/NC metals exhibit a very high potential for successful use in engineering applications in which high fatigue strength is required.

4. Fracture and fatigue of thin metallic films on substrate

This section deals with the fracture and fatigue of thin metallic films on substrates as a natural transition from 3D bulk NC systems to freestanding 2D and 1D systems. Even though the substrate can be made of any materials, and there are indeed examples of metallic coatings on all families of materials, the focus here is on soft substrates only. Indeed, in that case, the mechanics of the deformation of the coating on the substrate differs from both 3D bulk and 2D freestanding systems. These systems are also essential in the context of flexible electronic devices for a wide range of applications involving paper-like displays [278], electronic sensitive skin [279], electronic eyes [280], implantable neurostimulation electrodes [281], dielectric elastomeric actuators [282], stretchable organic cells [283] or electrodes [284]. For all these applications, thin metallic or semi-conductor films constitute the electric circuit. The capacity to support large stretching and twisting distortions without cracking is essential to preserve electrical conduction. The progress in this field has been tremendous over the last few years, see several reviews [285–287] and one key aspect concerns the resistance to failure of the metallic films or lines.

We start by briefly reviewing the experimental testing methods and basics about the fracture mechanics of thin coatings specialized to the case of soft substrates. Then, we address the question of the specific failure scenarios in thin metallic coatings by static damage and fracture or by fatigue. Note also that the intrinsic physical failure mechanisms in the films will be discussed in details in the next Section 5 when dealing with freestanding systems.

4.1. Fracture and fatigue testing of metallic coatings on soft substrates

Testing the fracture and fatigue resistance of metallic films on a polymer substrate seems rather straightforward as it relies on classical macroscopic mechanical test machines. Nevertheless, if the overall strain in the film can be easily accessed using classical extensometry, it is more difficult to accurately extract the precise magnitude of the stress. One option is to perform independent tests on the polymer substrate, measure the load displacement response and finally subtract from the total load of the bilayer the load supported by the polymer only. If the substrate is an elastomer, the ratio of the elastic modulus of the film over the elastic modulus of the substrate E_f/E_s will be ~10^5 which makes this approach feasible even for very thin films; but, if the substrate is a thermoplastic, the ratio drops down to ~30–100 making this approach inaccurate for typical substrate thickness (~100 μm). Furthermore, the initial internal stress must be known as a reference point. Another approach is to use *in situ* X-ray diffraction (XRD) to extract the stress as well as additional information on the plastic deformation mechanisms. A powerful approach relies on *in situ* synchrotron XRD as in Lohmiller et al. [288] for Pd, Gruber et al. [289] for Cu or Frank et al. [290] for Ta films. All the films mentioned in these examples were deposited on a polyimide substrate, which is a thermoplastic with Young's modulus around 2 GPa.

If the interest, as here, is on looking at fracture, the occurrence of the first cracks must be determined and the complete cracking or percolation of the cracks must be characterized. This is typically done by *in situ* tests under an optical microscope, e.g. [291], in a SEM, e.g. [292], or under an AFM tip [293]. Finally, the stretchability can be directly characterized by the performance which ultimately matters in the application, i.e. the evolution of the electrical resistance with deformation, see [294]. An example of a typical test set up is shown in Fig. 15a involving both optical microscopy and electrical measurements during the test, from [295]. Other methods than uniaxial tension can provide information such as torsion of wires [281], bulge tests, and scratch tests of metallic films on flexible substrates [296]. Note that one extra aspect complicates the mechanical analysis of such tensile tests when performed at large strains. The fact that during plastic deformation the metallic film contracts laterally more than the polymer substrate due to an effective Poisson ratio equal to 0.5 for the metallic film during plastic deformation, generates transverse tensile stresses in the film. The stress state is thus never perfect uniaxial tension.

4.2. Basics of fracture mechanics of thin coatings

The application of fracture mechanics to thin coatings has been developed in the late 80's, early 90's and comprehensively covered in several review papers [297–299]. We limit the scope here to the problem of channel cracks with a specific focus on the case where the substrate is much softer than the film. Consider a crack of length a much larger than the coating thickness h under stress σ resulting from the internal stress and/or additional load due to the externally imposed deformation. The film and the substrate are assumed isotropic linear elastic. The crack propagates when the energy release rate, G, exceeds a critical value characteristic of the film material, G_c. The energy release rate can be expressed as [298].

$$G = Z(\alpha,\beta)\frac{\sigma^2 h}{E_f^*} \text{ with } E_f^* = \frac{E_f}{1-\nu_f^2} \tag{10}$$

where E_f and ν_f are the Young's modulus and Poisson ratio of the film, respectively, and E^* refers to the "plane strain" modulus. The non-dimensional coefficient Z is a function of the elastic mismatch between the coating and the substrate through the Dundurs' coefficients defined as

$$\alpha = \frac{E_f^* - E_s^*}{E_f^* + E_s^*} \text{ and } \beta = \frac{\mu_f(1-2\nu_s) - \mu_s(1-2\nu_f)}{2\mu_f(1-\nu_s) + 2\mu_s(1-\nu_f)} \tag{11}$$

where E_s and ν_s are the Young's modulus and Poisson ratio of the substrate, respectively; μ is the shear modulus. As shown in Ref. [300], the influence of β on Z is negligible for $\alpha > 0$. But Z

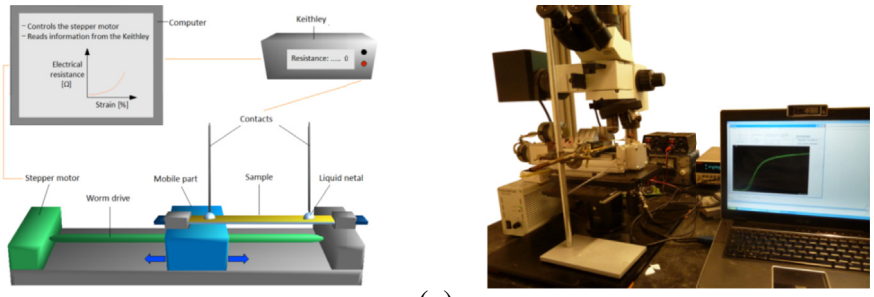

(a)

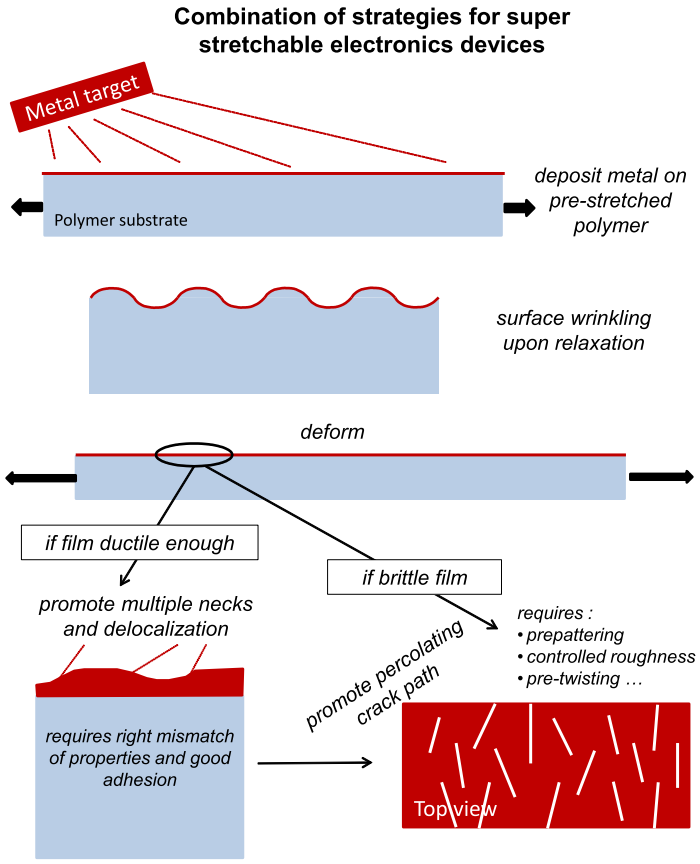

(b)

Fig. 15. (a) Instrumentation for in-situ stretching of metallic films on polymer substrates from [295]; (b) combination of strategies used to reach high stretchability (i.e. very large deformation without electrical failure).

depends much more significantly on α especially when α approaches 1. Several studies relying on finite element analysis have calculated the variation of G as a function of several parameters such as the crack density or the coating to substrate thickness ratio. Values of Z larger than 20 can be easily attained for metallic films on elastomers.

The analysis can be extended to the case of several parallel cracks with mean spacing S, each of them releasing the energy stored in a specific region around it. The work presented in [301] gives the value of Z computed by FE analysis as a function of α, of the substrate to film thickness ratio H/h, and of the crack spacing to film thickness ratio S/h. If the properties (E_f, E_s, h, H) are known, the results given in [301] directly provide, by interpolation, the value of Z corresponding to the measured crack spacing. Then, the energy release rate for crack propagation G is calculated from Eq. (10), provided that the value of the internal stress before cracking σ is known.

Other effects complicate an accurate determination of G. Finite element simulations have shown that for soft substrates, some amount of interfacial decohesion at the bottom of the crack will necessarily take place with a delamination width controlled by interface toughness [302]. The constraint factor Z increases with the delamination width and the impact on the energy release rate can be important for large elastic mismatch. Recently, Thouless et al. [303] showed that this implies also that cracks in stiff films will be drawn into the substrate, especially if its fracture toughness is low enough, and this will promote cracking of the film through a further increase of G. In addition to the stiffness mismatch, viscoelastic relaxation of the substrate impacts Z as well [304]. The question of the intrinsic meaning of the fracture toughness G_c as the

crack tip plastic deformation gets extensive also with respect to the plane stress/plane strain transition regime is an issue that has not been much studied in the present context - this question comes back in Section 5.3.

4.3. Fracture and fatigue mechanisms

The lack of ductility of thin metallic films has been repetitively discussed, e.g. [305,306], with potential negative impact on stretchability. For instance, based on a round robin performed by five different research teams, Tsuchiya et al. report average fracture strains in 500 nm thick freestanding Ti films varying between 0.4% and 2% depending on the group performing the measurements [307]. Results on freestanding Ni films vary between 0.9% and 2.3% [307]. Au films with thickness varying between 0.3 μm and 1 μm show fracture strains smaller than 1% [308]. Al films with thickness varying between 0.2 μm and 1 μm show fracture strains ranging between 1% and 7% depending on the width of the specimen [308]. Freestanding Cu films with thickness varying between 0.2 μm and 1 μm show fracture strains between 1% and 2% [308]. Even though the topic of freestanding films is the subject of Section 5, these examples show that, as a starting point, thin metallic films are intrinsically not ductile. Instead of looking at intrinsic ways to improve ductility by microstructure engineering and composition, scientists working in the field of flexible electronics, and coming from mechanics, electronics and chemistry more than from metallurgy, have proposed a set of innovative extrinsic workarounds, summarized in Fig. 15b, capitalizing on the mechanical interactions with a soft substrate combined or not with patterning of the conductive track. This approach is somewhat analogous to the "architectured materials" paradigm which aims at improving the material system performances by combining different materials and configurations [309]. The extrinsic ductilization strategies are explained hereafter.

A first very successful method to artificially impart ductility to a film is through inducing the wrinkling of the surface [285–287,310–312]. The idea is to deposit the film on a pre-stretched substrate in order to generate, after relaxation, surface wrinkles. When the system is stretched again, the surface must first flatten before a tensile load starts developing in the film up to the failure by plastic localization and cracking. There is an optimum level of pre-stretching to be found by considering also the transverse deformation of the film with respect to the substrate. Complex controlled wrinkling morphologies can be generated by pre-patterning the surface of the substrate such as to induce local stiffness variations and/or local internal stress fields, which upon thermal cooling (after deposition of the film for instance) will lead to surface instabilities [310,313].

Another possible source of ductilization is by properly matching the stiffness of the polymer substrate with the metallic film in order to delocalize deformation and to retard plastic localization occurring under tensile loading conditions [305,306,314,315]. If the Young's modulus of the substrate E_s and the hardening law of the film has the following form $\sigma = K\varepsilon^n$ (with a small strain hardening exponent n), three behaviors are possible under plane strain conditions: (i) if the elastomer is very compliant, i.e. E_s/K is small (e.g. $E_s/K < 0.2$), then the metal film forms a single neck at small strain as it was a freestanding film; (ii) if the elastomer has an intermediate compliance (e.g. $E_s/K = 1$), then the metal film forms multiple necks allowing much larger overall elongation, see Fig. 15b; (iii) if the elastomer is stiff, i.e. E_s/K is large (e.g. $E_s/K > 2$), then the metal film deforms uniformly to large strains. A substrate with the proper stiffness stabilizes the necking process through an elevation of the local stiffening resulting from the large local elongation of the underneath substrate region. The delamination of the film from the substrate must be avoided, otherwise the film becomes freestanding which suppresses the beneficial interaction with the soft substrate [305,306], see Fig. 16 from [316]. The same problem generalized under biaxial loading conditions has been recently revisited [317]. The occurrence of a delamination patch at the interface between the film and the substrate has a negative effect by preventing this delocalizing mechanism to occur. In addition to all possible surface treatments and activation methods providing high adhesion, the presence of a substrate roughness has been shown to delay interfacial crack propagation [318–320]. When fracture is caused by a brittle mechanism such as intergranular cleavage, the presence of the compliant substrate does little to postpone rupture [314].

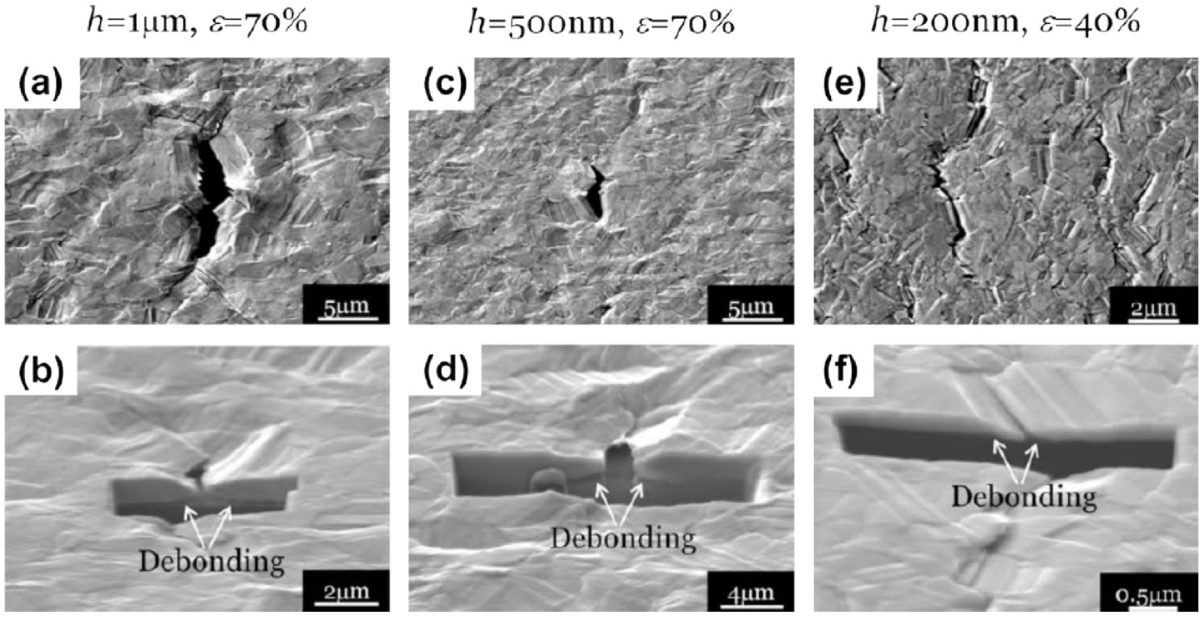

Fig. 16. Surface and cross-sectional views of (a, b) 1000, (c, d) 500 and (e, f) 200 nm thick Cu films stretched by 70%, 70% and 40%, respectively, on their polyimide substrate; loading is along horizontal direction for all micrographs; from [316].

Whether or not the wrinkling strategy is used and the delocalization process is effective, channel cracks are ultimately generated in the films. For electronic applications, failure is defined as when the film loses its electrical conductivity. The initiation of cracks is thus not the end of life of the system. The essential aspect is to delay the percolation of the cracking pattern essentially by avoiding the propagation of long straight cracks, see Fig. 15b. One way to promote complex branched crack patterns in the case of wires coated with a metallic film is by pre-twisting the system in addition to pre-stretching [281]. Another method is to create, on purpose, specific cracking patterns such as tri-branched micro-cracks [321]. Recently, the tuning of the roughness of the polymer substrate has been demonstrated to postpone by more than a factor 50 the strain corresponding to electrical failure through favouring a random cracking pattern with mutual shielding effects [295]. Note that the width and thickness of the film also play a role on the crack morphology [295,312].

The resistance to fatigue is essential for flexible electronics devices that must be repetitively stretched, rolled or twisted up to large strains. Early works by Lacour and co-workers [322] demonstrated the capacity of cyclically deforming 25 nm thick Au films deposited on 5 nm Cr and PDMS substrate between 0% and 15% without electrical failure. The conditions necessary to maintain an electrical pathway are the same as for static deformation, and exactly the same strategies as described above can be followed to improve the resistance to fatigue to larger strain amplitudes, see recent example of cyclic deformation tests with strain amplitude up to 50% with no deterioration of the electrical conductivity [295]. The failure mechanisms that give rise to a starter crack and then to its propagation are, on the other hand, different than under static conditions. Schwaiger, Kraft and co-workers [323–327] have shown that in Ag and Cu films, surface extrusions and voids at the coating/substrate interface dominate the fatigue life. Once again, the decohesion from the substrate during here cyclic deformation, leads to freestanding sections, which are more prone to localized plasticity and extrusion mechanisms, as recently confirmed on Ag films [328]. We will get back to the fatigue mechanisms in thin metallic films in Section 5.4.

Even though all the extrinsic ductilization methods mentioned above cannot be directly adapted to improve the resistance to failure of bulk NC systems, they offer interesting ways of thinking from a “system” viewpoint the resistance to failure. The idea to arrest cracks and to avoid long straight cracks is one of the interest of the graded system mentioned in Section 3 - a method also very much used by nature to toughen intrinsically brittle materials, such as bone or nacre, see e.g. [329]. Very successful progress in flexible electronics have been made without looking at the full potential of improving the intrinsic ductility of the films through in depth analysis of the fracture mechanisms leaving open new progress in this field.

5. 1D and 2D freestanding micro and nano-scale metallic systems

Freestanding sub-micron films, beams and wires are important in a variety of modern technologies, involving different MEMS configurations, several types of membrane applications, micro-sensors, etc. These small freestanding materials constitute also attractive systems for fundamental scientific works owing to the near ideal defect free conditions, the simplicity of the microstructure, the absence of perturbation from the constraint of a substrate, and/or the small size allowing direct TEM analysis. Note that a film can be freestanding also due to a local decohesion from an underlying substrate, a phenomenon that has been already discussed in the context of Section 4. Significant progress has been made over the last 10 years in the development of nanomechanical testing techniques that allow deforming nano-objects up to fracture under well-defined loading conditions, while allowing also *in situ* characterization. We review these aspects first before addressing successively the plastic localization, static damage and fracture, and fatigue mechanisms. Some of the sub-sections will extend discussions already initiated earlier in the paper.

5.1. Fracture testing methods of freestanding specimens

Several reviews have recently covered the topic of nanomechanical testing, e.g. [330–334]. The first key element when testing freestanding thin films or nanowires is the extraction, manipulation and positioning of the specimens. In the tests described hereafter, three categories can be roughly distinguished. In the first relatively conventional approach, thin films or nanowires are “detached” from a template, attached to a nanomanipulator and transported to the testing frame, to be welded or glued at the anchoring points. The second approach is the opposite and consists in “bringing” the loading device to the test specimen still attached in a way or another to the original frame. The third approach is to deposit or grow the material directly on the test platform. Whatever the choice, micro- and/or nanofabrication methods are needed to prepare the specimens, either by lithography and etching or by FIB, or by a combination of techniques, see Section 2. The second key issue is the application of very small loads and the extraction of accurate stress and strain.

The two probably most widely used and familiar methods in nanomechanics which are nanoindentation and micro- or nano-pillars compression, involve dominantly compressive loading conditions, which is not adapted for testing fracture and fatigue properties. Other classical techniques devoted to the measurement of the mechanical properties of thin films such as the wafer curvature method, see e.g. [137], under thermal loadings or other bending type methods, e.g. [156,335], involve strains that are often not sufficient to promote fracture in ductile films; furthermore the first technique is not adapted to freestanding films. Fig. 17 gathers a series of test method, involving dominantly tensile loading configurations, and which have been successfully applied to freestanding nano-sized metallic specimens. These test methods include:

(1) Various “top down” tensile testing set ups involving miniaturized version of macroscopic tensile tests. Fig. 17a shows a version of the micro-tensile testing stages concept, as initially proposed by Sharpe and coworkers [331,336] and Tsuchiya et al. [337,338]. Piezoelectric [339,340] and electrostatic [337] external actuators have been used to pull on the films. These testing platforms can be designed to allow cyclic loadings for fatigue analysis, see for instance [341–343]. High resolution CCD camera and optical microscope can be adapted to look at the specimens during deformation and, if needed, apply digital image correlation analysis to extract strain fields afterwards. Sometimes, the nano-manipulator used to transport thin ribbons or nanowires plays the role of actuator for deforming the test material, while gluing the opposite side to a force sensor [61,344], see Fig. 17b. Also AFM equipments [345] or other specific gripping tools were used to attach small metallic wires, beams or columns to pull them in tension [346,347], allowing *in situ* observations within a SEM, see e.g. Fig. 17c. Recently, water was used as a frictionless sliding support for the specimen to facilitate the attachment and positioning procedures of the load and actuating cells [348]. The proper alignment of the specimen is always a very critical issue as

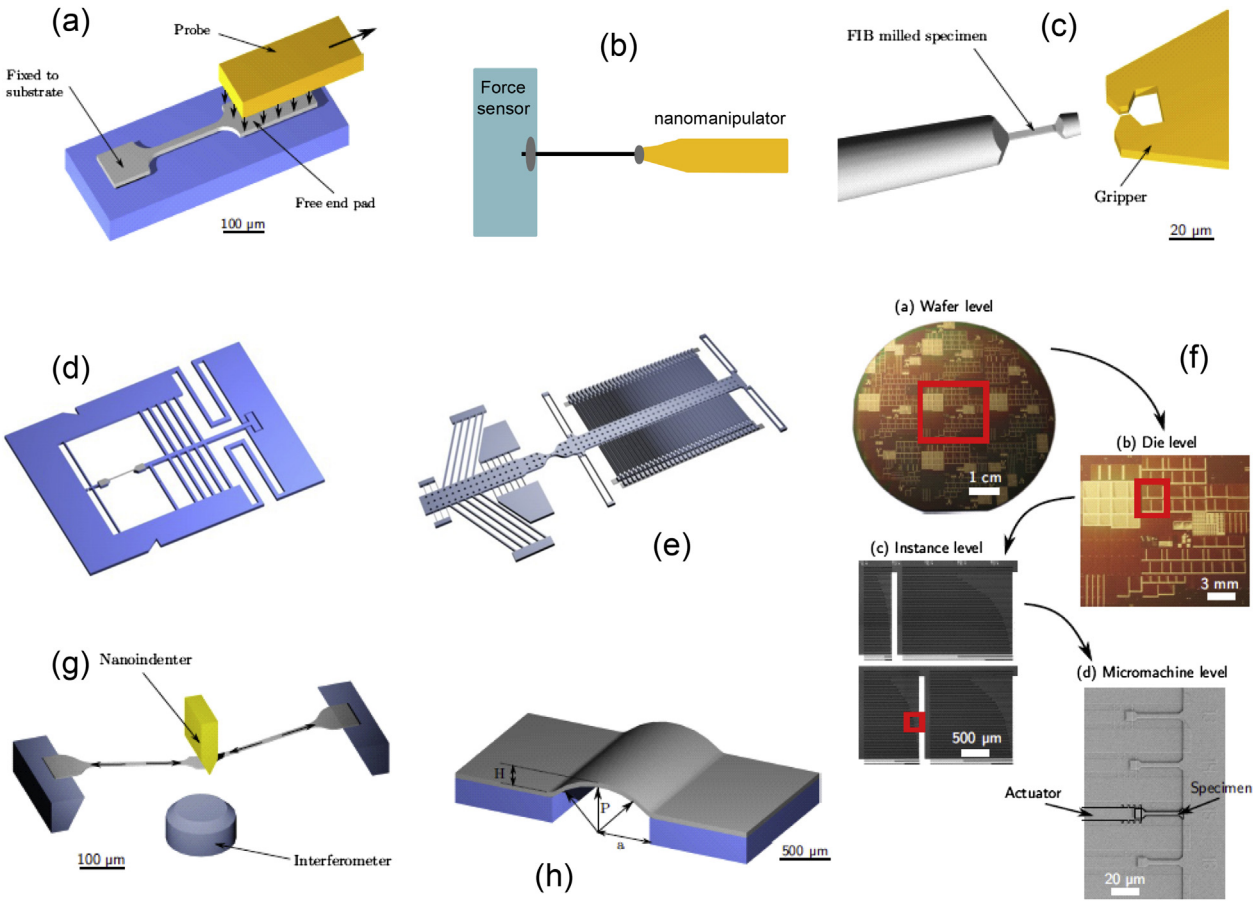

Fig. 17. Various set ups for testing the fracture and fatigue properties of freestanding thin films, nanoribbons and nanowires; (a) tensile stage by Tsuchiya and co-workers [338]; (b) nanomanipulator directly used to apply the deformation [61,344]; (c) FIB machined microgrips [347]; (d) MEMS based test frame by Haque and Saif [333,351,352]; (e) MEMS tensile testing stage by Espinosa and coworkers [354,355]; (f) on chip nanomechanical testing laboratory with internal stress based actuated elementary structures [358,359]; (g) tensile loading through deflection [308,366]; (h) bulge test configuration.

recently addressed in details by Kang and Saif [349,350] - a few degrees of misalignment invalidates the extraction of accurate elastic and plastic properties.

(2) Fig. 17d-f show examples of tensile testing methods based on MEMS fabrication techniques. Fig. 17d represents the seminal MEMS test frame proposed by Haque and Saif [333,351,352], see also [353]. This test method still requires external piezo actuation as well as the use of electron microscopy to measure the displacement of markers. Fig. 17e shows a very integrated MEMS based stage proposed by Espinosa and co-workers [354,355] with both actuation and sensing at the chip level. These testing methods, even though requiring sophisticated design and calibration analysis, have already led to very successful results, sometimes on truly nano-scale specimens. These testing stages are amenable to *in situ* TEM characterization by performing the back etching of the wafer under the test specimen, see [354] and also [356,357] for applications to fatigue analysis. A MEMS based testing frame based on a concept of "on chip" actuation of elementary tensile testing structures through internal stress has recently been developed and applied to different deformation and fracture investigations of free-standing metallic thin films [358–362]. This method schematically depicted in Fig. 17f allows the simultaneous testing of thousands of thin ribbons or nanowires under uniaxial tension, shear, notched or equibiaxial tension, with a capacity to allow direct TEM analysis [152]. All these test frames can be processed either in house with laboratory scale clean room infrastructures, or through industrial fabs that perform the micro-fabrication steps to produce the MEMS based on the provided masks, or directly purchased as commercial test equipment, see e.g. the so-called "push to pull" concept [363]. These MEMS based equipments have been used to perform *in situ* tests on metallic nanowires, e.g. [364,365]. Fracture mechanics tests can also be performed after the introduction of a sharp pre-crack for instance by FIB.

(3) The tensile deformation needed to reach fracture can be driven through other loading configurations. Fig. 17g shows a method based on the deflection of free-standing cantilevers using a nano-indenter with approximate uniaxial tension conditions within the gauge section [308,366]. Interferometry provides the strain from displacements and the stress is related to the nano-indentor load. The bulge test shown in Fig. 17h, see e.g. [367–369], involves biaxial conditions which can be varied from plane strain to equibiaxial depending on the aspect ratio of the membrane. The clamping conditions involving local stress concentration make difficult the extraction of the true fracture strain under a well-defined stress state. The bulge test can be used in the context of fracture mechanics analysis if a pre-crack is introduced [370] or of low cycle fatigue experiments [371].

(4) Failure can also be investigated on small size specimens under bending conditions. FIB is used to carve a beam

bending sample which is loaded using a nano-indentor [372,373]. Strains under bending might not be large enough to attain fracture and notches or pre-cracks can be machined to induce a stress concentration. The validity of the application of fracture mechanics theory on samples with "pre-cracks" induced by FIB [374,375] is a critical question that will be addressed later. Note that fatigue beam bending tests have also been performed using a nano-indentor or an AFM tip to force the oscillation of the test beam [376,377]. Effects related to local bending and/or to the real boundary conditions (which are never perfectly clamped conditions) are not easily taken into account.

5.2. Plastic localization in freestanding thin films and nanowires

Plastic localization is often the dominant failure mechanism in thin films when deformation takes place under freestanding conditions. Fig. 18 shows examples of plastic localization in thin metallic films or nanowires. The parameters dictating the resistance to necking in metallic films are the same as for NC bulk systems and have been covered in Section 3.2. Indeed, thin metallic films constitute a subclass of NC materials, with the same tendency for low strain hardening capacity and high rate sensitivity compared CG metals. But, with small scale test structures, attention must be paid to two additional effects described hereafter:

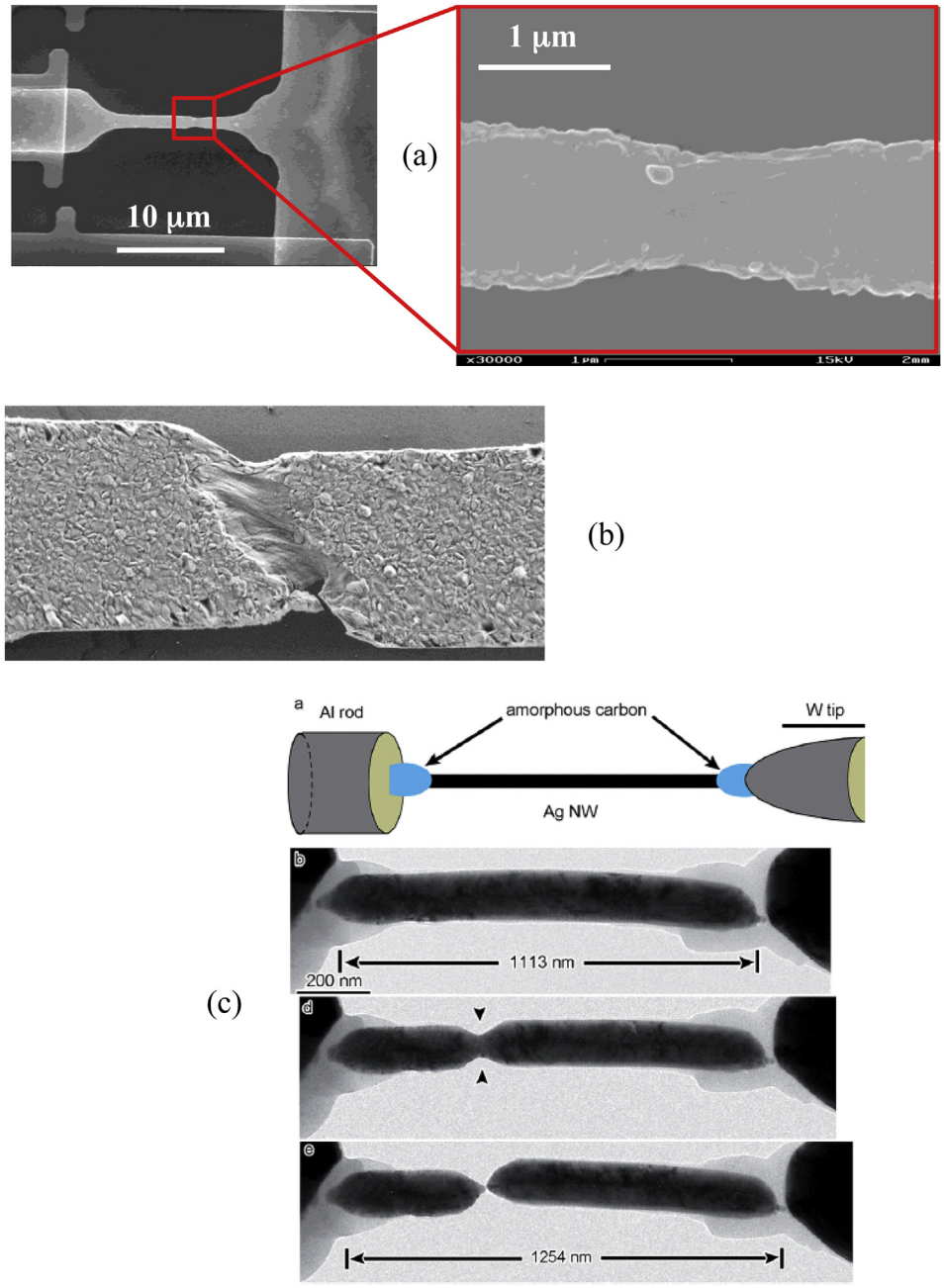

Fig. 18. Examples of necking in metallic films and nanowires; (a) and (b) SEM micrographs of 205 nm-thick Al specimens deformed in tension with the internal stress based actuation method [358,359]; (c) necking down to a single point in Ag nanowires, reproduced from [365].

(1) *Impact of free surface*. The presence of free surfaces can indirectly affect the resistance to necking in many different ways. As explained in Section 2, diffusion mechanisms are promoted along free surface. Also, grain growth and grain rotation are easier in columnar films than in bulk NC as the distortion of the material is not restricted by the presence of other grains in the out of plane direction. These mechanisms are thermally activated and lead to large rate sensitivity, often much larger than in bulk form. This explains why, sometimes, the resistance to necking is found to be quite large such as in some Al films with $\varepsilon_u > 20\%$, see e.g. [12,13,378]. In [149], a transition is predicted using MD simulations in the localization process from almost pure shear localization sliding along one well oriented GB in the case of a bamboo structure to a more conventional necking process, such as shown in Fig. 18, when the system involves multiple grains in the cross-section. The surface is also a source of imperfections when considering the small thickness. Indeed, a small surface roughness amplitude or the presence of surface etch pits, of lithography undulations or of grain boundary grooves on the order of a few nm lead to what can be considered as a significant imperfection in a 100 nm thick film. Also, the presence of an oxide at the surface can lead to an evolution of the constraint imposed to the plastic flow if it breaks during deformation [145] inducing a sudden local softening that favours plastic localization. The importance of imperfections and the statistical effects that result from the distribution of these imperfections as a function of specimen size have been recently demonstrated in the study by Coulombier et al. [13] in which hundreds of data were collected on Al films. The resistance to plastic localization involves a significant scatter which depends on specimen size.

(2) *Strain gradient plasticity effects*. Freestanding films with submicron thickness can also involve micron or submicron size in the second transverse direction, as in nanoribbons or nanowires. When plastic localization sets in, very large plastic strain gradients develop which can lead to so-called strain gradient plasticity effects, e.g. [70,73]. A very large density of GNDs is indeed necessary to accommodate the gradients associated to the development of a neck in micron or submicron sized structures, leading to an additional resistance to plastic flow when compared to a purely isotropic hardening contribution dictated by the accumulation of statistically stored dislocations only. This leads to a stabilization of the necking process, as represented by *curve 8* of Fig. 7. This phenomenon has been studied by Niordson and coworkers [379,380] using 2D FE simulations based on the strain gradient constitutive model of Fleck and Hutchinson [70]. A similar approach has been followed by Brugger et al. [145] specifically focusing on the necking in thin columnar metallic films. The loss of resistance to necking induced by the increasing strength when reducing film thickness can be compensated by the strain gradient effect [145]. A much more simple approach based on a 1D imperfection analysis, accounting for strain gradient effects, has been recently proposed by Pardoen [171] and validated towards the FE calculations of Niordson [380]. A direct experimental proof of the impact of strain gradient plasticity effects on necking in small dimensions systems is, to our knowledge, still lacking. In this context, it is worth noting the development in Fig. 18a of a neck which appears particularly more elongated than what is expected for a material with a strain hardening exponent on the order of $n \approx 0.1$, possible reflecting some stabilization by strain gradient effects. Now, this stabilization effect is only meaningful if the mechanism accommodating the strain gradients is through the generation of GNDs and not through other grain boundary sliding or grain rotation mechanisms, see the discussion in Section 5.3 where experimental evidences of gradients released by grain rotation mechanisms will be presented.

A general picture regarding the competition between all these effects can be sketched using the recent imperfection based localization analysis proposed in [171]. Compared to the result shown in Section 3, the initial yield stress involves now a term depending also on the film thickness, see [136,381],

$$\sigma_0 = \sigma_{00} + K_{HP1}\Big/\sqrt{d} + K_{HP2}/h \tag{12}$$

where h is the film thickness and K_{HP2} is a hardening parameter. Fig. 19 shows the evolution of the strain at necking normalized by the strain hardening exponent, here $n = 0.25$, as a function of the film thickness for a material involving a grain size dependent strength and rate sensitivity. Three characteristic lengths are considered. The length l^*, which is the intrinsic length scale entering the gradient plasticity model, is set equal to 0, 0.5 or 1 μm. The strain gradient plasticity effects are turned off below a grain size equal to d_c at which classical plasticity mechanisms are expected not to play a role anymore (see Section 2), taken here equal to 250 nm. The imperfection entering the model is taken small, $f = 0.999$, which means a 0.1% local reduction of thickness. Fig. 19 illustrates the complex competition between the different contributions taken into account in the analysis. The drop of ductility would be more significant in the case of larger imperfections and if a decrease of strain hardening capacity would also be taken into account. The scenario that emerges from Fig. 19 implies two transitions controlled by l^* and d_c. When $h = d < d_c$, we anticipate a high rate sensitivity but no strain gradient plasticity effect. When $h = d > l^*$, we anticipate no size effect except through the Hall-Petch effect which raises the strength, leading to a decrease of the ductility. When $d_c < h = d < l^*$, strain gradient plasticity effects can

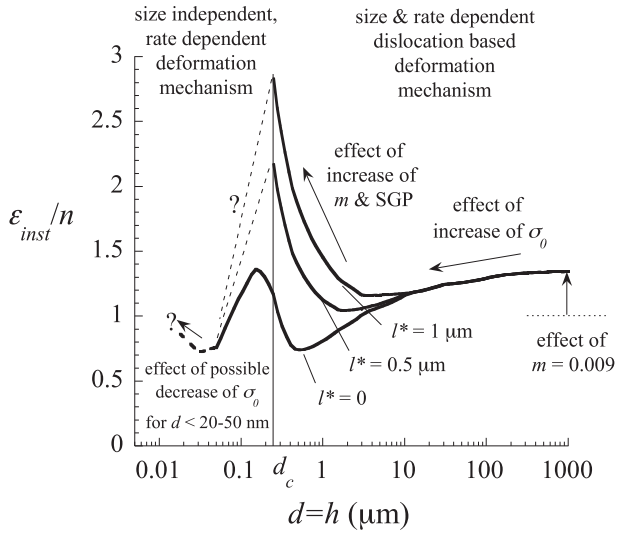

Fig. 19. Variation of the strain at necking ε_{inst} normalized by the strain hardening exponent n as a function of the film thickness h (taken equal to grain size d) for a material involving a grain size dependent strength and rate sensitivity, reproduced from [171]. Three characteristic lengths are considered: $l^* = 0$, 0.5 or 1 μm. The SGP effects are turned off below a grain size equal to $d_c = 250$ nm at which the rate dependent thermally activated mechanisms start dominating the deformation process. The imperfection is taken small $f = 0.999$.

improve the ductility. This is certainly not yet the full picture as one should also account for localized necks developing at an angle. Indeed, if the straining is not homogenous, diffuse necking will probably not occur and only localized necking will take place. Fig. 18b shows for instance a more localized neck developing at an angle in a thin Al films.

The discussion above shows that many routes can be followed to modify and improve the resistance to necking of thin films or nanowires. The first option is obviously through increasing the strain hardening capacity as in bulk NC specimens. Accumulation of dislocations in thin films with grains as small as 10–30 nm has been recently demonstrated in different fcc films [176–178], see Section 2.2. Same as for bulk NC systems, sources of strain hardening associated to the presence of nanotwins in thin metallic films have been demonstrated for instance in thin Pd films [52,111,182]. Growth nanotwins in Pd films are favoured by processing methods that lead to weak textures (here e-beam evaporation) which allows the mechanism of GB migration to operate during deposition [51]. More generally, texture effects can be very strong in thin films. In the study by Lu et al. [316] on Cu films with thickness from 50 nm to 1 μm sputter deposited on polyimide foils (see also Section 4.3) deformed in tension, films thicker than 200 nm exhibit co-evolution of necking and debonding from the substrate, see Fig. 16. The debonding patches allows looking at the response of the film in locally freestanding (plane strain) conditions, owing to FIB cross-sections. The ductility is found to decrease for film thickness above 500 nm. The origin of this decrease is related to an increasing fraction of (100) grains in the (111) dominant texture when increasing the thickness. The softer (100) grains lead to earlier localization and faster neck development. In all these systems, heterogeneities in the grain size and nanotwins distribution add to the grain orientation effect and lead to very significant back stresses, as explained in Section 2.2. A major contribution to strain hardening in thin metallic films is often from kinematic origin. The key here is to allow kinematic hardening effects to play a role up to sufficiently large strains in order to postpone necking, such as with TRIP and TWIP effects in bulk systems. A multiscale back stress engineering strategy holds much promise for improving the resistance to localization in thin or bulk NC metals.

A second route to increase the resistance to necking is to favour thermally activated mechanisms in order to enhance the rate sensitivity. This discussion is true also for bulk NC metals, even though freestanding thin films are more prone to GB relaxation mechanisms because of the absence of constraint in the thickness direction. The chemical composition of the GB is also a key factor. Tang et al. [173] have shown that low pressure deposition allows decreasing the amount of oxygen at the GB in sputter deposited Al films, favouring grain growth mechanisms and leading to m values sometimes larger than 0.1. On the other hand, Zhang et al. [382], recently proved that adding a small amount of Zr (0.5%) segregating at the GBs of Cu thin films, was promoting grain growth mechanisms, hence improving the ductility. The proposed reason is an indirect effect of the presence of Zr which favours the formation of (110) grains, leading to the coexistence of three types of orientations, i.e. (111), (100) and (110) grains, whose cooperative interplay is known to encourage grain growth [383]. Note finally that the application of low deformation rates sometimes lead to higher m values such as demonstrated in Au films [151].

The third route to delay necking is to minimize imperfections by avoiding GB grooves, roughness and lithography defects. Also, promoting thin film structures or membranes with many grains over the width is a way to limit the probability of weak grain clusters that can decrease the resistance to plastic localization.

The issue of plastic localization in sub-micron metallic systems is a rich and very open field of investigation. The theoretical approaches developed mainly by the metal forming community, see e.g. [170], have to be substantially adapted to account for the complex interplay of deformation mechanisms discussed above.

5.3. Damage and fracture in freestanding small scale metallic systems

As already mentioned in Section 3.2, direct observations of damage and of its accumulation in NC materials have been essentially obtained from investigations of freestanding thin films. Indeed, methods used in CG metals, based on careful polishing of cross-sections of deformed or broken samples, e.g. [200], or modern X-ray microtomography, e.g. [201,202], are not applicable to NC bulk samples due to the very small void sizes. In particular, the *in situ* TEM tensile test methods described in Section 5.1 have recently provided a realm of interesting data that are reviewed in this section about the failure scenario under homogenous deformation conditions as well as in the presence of pre-cracks/notches typically machined by FIB.

Before looking at high magnification TEM characterizations, a good starting point regarding the competition between failure modes comes from the study of Lu et al. [316], as already addressed in Section 4, on sputter deposited Cu films. Films with thickness below 100 nm fail by intergranular fracture due to the very large stress building up as a result of the large yield stress, leading to small elongation at fracture. (Note that these authors have not searched for possible GB embrittlement cause.) Thicker films all exhibit co-evolution of necking and debonding from the substrate, see Fig. 16, followed by transgranular fracture. The 200 nm films seem to neck down to zero thickness with no damage, while thicker films show a finite broken cross-section area indicating the existence of a cracking mechanism. The details of the damage mechanisms cannot be resolved by SEM. This study shows that the later the onset of necking, the larger the fracture strain as discussed earlier. The competition between a ductile damage failure mechanism and a brittle intergranular fracture with no significant plasticity controlled damage growth has been observed in other systems exhibiting very marked change of ductility. Gianola et al. [378] found almost no ductility in 200 nm thick 99.999% pure Al films sputter deposited at a base pressure of 10^{-5} Torr, while when the deposition is at lower pressure, the elongation to fracture was larger than 15%. In the last case, a relaxation mechanism by grain growth limits the yield stress and thus the magnitude of the load seen by the GBs. The authors demonstrated later [173], for the first case, using atom probe tomography a significant enrichment in O at GB suppressing the grain growth mechanism, elevating the stress, and, perhaps (this is our interpretation) lowering also the GB cohesion.

The mechanism of ductile fracture in thin metallic films revealed by *ex-* or *in-situ* TEM analysis is essentially by the nucleation, growth and coalescence of voids. Voids primarily nucleate at triple junctions or at GBs as shown for instance for 60 nm thick sputtered Ag film [384], 100 nm thick EB-PVD Cu films [385], and 300 nm evaporated pure Al film [147]. This is similar to bulk NC metals and in agreement with the MD simulation predictions on Ni with 10 nm grain sizes [216] except for the pure GB sliding failure occuring as in the case of a bamboo structure [149]. Recently, it has been convincingly shown for 150 nm diameter Ag nanowires pulled in tension within a TEM that voids can also nucleate in the vicinity of TBs [365].

After nucleation, voids grow owing to the different deformation mechanisms reported in Section 2.2. Emission of dislocation loops from the surface of nano-sized voids is one factor driving dilatation [386]. As explained in [365], the time scale for growth by diffusion mechanisms is too slow to explain the void growth rates observed

in metallic films or nanowires when deformed at moderate strain rates. GB sliding can lead to the distortion of the void morphology. Further GB decohesion leads also to the enlargement of the void in the direction of the GB. The coexistence of these different void growth mechanisms has been observed in [384] on 60 nm thick Ag films as well as captured by MD simulations on NC Ni [149]. In these simulations, the growth of the void, involving grain boundary sliding and decohesion, is sometimes stopped when the void surface reaches a triple junction. Triple junctions can thus act as void nucleation sites but also as void growth arrestors. The fracture surfaces of Au films show clear dimples which is a clear proof of the void growth based nature of the damage mechanism [387].

The voids finally coalesce with one another through an intervoid necking mechanism, as clearly observed in the Ag films [384] or in MD simulations of Ni nanowires [149] as discussed above. The coalescence process is reminiscent of the mechanism occurring in CG metals [1,388]. Fig. 20 shows a micrograph of 210 nm thick freestanding Al notched specimen near to final failure after deformation using the on chip tensile testing method described in Section 5.1. Cracking starts at the notch root and propagates in the sample by repeated coalescence with discrete voids. The fracture process involves about 10 voids. The ligament size is approximately 2 μm, meaning that the void spacing is on the order of 200 nm, which is roughly equal to the grain size. Compared to the few results obtained on bulk NC metals, e.g. [38,67,203], where the void spacing was significantly larger than the grain size, there is here a one to one relationship. This example shows that even though *in situ* TEM tests on thin metallic films can enlighten the damage mechanism occurring in all NC (bulk or thin film) systems in general, the connection might only remain qualitative and dependent on the material. The peculiar nature of thin films with a columnar grain structure leading to a single row of through-the-thickness voids under specific mechanical constraint is not fully representative of the damage occurring inside a bulk system.

Although this process of fracture by successive nucleation, growth and coalescence of voids is common to CG polycrystals, the models developed for bulk CG metals as described in Part I of this series of overviews [1] are not directly applicable to NC metals in bulk or thin film form; this part of the present discussion extends thus also Section 3.3. First of all, void nucleation essentially occurs by decohesion at GBs, mostly at triple junctions, due to large overall stress levels, which are amplified by local stress concentrations caused by dislocation accumulation and GB sliding. Most models developed for CG alloys rely on a different mechanism associated with the decohesion or fracture of second phase inclusions, e.g. [1,389]. Next, one contribution to void growth in NC metals is by dislocation mechanisms, just like in CG metals but at a scale where strain gradient plasticity effects cannot be neglected. Voids with dimensions below 1 μm grow more slowly than larger voids due to the accumulation of a high density of GNDs as needed to accommodate the large local strain gradients, see e.g. [70,390–392] (note that void sizes typically smaller than 20–50 nm cannot anymore be treated with continuum theories but require dislocation dynamics or atomistics, e.g. [393,394]). Furthermore, as explained above, void distortion and enlargement can be caused also by a combination of evolving GB decohesion and GB sliding at the void tip. Models for the description of the void evolution will thus have to incorporate many aspects related to the intrinsic resistance of the interface which itself depends on the character of the GB and local chemistry, to the blunting of the void tip and to the stress triaxiality near the GB. One aspect of this problem has recently been investigated by Yerra et al. [395], although in a totally different context of CG multiphase alloys. The analysis of the decohesion at an interface between two phases shows the competition, after a first small decohesion along a weak interface spot, between the propagation of the decohesion and the plastic opening/blunting of the void [395]. A full micromechanics based model should finally account for the possibility of purely intergranular brittle fracture if the strength gets very high due to the small grain size or if GB embrittlement is so significant that GB decohesion proceeds without any significant plastic relaxation. The formulation of such a model is challenging and certainly open. Perhaps, the coalescence mechanism, because of its intrinsic geometrical nature, may be more directly amenable to a treatment with models developed for

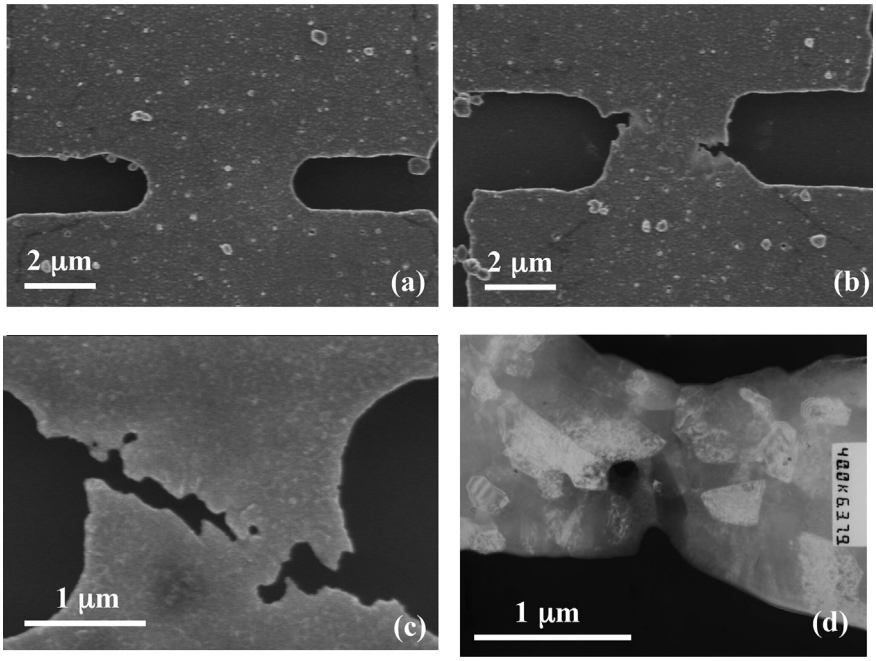

Fig. 20. Damage by void growth and coalescence in 210 nm thick aluminium films; (a)–(c) micrographs of three notched specimens deformed using the internal stress driven testing method described in [359] up to different levels of deformation; (d) TEM micrograph showing a cavity growing along a GB in the necking zone of a tensile test specimen.

CG metals, see [1].

Fig. 21 is a tentative schematic synthesis that we propose, based on the data reviewed before and some physical speculations, for the evolution of the fracture strain in metallic thin films as a function of yield stress (or of the reduction of grain size following $1/d^{\alpha}$). One evolution line corresponds to the ductile fracture locus while a transition into intergranular low ductility fracture can set up at a given stress level depending on the intrinsic resistance and on the distribution of GB misorientation, on impurity segregation and on other local stress concentrator factors. Note that the transition is not drawn as being perfectly sharp. Indeed, the nucleation of voids for the ductile mechanism also proceeds by local GB decohesion process. There must be a range of conditions in which the amount of void growth decreases while pure GB decohesion becomes more and more dominant. The ductile fracture locus is characterized by a fracture strain that first decreases with increasing yield stress due to more rapid void nucleation and lower strain at necking (faster necking means earlier generation of a region with higher stress triaxiality). When the grain size (and or film thickness) is below typically 100 nm, the rate sensitivity significantly increases, which means a retardation of necking, but also a lower void growth rate and coalescence if we rely on existing damage models for CG materials [1,396,397]. In this range of grain size, the fracture strain can be expected to increase but with higher dispersion due to imperfections that are more difficult to control. In the best case, the true fracture is locally infinite (pure necking to a point) if damage is fully suppressed. Finally, an increase of the strain rate will favour intergranular fracture due to the larger stress building up as if the yield stress was larger. This general scenario of Fig. 21 requires validation from dedicated experimental programs and/or careful advanced numerical simulations. Such a genuine understanding is needed to guide metallurgists in the design of more ductile NC metals.

In macroscopic material coupons, the resistance to fracture is usually considered to be best quantified by the fracture toughness, which, opposite to the fracture strain, should in principle be an intrinsic quantity. But, the transfer of fracture mechanics concepts at the scale of submicron metallic films and of specimens which are micrometers wide is very questionable. First, the plastic zone size can easily become larger than the width of the specimen leading to fully plastic conditions with extended zones of finite deformation and a loss of validity even of the J integral concept. Furthermore, plane stress conditions will prevail in micron and submicron thick components, and the fracture toughness is never well defined under near plane stress conditions [206,207]. The question of the sharpness of the initial pre-crack, often produced by FIB, is another key issue - fracture mechanics concepts can be applied only if the initial pre-crack opening is much smaller than the CTOD at cracking initiation δ_c. Based on typical G_{Ic} values for thin metallic films ranging between 10 and 1000 J/m^2 (based on K_{Ic} data given later), the δ_c for 1 GPa yield stress will typically vary between 5 and 500 nm. For the lower range of fracture toughness, the initial crack opening has to be smaller than a few tens of nm or below, which is not possible with FIB, while for the upper range, the initial sharpness may be sufficient. Finally, a recent set of investigations by Kumar et al. [398,399] on the fracture behavior of evaporated 100 nm thick Al films (50 nm grain size), with notch, combining in-situ TEM testing and MD simulations proved that the concept of stress concentration can sometimes not be valid at all at this small scale. Significant grain rotation driven by GB diffusion was observed at the notch tip, relaxing completely the stress gradient, with fracture occurring far away from the notched zone. The reduction of the stress concentration at notches in submicron material specimens has been also demonstrated for Pt nano-cylinders, although fracture was, in this study, still taking place in the notched region [400]. Even though this phenomenon cannot probably be generalized (see e.g. the fracture mechanisms of Fig. 20 also on Al films but with slightly larger grain sizes and loaded much faster), it must be reminded when applying fracture mechanics arguments.

Keeping in mind the theoretical and practical difficulties mentioned above, it is worth reviewing a few crack propagation studies in metallic thin films. Hirakata et al. [401] measured the

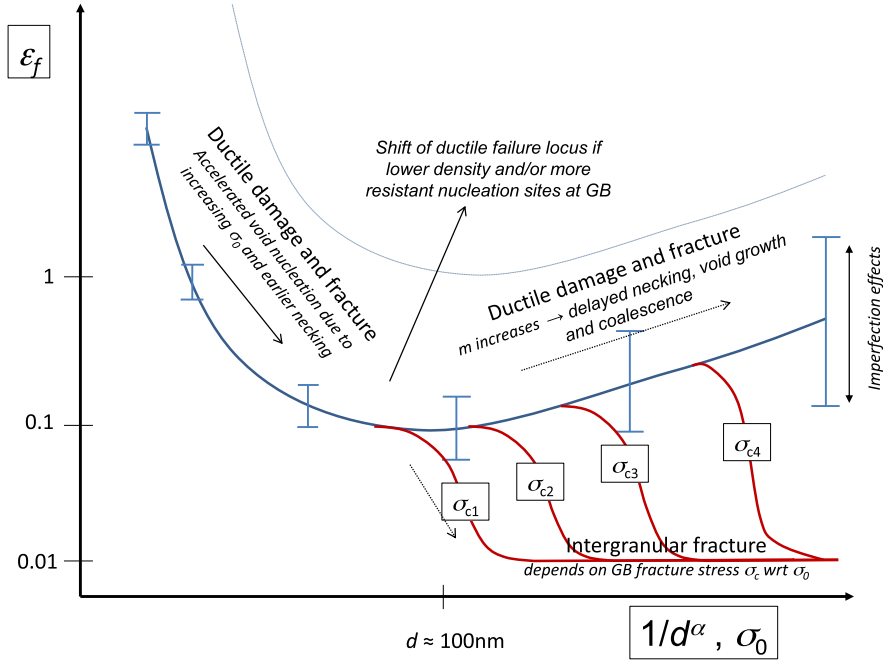

Fig. 21. Schematic illustration of the variation of the true fracture strain with respect to the yield stress (which is directly connected to the grain size d or film thickness). It shows the variation of the fracture strain as controlled by a ductile damage mechanism involving different factors that can play a role when changing grain size and the competition with a more brittle intergranular failure mode which primarily depend on the cohesion of GBs.

fracture toughness of freestanding evaporated Cu films with thickness between 100 and 800 nm demonstrating an increase of K_{Ic} from 2.3 MPa$\sqrt{m}$ to 7.8 MPa$\sqrt{m}$, in agreement with earlier measurements by Keller [402]. The specimens were much larger than the plastic zone size. We propose to re-analyze here these results in the context of the known linear dependence of the crack tip necking energy as a function of thickness in thin sheets as addressed in [207] but with the additional complexity that the yield stress decreases with increasing thickness. The yield stress of the 100 nm film is around 3 times larger than in 800 nm thick films, giving, to first order, an expected factor 8/3 increase of K_{Ic}, which agrees well with the measurements. Hosakawa et al. [403] measured $K_{Ic} = 0.45$ MPa$\sqrt{m}$ in ~250 nm Au films and $K_{Ic} = 0.5$ MPa$\sqrt{m}$ in Al films. These low values prove again, as explained in Section 3.3, that a high fracture toughness necessarily requires a large fracture process zone to allow for enough dissipation and for crack tip shielding over a sufficiently large volume of material, and there is thus an unavoidable size constraint on the possible enhancement of the fracture toughness in thin films. Nevertheless, toughening mechanisms can still be promoted with possible modest improvement of the resistance to tearing. For instance, Hattar et al. [404] have shown that in 200-nm thick sputter deposited Al involving small grain sizes down to 35 nm, the larger grains (up to 420 nm size) stop intergranular cracks by crack tip blunting through GB mediated deformation mechanisms. This is another example of the interest of bimodal structures, here to arrest cracks. Nanotwins have also the potential to improve the tearing resistance by a crack blunting and bridging mechanisms, as shown by Kim et al. on Cu films [405], or by forcing crack blunting, deflection, twinning/detwinning and slip transmission across the CTBs such as recently found in Ag films [406]. Note that in the study by Kim et al. [405], they found, in agreement with the beginning of the message of this section, a transition between brittle intergranular fracture and a ductile mechanism assisted by the nanotwin bridging mechanism when increasing thickness above 40 nm. Kumar et al. [407] observed an unexpected phase transformation in 200 nm thick Al films with 60 nm grain size, owing to the extremely large stresses building up as a result of the absence of dislocation activity and diffusion mechanisms, with a significant toughening potential. A final example of toughening by composite microstructure has been recently demonstrated for 100 nm thick Cu matrix - Cr pillar inclusions films [408] where the weak interface favours crack deviation. There are still only very few studies on crack propagation in thin metallic films and the modelling of the link between the microstructure, deformation mechanisms and crack initiation and tearing resistance is almost absent from the current literature.

5.4. Fatigue

The fatigue of thin metallic films presents many commonalities with bulk NC systems. The impossibility to create dislocation fatigue substructures and to form persistent slip bands has been demonstrated in many research studies. A majority of studies deal with films cyclically deformed on polymer substrates, as already partly addressed in Section 4.3, but not from the viewpoint of the underlying physical mechanisms. In an investigation on the cyclic behavior of magnetron sputter deposited Cu films with thickness from 0.4 to 3 μm and grain size from 250 to 750 nm or from 1 to 2.5 μm after annealing, Zhang and coworkers (see [326] and also references therein) have concluded that both the grain size and film thickness affect the fatigue behavior. Only grain sizes above 3 μm involve the generation of clear dislocation walls while only individual dislocations develop for grain size below 1 μm. Extrusions, whose dimensions have been quantitatively measured in the same study, occur in the large grains for almost all films, with dimensions decreasing with decreasing grain size and film thickness. GB and TB damage become the dominating crack initiation mechanisms at the smallest grain sizes. This work confirms earlier findings on Cu films [325,327], which were also recently found in Ag films [328].

Only a very small number of studies have been devoted to the fatigue of truly freestanding submicron metallic films. Recently, Hosseinian and Pierron [356] used their novel *in situ* TEM MEMS based set up, see Section 5.1, to perform cyclic tests on e-beam evaporated 100 nm thick, 100 μm long, 1.5 μm wide Au samples, with a grain size distribution spread over the range 10 to 400 nm. A ratcheting behavior under tension-tension cyclic loading was observed under stress controlled loading conditions. Nanosized fatigue cracks were observed after 7000 cycles at a maximum stress equal to 75% of the tensile strength. Large amounts of dislocations were observed at the tip of these fatigue cracks. On the contrary, Kumar et al. [409] did not observe any formation of fatigue cracks after 10 million cycles in Al thin films when deformed cyclically with maximum applied strain equal to 0.4%. Meirom et al. [342] measured the $\Delta a/\Delta N$ versus ΔK response in 1 μm thick Pt films involving either very elongated columnar grains or multiple equiaxed grains along the thickness (these two morphologies exhibit almost identical uniaxial stress strain response), see also [410]. The fatigue crack resistance was found independent of the grain morphology. An intriguing transition was observed from intergranular crack growth at low ΔK to transgranular at large ΔK. Recently, Zhang et al. [382] proved that the doping of GB of Cu thin films (on polymer substrate) with significant Zr (in the form of an amorphous phase) could lead to prolonged fatigue lifetime through depressing microcrack nucleation and through the arrest of intergranular cracks. These few examples show that the fatigue of thin metallic films remains a very open field of research due to the possible complex interplay of the possible deformation and fracture mechanisms.

6. Conclusion and perspectives

The “Achilles' heel” of nanostructured metals is their resistance to failure. This overview has shown that when looking carefully at the data, the problem is most often related to either a lack of resistance to plastic localization or to processing defects, and not primarily to a true lack of resistance to damage, except when interface and grain boundaries are weakened, or to a problem of resistance to fatigue.

The resistance to plastic localization has been studied using different kinds of models, from advanced strain gradient plasticity approaches to more simple imperfection based analyses. Over the past decade, many remedies have been proposed to enhance resistance to diffuse or localized necking:

- Increase the intrinsic strain hardening capacity of the deformation mechanisms without too much lowering the initial strength by favouring the presence of nano-twins, by triggering TRIP and TWIP mechanisms in retained austenite, by playing with bimodal or multimodal grain size distribution, through multiphase architecturing, and/or by lowering the temperature. The question of the respective and optimum contributions of isotropic versus kinematic hardening contribution is not fully resolved, but it is clear that favouring kinematic and isotropic hardening effects at large strains (such as with TRIP or TWIP based effects) should be more systematically investigated in NC metals. Moreover, the tensile properties of these new materials should be investigated over a wider range of temperature and strain rate.

- Increase the strain rate sensitivity by favouring thermally activated mechanism such as GB sliding, grain growth dislocation nucleation dominated plasticity, though not at the expense of a too large reduction of strength and strain hardening. This last trade off requires more investigations. Sometimes, deforming at low rates is a way to reach high rate sensitivity, an option that can be used for forming operations.
- By extrinsic delocalization of necking through matching the metal with a soft polymer substrate or by playing with multilayered or graded structures.

The application to thin films of advanced localization/bifurcation analyses accounting for imperfections, rate sensitivity and texture is a very open field of investigation.

The fracture mechanisms are primarily intergranular brittle type or growth and coalescence of voids nucleated at GBs and triple junctions. Experimental tools exist nowadays to investigate these physical mechanisms quantitatively owing to *in situ* methods. Atomistic simulations are also available, but micromechanical models are very much lacking. The fracture strain can be enhanced by:

- Favouring clean GB with the best possible character to resist decohesion, which is positive for both mechanisms. More researches are needed on GB characterization (e.g. with atom probe methods) and engineering for NC metals. Of course, there is an intrinsic limit which is reached when the yield stress is so large it leads to stress near the theoretical interface or grain boundary stress.
- Limiting the yield stress to a level that prevents vast intergranular decohesion in order to maintain a high strength/fracture strain balance.
- Limiting the sources for GB damage in the form of second phase precipitates.

Regarding the initiation and propagation of cracks, the difficulty is first to validate the use of fracture mechanics due to small size of samples or natural small thickness of thin films which can make irrelevant comparisons among test data for different materials. There are still very few results showing the influence of test temperature. This parameter can play a key role in materials exhibiting a strong strain rate effect or in NC steels containing unstable austenite. Also, relaxation mechanisms by grain growth or grain boundary sliding can sometimes be so active that stress singularity cannot build up and the simple notion of stress concentration loses significance. Another key issue is that high fracture toughness requires triggering damage phenomena over large regions in order to allow dissipation in large fracture process zone and offer high crack tip shielding. The hybridization strategy by combining a NC structure with additional features like nanotwins, graded layer, multiphases, predefined non percolating crack paths offer different ways to improve fracture resistance.

Regarding fatigue, the investigations are still essentially limited to pure metals such as Ni and Cu. Very few results on engineering structural materials (Al alloys, steels, Zr alloys, etc.) are available. A special attention must be given to the preparation of the free surface of the samples and in testing the materials over a wide range of fatigue life. This is especially true for fatigue loading which is extremely sensitive to the preparation of the free surface. The existing results show that the conventional fatigue endurance of NC metals tends to be larger than in CG counterparts. The effect of residual stresses on these results is not known. The fatigue crack growth rate of these NC materials is usually larger than that of CG metals, except in Ni-Co alloys. The role of existing twins in NC/NT materials seems to play a predominant role to control the crack propagation rate. This suggests that both the crack initiation behavior and crack propagation rates can be improved in low stacking fault energy alloys using NC microstructures, provided that the microstructure is stabilized to limit the de-twinning effect. This would require further fundamental and detailed studies on the interaction between intersecting twins and on the interaction between moving dislocations and existing twins, with a special emphasis on cyclic loading.

A systematic scientific strategy which integrates all the solutions indicated above in order to develop high performance NC metals in terms of enhanced balance of strength, resistance to localization, fracture and fatigue, using a multiscale approach of architectured materials remains in its infancy. Bimodal structures if properly designed are usually beneficial to the resistance to plastic localization, to static cracking and to fatigue. Control of the defects along the interfaces whether these are precipitates, ledges or chemical impurities, is one of the grand challenges. Finding the best trade-off between strain hardening and rate sensitivity is a very open question as well. The cross-fertilization between the discoveries and idea put forward in the different sub-communities dealing with bulk UFG/NC metals, flexible electronics and metallic thin films and nanowires research offers many opportunities along these lines.

Acknowledgments

The support of the Belgian Science Policy through the IAP 7/21 project as well as of the “Communauté Française de Belgique” under the program “Actions de Recherche Concertées” ARC 05/10-330 and ARC Convention No11/16-037 are gratefully acknowledged by TP. AAB acknowledges support from the National Science Foundation (Grant Number DMR-0844082) through the International Institute for Multifunctional Materials for Energy Conversion (IIMEC) established at Texas A&M University. A. Pineau would like to acknowledge the Ecole des Mines, the Ministry of Industry, the French CNRS, industry laboratories such as Snecma, ArcelorMittal, EDF, AREVA and many others, and research organizations, such as CEA and Onera, which have largely contributed to the development of his research. He would like, together with AAB and TP, to thank also all of his undergraduate and PhD students. Without them it would have been impossible to develop his research agenda.

References

[1] A. Pineau, A.A. Benzerga, T. Pardoen, Acta Mater. 107 (2016) 424–483.
[2] A. Pineau, D.L. McDowell, E.P. Busso, S.D. Antolovich, Acta Mater. 107 (2016) 484–507.
[3] H. Gleiter, Prog. Mater. Sci. 33 (1989) 223–315.
[4] M.A. Meyers, A. Mishra, D.J. Benson, Prog. Mater. Sci. 51 (2006) 427.
[5] K.S. Kumar, H. Van Swygenhoven, S. Suresh, Acta Mater. 51 (2003) 5743–5774.
[6] J.R. Greer, J.T.M. De Hosson, Prog. Mater. Sci. 56 (2011) 654–724.
[7] M. Dao, L. Lu, R.J. Asaro, J.T.M. De Hosson, E. Ma, Acta Mater. 55 (2007) 4041.
[8] M.D. Uchic, P.A. Shade, D.M. Dimiduk, Ann. Rev. Mater. Res. 39 (2009) 361–386.
[9] X. Li, Y. Wei, L. Lei, K. Lu, H. Gao, Nature 464 (2010) 877–880.
[10] J.W. Hutchinson, Z. Suo, Adv. Appl. Mech. 29 (1992) 63.
[11] T. Li, Z. Suo, Int. J. Solids Struct. 43 (2006) 2351–2363.
[12] D.S. Gianola, D.H. Warner, J.F. Molinari, K.J. Hemker, Scr. Mater. 55 (2006) 649.
[13] M. Coulombier, A. Boe, C. Brugger, J.P. Raskin, T. Pardoen, Scr. Mater. 62 (2010) 742–745.
[14] R.Z. Valiev, R.K. Islamgaliev, I.V. Alexandrov, Prog. Mater. Sci. 45 (2000) 103–189.
[15] R.Z. Valiev, T.G. Langdon, Prog. Mater. Sci. 51 (2006) 881–981.
[16] Y. Estrin, A. Vinogradov, Acta Mater. 61 (2013) 782–817.
[17] Y.M. Wang, E. Ma, Acta Mater. 52 (2004) 1699–1709.
[18] J.S. Carpenter, S.C. Vogel, J.E. LeDonne, D.L. Hammon, I.J. Beyerlein, N.A. Mara, Acta Mater. 60 (2012) 1576–1586.
[19] S.J. Zheng, I.J. Beyerlein, J. Wang, J.S. Carpenter, W.Z. Han, N.A. Mara, Acta Mater. 60 (2012) 5858–5866.

[20] B. Huang, K.N. Ishihara, P.H. Shingu, J. Mater. Sci. Lett. 19 (2000) 1763–1765.
[21] Y. Watanabe, K.N. Ishihara, P. Hideo Shingu, Scr. Mater. 44 (2001) 1853–1857.
[22] H.S. Shahabi, M. Eizadjou, H. Danesh Manesh, Mater. Sci. Eng. A 527 (2010) 5790–5795.
[23] L. Thilly, O. Ludwig, M. Veron, F. Lecouturier, J.P. Peyrade, S. Askenazy, Philos. Mag. A 82 (2002) 925.
[24] T.H. Fang, W.L. Li, N.R. Tao, K. Lu, Science 33 (2011) 1587–1590.
[25] X. Wu, P. Jiang, L. Chen, F. Yuan, Y.T. Zhu, Proc. Natl. Acad. Sci. U.S.A. 111 (2014) 7197.
[26] S. Jin, D. Huang, J.W. Morris, Metall. Trans. 7A (1976) 637–645.
[27] A. Lambert, J. Drillet, A.F. Gourgues, T. Sturel, A. Pineau, Sci. Technol. Weld. Joining 5 (2000) 168–173.
[28] F. Maresca, V.G. Kouznetsova, M.G.D. Geers, J. Mech. Phys. Solids 73 (2014) 69–83.
[29] G. Gao, H. Zhang, X. Gui, P. Luo, Z. Tun, B. Bai, Acta Mater. 76 (2014) 425–433.
[30] H.-W. Yen, S.W. Ooi, M. Elzadjou, A. Breen, C.-Y. Huang, H.K.D.H. Bhadeshia, S.P. Ringer, Acta Mater. 82 (2015) 100–114.
[31] R.J. Perez, B. Huang, E.J. Lavernia, Nanostruct. Mater. 7 (1996) 565–572.
[32] B.Q. Han, Z. Lee, D. Witkin, S. Nutt, E.J. Lavernia, Metall. Mater. Trans. A 36 (2005) 957–965.
[33] F. Zhou, X.Z. Liao, Y.T. Zhu, S. Dallek, E.J. Lavernia, Acta Mater. 51 (2003) 2777–2791.
[34] S. Cheng, E. Ma, Y.M. Wang, L.J. Kecskes, K.M. Youssef, C.C. Koch, U.P. Trociewitz, K. Han, Acta Mater. 53 (2005) 1521–1533.
[35] Y. Zhao, Topping, J.F. Bingert, J.J. Thornton, A.M. Dangelewicz, Y. Li, W. Liu, Y. Zhu, Y. Zhou, E.J. Lavernia, Adv. Mater. 20 (2008) 3028–3033.
[36] Q. Huang, N. Baluc, Y. Dai, S. Jitsukawa, A. Kimura, J. Konys, R.J. Kurtz, R. Lindau, T. Muroga, G.R. Odette, B. Raj, R.E. Stoller, L. Tan, H. Tanigawa, A. Tavassoli, T. Yamamoto, F. Wan, Y. Wu, J. Nucl. Mater. 442 (2013) S2–S8.
[37] U. Erb, Nanostruct. Mater. 6 (1995) 533–538.
[38] K.S. Kumar, S. Suresh, M.F. Chisholm, J.A. Horton, P. Wang, Acta Mater. 51 (2003) 387–405.
[39] Z. Budrovic, H. Van Swygenhoven, P.M. Derlet, S. Van Petegem, B. Schmitt, Science 304 (2004) 273.
[40] M. Dao, L. Lu, Y.F. Shen, S. Suresh, Acta Mater. 5421 (2006) 5421–5432.
[41] Q.S. Pan, L. Lu, Acta Mater. 81 (2014) 248–257.
[42] L. Lu, Y.F. Shen, X.H. Chen, L.H. Qian, K. Lu, Science 304 (2004) 422–426.
[43] H. Natter, M. Schmelzer, R. Hempelmann, J. Mater. Res. 13 (1998) 1186–1197.
[44] A.J. Detor, C.A. Schuh, Acta Mater. 55 (2007) 371–379.
[45] K. Lu, J.T. Wang, W.D. Wei, J. Appl. Phys. 69 (1991) 522–524.
[46] K. Lu, Mater. Sci. Eng. R 16 (1996) 161–221.
[47] V. Haas, H. Gleiter, R. Birringer, Scr. Metall. 28 (1993) 721–724.
[48] P.G. Sanders, G.E. Fougere, L.J. Thompason, J.A. Eastma, J.R. Weertman, Nanostruct. Mater. 8 (1997) 243–252.
[49] J.Q. Su, T.W. Nelson, C.J. Sterling, J. Mater. Res. 18 (2003) 1757–1760.
[50] X. Zhang, A. Misra, Scr. Mater. 66 (2012) 860–865.
[51] B. Wang, H. Idrissi, H. Shi, M.S. Colla, S. Michotte, J.P. Raskin, T. Pardoen, D. Schryvers, Scr. Mater. 66 (2012) 866–871.
[52] B. Wang, H. Idrissi, M. Galceran, M.S. Colla, S. Turner, S. Hui, J.P. Raskin, T. Pardoen, S. Godet, D. Schryvers, Int. J. Plast. 37 (2012) 140–156.
[53] M. Verdier, H. Huang, F. Spaepen, J.D. Embury, H. Kung, Philos. Mag. 86 (2006) 5009–5016.
[54] E.G. Fu, Li Nan, A. Misra, R.G. Hoagland, H. Wang, X. Zhang, Mater. Sci. Eng. A 493 (2008) 283–287.
[55] D. Bhattacharyya, N.A. Mara, P. Dickerson, R.G. Hoagland, A. Misra, J. Mater. Res. 24 (2009) 1291–1302.
[56] T.A. Wynn, D. Bhattacharyya, D.L. Hammon, A. Misra, N.A. Mara, Mater. Sci. Eng. A 564 (2013) 213–217.
[57] D. Kiener, C. Motz, M. Rester, M. Jenko, G. Dehm, Mater. Sci. Eng. A 459 (2007) 262–272.
[58] M.B. Lowry, D. Kiener, M.M. Leblanc, C. Chisholm, J.N. Florando, J.W. Morris, A.M. Minor, Acta Mater. 58 (2010) 5160–5167.
[59] H. Idrissi, S. Turner, M. Mitsuhara, B. Wang, S. Hata, M. Coulombier, J.P. Raskin, T. Pardoen, G. Van Tendeloo, D. Schryvers, Microsc. Microanal. 17 (2011) 983–990.
[60] J. Eymery, X. Chen, C. Durand, M. Kolb, G. Richter, C. R. Phys. 14 (2013) 221–227.
[61] G. Richter, K. Hillerich, D.S. Gianola, R. Mönig, O. Kraft, C.A. Volkert, Nano Lett. 9 (2009) 3048–3052.
[62] U.F. Kocks, H. Mecking, Prog. Mater. Sci. 48 (2003) 171–273.
[63] E.O. Hall, Proc. Phys. Soc. London, Sect. B 64 (1951) 747.
[64] N.J. Petch, J. Iron Steel Inst. London 173 (1953) 25.
[65] T.J. Massart, T. Pardoen, Acta Mater. 58 (2010) 5768–5781.
[66] C.Y. Yu, P.W. Kao, C.P. Chang, Acta Mater. 53 (2005) 4019.
[67] P. Bhaskar, A. Dasgupta, V.S. Sarma, U.K. Mudali, S. Saroja, Mater. Sci. Eng. A 616 (2014) 71–77.
[68] C.W. Sinclair, W.J. Poole, Y. Bréchet, Scr. Mater. 55 (2006) 739–742.
[69] M. Delincé, P.J. Jacques, Y. Bréchet, J.D. Embury, M.G.D. Geers, T. Pardoen, Acta Mater. 55 (2007) 2337–2350.
[70] N.A. Fleck, J.W. Hutchinson, J. Mech. Phys. Solids 49 (2001) 2245–2271.
[71] C.J. Bayley, W.A.M. Brekelmans, M.G.D. Geers, Int. J. Solids Struct. 43 (2006) 7268–7286.
[72] M. Kuroda, V. Tvergaard, J. Mech. Phys. Solids 56 (2008) 1591–1608.
[73] A.G. Evans, J.W. Hutchinson, Acta Mater. 57 (2009) 1675–1688.
[74] N.A. Fleck, J.R. Willis, J. Mech. Phys. Solids 57 (2009) 1045–1057.
[75] P. Gudmundson, J. Mech. Phys. Solids 52 (2004) 1379–1406.
[76] K.E. Aifantis, J.R. Willis, Mech. Mater. 38 (2006) 702–716.
[77] C.F.O. Dahlberg, J. Faleskog, C.F. Niordson, B.N. Legarth, Int. J. Plast. 43 (2013) 177–195.
[78] D.S. Balint, V.S. Deshpande, A. Needleman, E. Van der Giessen, Int. J. Plast. 24 (2008) 2149–2172.
[79] A.A. Benzerga, Y. Bréchet, A. Needleman, E. Van der Giessen, Modell. Simul. Mater. Sci. Eng. 12 (2004) 159–196.
[80] A.A. Benzerga, Y. Bréchet, A. Needleman, E. Van der Giessen, Acta Mater. 53 (2005) 4765–4779.
[81] P.J. Guruprasad, Scale Effects in Crystal Plasticity (Ph.D. thesis), Texas A&M University, 2010.
[82] H. Van Swygenhoven, P.M. Derlet, A.G. Froseth, Acta Mater. 54 (2006) 1975–1983.
[83] W. Lojkowski, H. Kirchner, M. Grabski, Scr. Metall. 11 (1977) 1127.
[84] Y. Ivanisenko, L. Kurmanaeva, J. Weissmueller, K. Yang, J. Markmann, H. Rosner, T. Scherer, H.J. Fecht, Acta Mater. 57 (2009) 3391–3401.
[85] P. Liu, S. Mao, L. Wang, X. Han, Z. Zhang, Scr. Mater. 64 (2011) 343–346.
[86] T. Rupert, D. Gianola, Y. Gan, K. Hemker, Science 326 (2009) 1686–1690.
[87] K. Zhang, J.R. Weertman, J.A. Eastman, Appl. Phys. Lett. 87 (2005) 061921.
[88] D.S. Gianola, S. Van Petegem, M. Legros, S. Brandstetter, H. Van Swygenhoven, K.J. Hemker, Acta Mater. 54 (2006) 2253–2263.
[89] M. Legros, D.S. Gianola, K.J. Hemker, Acta Mater. 56 (2008) 3380–3393.
[90] T. Gorkaya, D.A. Molodov, G. Gottstein, Acta Mater. 57 (2009) 5396–5405.
[91] F. Mompiou, D. Caillard, M. Legros, Acta Mater. 57 (2009) 2198–2209.
[92] L. Li, S. Van Petegem, H. Van Swygenhoven, P.M. Anderson, Acta Mater. 60 (2012) 7001–7010.
[93] G. Saada, T. Kruml, Acta Mater. 59 (2011) 2565–2574.
[94] J. Chen, L. Lu, K. Lu, Scr. Mater. 54 (2006) 1913–1918.
[95] Q. Wei, J. Mater. Sci. 42 (2007) 1709–1727.
[96] S. Van Petegem, S. Brandstetter, H. Van Swygenhoven, J.L. Martin, Appl. Phys. Lett. 89 (2006) 073102.
[99] J.W. Christian, S. Mahajan, Prog. Mater. Sci. 39 (1995) 1–157.
[100] L. Remy, Metall. Trans. 12A (1981) 387–408.
[101] L. Remy, Acta Mater. 26 (1978) 443–451.
[102] Y.T. Zhu, X.Z. Liao, X.L. Wu, Prog. Mater. Sci. 57 (2012) 1–62.
[103] L. Zhu, H. Ruan, X. Li, M. Dao, H. Gao, J. Lu, Acta Mater. 59 (2011) 5544–5557.
[104] Y.T. Zhu, X.Z. Liao, X.L. Wu, J. Narayan, J. Mater. Sci. 48 (2013) 4467–4475.
[105] V. Yamakov, D. Wolf, S.R. Phillpot, A.K. Mukherjee, H. Gleiter, Nat. Mater. 1 (2002) 45–49.
[106] L. Lu, R. Schwaiger, Z.W. Shan, M. Dao, K. Lu, S. Suresh, Acta Mater. 53 (2005) 2169–2179.
[107] R.J. Asaro, S. Suresh, Acta Mater. 53 (12) (2005) 3369–3382.
[108] P. Gu, M. Dao, S. Suresh, Acta Mater. 67 (2014) 409–417.
[109] K.A. Afanasyev, F. Sansoz, Nano Lett. 7 (2007) 2056–2062.
[110] Z.H. Jin, P. Gumbsch, K. Albe, E. Ma, K. Lu, H. Gleiter, H. Hahn, Acta Mater. 56 (2008) 1126–1135.
[111] H. Idrissi, M.S. Colla, B. Wang, D. Schryvers, J.P. Raskin, T. Pardoen, Adv Mater. 23 (2011) 2119–2122.
[112] S.R. Agnew, A. Yu, A.Y. Vinogradov, S. Hashimoto, J.R. Weertman, J. Electron. Mater. 28 (1999) 1038–1044.
[113] A. Pineau, Philos. Trans. R. Soc. A 373 (2015) 20140131.
[114] B.-G. Yoo, S.T. Boles, Y. Liu, X. Zhang, R. Schwaiger, C. Eberl, O. Kraft, Acta Mater. 81 (2014) 184–193.
[115] J. Wang, N. Li, O. Anderoglu, X. Zhang, A. Misra, J.Y. Huang, J.P. Hirth, Acta Mater. 58 (2010) 2262–2270.
[116] Y.B. Wang, M.L. Sui, E. Ma, Philos. Mag. Lett. 87 (2007) 935–942.
[117] Z. Shan, L. Lu, A. Minor, E. Stech, S. Mao, JOM 60 (2008) 71–74.
[118] J.P. Hirth, R.C. Pond, J. Lothe, Acta Mater. 54 (2006) 4237–4245.
[119] J.W. Cahn, Y. Mishin, A. Suzuki, Acta Mater. 54 (2006) 4953–4975.
[120] H. Mirkhani, S.P. Joshi, J. Mech. Phys. Solids 68 (2014) 107–133.
[121] P.B. Chowdhury, H. Sehitoglu, R.G. Rateick, H.J. Maier, Acta Mater. 61 (2013) 2531–2547.
[122] Y. Wang, M. Chen, F. Zhou, E. Ma, Nature 419 (2002) 912–915.
[123] T. Pardoen, T.J. Massart, C. R. Méc. 340 (2012) 247–260.
[124] Y. Mine, H. Takashima, M. Matsuda, K. Takashima, Mater. Sci. Eng. A560 (2013) 535–544.
[125] L. Mazzoni, T. Pardoen, T.J. Massart, Eur. J. Mech. A. Solids 29 (2010) 132–142.
[126] L. Mazzoni, T. Pardoen, T.J. Massart, Int. J. Solids Struct. 45 (2008) 5397–5418.
[127] J. Wang, A. Misra, Curr. Opin. Solid State Mater. Sci. 15 (2011) 20–28.
[128] J.D. Embury, J.P. Hirth, Acta Metall. Mater. 42 (1994) 2051–2056.
[129] J. Wang, R.G. Hoagland, J.P. Hirth, A. Misra, Acta Mater. 56 (2008) 3109–3119.
[130] I.J. Beyerlein, J.R. Mayeur, R.J. McCabe, S.J. Zheng, J.S. Carpenter, N.A. Mara, Acta Mater. 72 (2014) 137–147.
[131] S.B. Lee, LeDonne, S.C.V. Lim, Beyerlein, A.D. Rollett, Acta Mater. 60 (2012) 1747–1761.
[132] J.S. Carpenter, S.C. Vogel, J.E. LeDonne, D.L. Hammon, I.J. Beyerlein, N.A. Mara, Acta Mater. 60 (2016) 1576–1586.
[133] A. Bellou, C.T. Overman, H.M. Zbib, D.F. Bahr, A. Misra, Scr. Mater. 64 (2011) 641–644.

[134] W. Guo, E.A. Jagle, P.P. Choi, J. Yao, A. Kostka, J.M. Schneider, D. Raabe, Phys. Rev. Lett. 113 (2014) 035501.
[135] J.Y. Zhang, Y. Liu, J. Chen, Y. Chen, G. Liu, X. Zhang, J. Sun, Mater. Sci. Eng. A 552 (2012) 392–398.
[136] R. Venkatraman, J.C. Bravman, Mater. Res. 7 (1992) 2040.
[137] L.B. Freund, S. Suresh, Thin Film Materials, Cambridge University Press, U.K., 2003.
[138] J.W. Matthews, S. Mader, T.B. Light, J. Appl. Phys. 41 (1970) 3800–3804.
[139] S.I. Rao, D.M. Dimiduk, T.A. Parthasarathy, M.D. Uchic, M. Tang, C. Woodward, Acta Mater. 56 (2008) 3245–3259.
[140] A.A. Benzerga, Int. J. Plast. 24 (2008) 1128–1157.
[141] A.A. Benzerga, N.F. Shaver, Scr. Mater. 54 (2006) 1937–1941.
[142] T.A. Parthasarathy, S.I. Rao, D.M. Dimiduk, M.D. Uchic, D.R. Trinkle, Scr. Mater. 56 (2007) 313–316.
[143] J.A. El-Awady, Nat. Commun. 6 (2015) 5926.
[144] A.A. Benzerga, J. Mech. Phys. Solids 57 (2009) 1459–1469.
[145] C. Brugger, M. Coulombier, T.J.M. Massart, J.P. Raskin, T. Pardoen, Acta Mater. 58 (2010) 4940–4949.
[146] L. Nicola, E. van der Giessen, A. Needleman, Thin Solid Films 479 (2005) 329–338.
[147] F. Mompiou, M. Legros, M. Coulombier, J.P. Raskin, T. Pardoen, Acta Mater. 61 (2013) 205–216.
[148] H. Idrissi, A. Kobler, B. Amin-Ahmadi, M. Coulombier, M. Galceran, J.P. Raskin, S. Godet, C. Kubel, T. Pardoen, D. Schryvers, Appl. Phys. Lett. 104 (2014) 101903.
[149] Z.X. Wu, Y.W. Zhang, M.H. Jhon, D.J. Srolovitz, Acta Mater. 61 (2013) 5807–5820.
[150] M. Coulombier, Nanomechanical la on-chip for Testing Thin Film Materials and Application to Al and Al(Si)(Ph.D. dissertation), Université catholique de Louvain, 2012.
[151] K. Jonnalagadda, N. Karanjgaokar, I. Chasiotis, J. Chee, D. Peroulis, Acta Mater. 58 (2010) 4674–4684.
[152] M.S. Colla, B. Amin-Ahmadi, H. Idrissi, L. Malet, S. Godet, J.P. Raskin, D. Schryvers, T. Pardoen, Nat. Commun. 6 (2015) 5922.
[153] M.S. Colla, Plasticity and creep in thin free-standing nanocrystalline Pd films (Ph.D. dissertation), Université catholique de Louvain, 2014.
[154] G. Guisbiers, M.S. Colla, M. Coulombier, J.P. Raskin, T. Pardoen, J. Appl. Phys. 113 (2013) 024513.
[155] D. Weiss, H. Gao, E. Arzt, Acta Mater. 49 (2001) 2395–2403.
[156] J.S. Stolken, A.G. Evans, Acta Mater. 46 (1998) 5109–5115.
[157] N.A. Fleck, G.M. Muller, M.F. Ashby, J.W. Hutchinson, Acta. Metall. Mater. 42 (1994) 475–487.
[158] H.H.M. Cleveringa, E. Van der Giessen, A. Needleman, Int. J. Plast. 15 (1999) 837–868.
[159] E. Tarleton, D.S. Balint, J. Gong, A.J. Wilkinson, Acta Mater. 88 (2015) 271–282.
[160] D.S. Balint, V.S. Deshpande, A. Needleman, E. Van der Giessen, J. Mech. Phys. Solids 54 (2006) 2281–2303.
[161] P.J. Guruprasad, A.A. Benzerga, J. Mech. Phys. Solids 56 (2008) 132–156.
[162] D. Kiener, P.J. Guruprasad, S.M. Keralavarma, G. Dehm, A.A. Benzerga, Acta Mater. 59 (2011) 3825–3840.
[163] L. Nicola, Y. Xiang, J.J. Vlassak, E. Van der Giessen, A. Needleman, J. Mech. Phys. Solids 54 (2006) 2089–2110.
[164] J. Rajagopalan, J.H. Han, M.T. Saif, Science 315 (2007) 1137580.
[165] J. Rajagopalan, J.H. Han, M.T. Saif, Scr. Mater. 59 (2008) 921–926.
[166] J.G. Speer, E. De Moor, K.O. Findley, D.K. Matlock, B.C. De Cooman, D.V. Edmonds, Met. Trans. 42A (2011) 3591–3601.
[167] J.A. Sharon, H.A. Padilla, B.L. Boyce, J. Mater. Res. 28 (2013) 1539–1552.
[168] Z. Marciniak, K. Kuczynski, Int. J. Mech. Sci. 9 (1967) 609–620.
[169] J.W. Hutchinson, K.W. Neale, Acta Metall. 25 (1977) 839–846.
[170] W.F. Hosford, R.M. Caddell, Metal Forming - Mechanics and Metallurgy, Prentice Hall, 1993.
[171] T. Pardoen, J. Mech. Phys. Solids 62 (2014) 81–98.
[172] R. Schwaiger, I.S. Choi, M. Ames, R. Birringer, T. Neithardt, A. Castrup, O. Kraft, Submitted For Publication.
[173] F. Tang, D.S. Gianola, M.P. Moody, K.J. Hemker, J.M. Cairney, Acta Mater. 60 (2012) 1038–1047.
[174] J.R. Rice, Theor. Appl. Mech. (Ed. W.T. Koiter), 1976, pp. 207–220.
[175] R. Hill, J.W. Hutchinson, J. Mech. Phys. Solids 23 (1975) 239–264.
[176] X. Wu, Y.T. Zhu, Y.G. Wei, Q. Wei, Phys. Rev. Lett. 103 (2009) 205504.
[177] J.H. Lee, T.B. Holland, A.K. Mukherjee, X. Zhang, H. Wang, Sci. Rep. 3 (2013) 1061.
[178] L. Wang, X. Han, P. Liu, Y. Yue, Z. Zhang, E. Ma, Phys. Rev. Lett. 105 (2010) 135501.
[179] L. Lu, X. Chan, X. Huang, K. Lu, Science 323 (2009) 607–610.
[180] Y.F. Shen, L. Lu, Q.H. Lu, Z.H. Jin, K. Lu, Scr. Mater. 52 (2005) 989–994.
[181] T. Zhu, J. Li, A. Samanta, H.G. Kim, S. Suresh, Proc. Natl. Acad. Sci. U.S.A. 104 (2007) 3031–3036.
[182] M.S. Colla, B. Wang, H. Idrissi, D. Schryvers, J.P. Raskin, T. Pardoen, Acta Mater. 60 (2012) 1795–1806.
[183] H.W. Höppel, Z.M. Zhou, H. Mughrabi, J.R. Van, J. Electron. Mater. 28 (1999) 1038–1044.
[184] O. Bouaziz, S. Allain, C. Scott, Scr. Mater. 58 (2008) 484–487.
[185] P. Jacques, Q. Furnémont, S. Godet, T. Pardoen, K. Conlon, F. Delannay, Philos. Mag. 86 (2006) 2371–2392.
[186] P.J. Jacques, Q. Furnémont, F. Lani, T. Pardoen, F. Delannay, Acta Mater. 55 (2007) 3681–3693.
[187] L. Delannay, P. Jacques, T. Pardoen, Int. J. Solids Struct. 45 (2008) 1825–1843.
[188] M.J. Santofimia, L. Zhao, R. Petrov, C. Kwakernaak, W.G. Sloof, J. Siestma, Acta Mater. 59 (2011) 6059–6068.
[189] M.J. Santofimia, L. Zhao, Siestma, Metall. Mater. Trans. 42 (2011) 3620–3626.
[190] E. De Moor, D.K. Matlock, J.G. Speer, M.J. Merwin, Scr. Mater. 64 (2011) 185–188.
[191] S. Yan, X. Liu, W.J. Liu, H. Lan, H. Wu, Mater. Sci. Eng. A 620 (2014) 58–66.
[192] A. Arlazarov, O. Bouaziz, J.P. Masse, F. Kegel, Mater. Sci. Eng. A 620 (2014) 293–300.
[193] K. Zhang, P. Liu, Li Wei, Z. Guo, Y. Rong, Mater. Sci. Eng. A 619 (2014) 205–211.
[194] S.C. Hong, J.C. Ahn, S.Y. Nam, H.C. Yang, J.G. Speer, D.K. Matlock, Met. Mater. Int. 13 (2007) 439–445.
[195] E.P. Bagliani, M.J. Santofimia, L. Zhao, J. Siestma, E. Anelli, Mater. Sci. Eng. A559 (2013) 486–495.
[196] M. Delincé, P.J. Jacques, Y. Bréchet, J.D. Embury, M.G.D. Geers, T. Pardoen, Acta Mater. 55 (2007) 2337–2350.
[197] G. Liu, G.J. Zhang, F. Jiang, X.D. Ding, Y.J. Sun, J. Sun, E. Ma, Nat. Mater. 12 (2013) 344–350.
[198] F.K. Yan, G.Z. Liu, N.R. Tao, K. Lu, Acta Mater. 60 (2012) 1059–1071.
[199] A. Cetin, C. Bernardi, A. Mortensen, Acta Mater. 60 (2012) 2265–2276.
[200] D. Chae, D.A. Koss, Mater. Sci. Eng. A 366 (2004) 299–309.
[201] L. Babout, E. Maire, J.Y. Buffiere, R. Fougere, Acta Mater. 49 (2001) 2055–2063.
[202] L. Lecarme, E. Maire, K.C.A. Kumar, C. De Vleeschouwer, L. Jacques, A. Simar, T. Pardoen, Acta Mater. 63 (2013) 130–139.
[203] W.M. Yin, S.H. Wang, R. Mirshams, C.H. Xiao, Mater. Sci. Eng. A 301 (2001) 18–22.
[204] I.A. Ovid'ko, A.G. Sheinerman, N.V. Skiba, Acta Mater. 59 (2011) 678–685.
[205] H. Li, F. Ebrahimi, Adv Mater. 17 (2005) 1969–1972.
[206] T. Pardoen, Y. Marchal, F. Delannay, J. Mech. Phys. Solids 47 (1999) 2093–2123.
[207] T. Pardoen, F. Hachez, B. Marchioni, P.H. Blyth, A.G. Atkins, J. Mech. Phys. Solids 52 (2004) 423–452.
[208] R.A. Mirshams, C.H. Xiao, S.H. Whang, W.M. Yin, Mater. Sci. Eng. A 315 (2001) 21–27.
[209] A. Hohenwarter, R. Pippan, Philos. Trans. A 373 (2015) 20140366.
[210] A. Hohenwarter, A. Taylor, R. Stock, R. Pippan, Metall. Mater. Trans. A 42 (2011) 1609–1618.
[211] A. Hohenwarter, C. Kammerhofer, R. Pippan, J. Mater. Sci. 45 (2010) 4805–4812.
[212] J.R. Rice, M.A. Johnson, in: M.F. Kanninen, W.F. Adler, A.R. Rosenfield, R.I. Jaffee (Eds.), Inelastic Behavior of Solids, McGraw-Hill, 1970, pp. 641–672.
[213] V. Tvergaard, J.W. Hutchinson, J. Mech. Phys. Solids 40 (1992) 1377–1397.
[214] A. Pineau, T. Pardoen, Failure mechanisms of metals, in: Comprehensive Structural Integrity Encyclopedia, vol. 2, Elsevier, 2007 (Chap. 6).
[215] T. Pardoen, J.W. Hutchinson, Acta Mater. 51 (2003) 133–148.
[216] D. Farkas, H. Van Swygenhoven, P.M. Derlet, Phys. Rev. B 66 (2002) 60101.
[217] D. Farkas, S. Van Petegem, H.P.M. Derlet, H. Van Swygenhoven, Acta Mater. 53 (2005) 3115–3123.
[218] G.Q. Xu, M.J. Demkowicz, Phys. Rev. Lett. 111 (2013) 145501.
[219] I.A. Ovid'ko, A.G. Sheinerman, Acta Mater. 58 (2010) 5286–5294.
[220] I.A. Ovid'ko, A.G. Sheinerman, Scr. Mater. 60 (2009) 627–630.
[221] E.W. Qin, L. Lu, N.R. Tao, J. Tan, K. Lu, Acta Mater. 57 (2009) 6215–6225.
[222] A. Singh, L. Tang, M. Dao, L. Lu, S. Suresh, Acta Mater. 59 (2011) 2437–2446.
[223] M. Li, D. Guo, T. Ma, G. Zhang, Y. Shi, X. Zhang, Mater. Sci. Eng. A 606 (2014) 330–333.
[224] M. Haddad, Y. Ivanisenko, E. Courtois-Manara, H.J. Fecht, Mater. Sci. Eng. A 620 (2015) 30–35.
[225] A.Y. Vinogradov, V.V. Stolyarov, S. Hashimoto, R.Z. Valiev, Mater. Sci. Eng. A 318 (2001) 163–173.
[226] J. Frontan, Y. Zhang, M. Dao, J. Lu, F. Galvez, A. Jerusalem, Acta Mater. 60 (2012) 1353–1367.
[227] W.Z. Han, E.K. Cerreta, N.A. Mara, I.J. Beyerlein, J.S. Carpenter, S.J. Zheng, C.P. Trujillo, P.O. Dickerson, A. Misra, Acta Mater. 63 (2014) 150–161.
[228] N.A. Mara, D. Bhattacharyya, R.G. Hoagland, A. Misra, Scr. Mater. 58 (2008) 874–877.
[229] H. Mughrabi, Proced. Eng. 2 (2010) 3–26.
[230] H. Mughrabi, H.W. Höppel, Int. J. Fatigue 32 (2010) 1413–1427.
[231] H.W. Höppel, M. Göken, Nanostructured metals and alloys. Processing, microstructure, mechanical properties and applications, in: Sung H. Whang (Ed.), Published by Woodhead, 2011, pp. 507–538 (Chap. 17).
[232] L. Kunz, Mechanical properties of copper processed by severe plastic deformation, in Copper alloys - Early applications and current performance - Enhancing processes, in: L. Collini (Ed.), Published by InTech, Rijeka, Croatia, 2012, pp. 93–126 (Chapter 5).
[233] H.A. Padilla, B.L. Boyce, Exp. Mech. 50 (2010) 5–23.
[234] M.K. Wong, W.P. Kao, J.T. Lui, C.P. Chang, P.W. Kao, Acta Mater. 55 (2007) 715–725.
[235] L.R. Saitova, H.W. Höppel, M. Göken, L.P. Semenova, R.Z. Valiev, Int. J. Fatigue 31 (2009) 322–331.
[236] A.Y. Vinogradov, V.V. Stolyarov, S. Hashimoto, R.Z. Valiev, Mater. Sci. Eng.

A318 (2001) 163–173.
[237] A.Y. Vinogradov, Y. Kanako, K. Kitagawa, S. Hashimoto, V. Stolyarov, R. Valiev, Scr. Mater. 36 (1997) 1345–1351.
[238] Q.S. Pan, L. Lu, Acta Mater. 81 (2014) 248–258.
[239] R. Klemm, Doctorate thesis Zyklische Plastizität von mikro- und submikrokristallinem Nickel, Technische Universität, Dresden, 2004.
[240] H.W. Höppel, Z.M. Zhou, H. Mughrabi, R.Z. Valiev, Philos. Mag. A 82 (2002) 1781–1794.
[241] T. Hanlon, Y.-N. Kwon, S. Suresh, Scr. Mater. 49 (2003) 675–680.
[242] T. Hanlon, E.D. Tabachnikova, S. Suresh, Int. J. Fatigue 27 (2005) 1147–1158.
[243] Y. Furuya, S. Matsuoka, S. Shimakura, T. Hanamura, S. Tarizuka, Scr. Mater. 52 (2005) 1163–1167.
[244] M.E. Kamaya, J. Adv. Maint. 5 (2013) 185–200.
[245] C. Blochwitz, S. Jacob, W. Tirschler, Mater. Sci. Eng. A 496 (2008) 59–66.
[246] F.P.E. Dunne, Curr. Opin. Solid State Mater. Sci. 18 (2014) 170–179.
[247] G.T. Gray III, Acta Mater. Metall. 36 (1988) 1745–1754.
[248] S. Mahajan, Scr. Mater. 68 (2013) 95–99.
[249] J. Man, T. Vystavel, A. Weidner, I. Kubena, M. Patrenec, T. Kruml, Polak, J. Int. J. Fatigue 39 (2012) 44–53.
[250] M.D. Sangid, T. Ezaz, H. Sehitoglu, I.M. Robertson, Acta Mater. 59 (2011) 283–296.
[251] M.D. Sangid, H.J. Maier, H. Sehitoglu, J. Mech. Phys. Solids 59 (2011) 595–609.
[252] M.D. Sangid, H.J. Maier, H.J. Sehitoglu, Int. J. Plast. 27 (2011) 801–821.
[253] G.M. Castelluccio, D.L. McDowell, J. Mater. Sci. 48 (2013) 2376–2387.
[254] S. Fintova, L. Kunz, in: 6th Int Conf on Nanomaterials by Severe Plastic Deformation, IOP conf series: Materials Science and engineering, vol. 63, 2014, pp. 1–8.
[255] A. Vinogradov, J. Mater. Sci. 42 (2007) 1797–1808.
[256] P. Cavaliere, Int. J. Fatigue 31 (2009) 1476–1489.
[257] J. Horsky, G. Khabiti, B. Weiss, M.J. Zehetbauer, J. Alloys Compd. 509S (2011) S323–S327.
[258] Y. Yan, N. Yao, B. Imasogie, W.O. Soboyejo, Acta Mater. 55 (2007) 4305–4315.
[259] L. Collini, Eng. Fract. Mech. 77 (2010) 1001–1011.
[260] L. Collini, Fatigue crack resistance of ultrafine-grained copper structures, in: L. Collini (Ed.) Copper alloys - Early applications and current performance - Enhancing processes, Published by InTech, Rijaka, Croatia, 2012, pp. 127–150 (Chapter 6).
[261] M.D. Sangid, G.J. Pataky, H. Sehitoglu, R.G. Rateick, T. Niendorf, H.J. Maier, Acta Mater. 59 (2011) 7340–7355.
[262] P. Lukas, L. Kunz, Z. Knesl, B. Weiss, R. Stickler, Mater. Sci. Eng. 70 (1985) 91–100.
[263] H.-K. Kim, M.-Il. Choi, C.-S. Chung, D.H. Shin, Mater. Sci. Eng. A 340 (2003) 243–250.
[264] M.D. Chapetti, H. Migata, T. Tagawa, T. Miyata, M. Fujioka, Int. J. Fatigue 27 (2005) 235–243.
[265] T. Niendorf, F. Rubitschek, H.J. Maier, D. Canadinc, I. Karaman, J. Mater. Sci. 45 (2010) 4813–4821.
[266] Y. Estrin, A. Vinagradov, Int. J. Fatigue 32 (2010) 898–907.
[267] E. Avtokratova, U. Sitdikov, R. Kaibyshav, Y. Watanabe, Mater. Sci. Forum 584&586 (2008) 821–826.
[268] P.B. Chowdhury, H. Sehitoglu, R.G. Rateick, Int. J. Fatigue 68 (2014) 277–291.
[269] B. Budianski, J.W. Hutchinson, J. Appl. Mech. Trans. 45 (1978) 267–276.
[270] Y.J. Kim, K.-H. Schwalbe, Eng. Fract. Mech. 68 (2001) 163–182.
[271] Y.J. Kim, K.-H. Schwalbe, Eng. Fract. Mech. 68 (2001) 183–199.
[272] A. Zak, M.J. Williams, Appl. Mech. 30 (1963) 142–143.
[273] A. Romeo, R. Ballarini, Int. J. Fract. 65 (1994) 183–196.
[274] A. Romeo, R.J. Ballarini, Appl. Mech. 62 (1995) 614–619.
[275] A.S. Kim, J. Besson, A. Pineau, Int. J. Solids Struct. 36 (1999) 1845–1864.
[276] O. Kolednik, J. Predan, N. Gubeljak, D.F. Fisher, Mater. Sci. Eng. A 519 (2009) 172–183.
[277] R. Pippan, K. Flechsig, F.O. Riemelmoser, Mater. Sci. Eng. A 283 (2000) 225–233.
[278] H.O. Jacobs, A.R. Tao, A. Schwartz, D.H. Garcia, G.M. Whitesides, Science 296 (2002) 323–325.
[279] V. Lumensky, M.S. Shur, S. Wagner, IEEE Sens. J. 1 (2001) 41–51.
[280] H.C. Ko, M.P. Stoykovich, J. Song, V. Malyarchuk, W.M. Choi, C.J. Yu, J. Geddes III, J. Xiao, S. Wang, Y.Y. Huang, J.A. Rogers, Nature 454 (2008) 748–753.
[281] S. Befahy, S. Yunus, T. Pardoen, P. Bertrand, Appl. Phys. Lett. 91 (2007) 141911.
[282] R. Pelrine, R. Kornbluh, G. Kofod, Adv. Mater. 12 (2000) 1223–1225.
[283] D.J. Lipomi, B.C.K. Tee, M. Vosgueritchian, Z. Bao, Adv. Mater. 23 (2011) 1771–1775.
[284] C. Wang, W. Zheng, Z. Yue, C.O. Too, G.G. Wallace, Adv. Mater. 23 (2011) 3580–3584.
[285] S. Wagner, S. Bauer, MRS Bull. 37 (2012) 207–213.
[286] J.A. Rogers, T. Someya, Science 327 (2010) 1603–1607.
[287] D.H. Kim, J.L. Xiao, J. Song, Y. Huang, J.A. Rogers, Adv. Mater. 22 (2010) 2108–2124.
[288] J. Lohmiller, R. Baumbusch, M.B. Kerber, A. Castrup, H. Hahn, E. Schafler, M. Zehetbauer, O. Kraft, P.A. Gruber, Mech. Mater. 67 (2013) 65–73.
[289] P.A. Gruber, E. Arzt, R. Spolenak, J. Mater. Res. 24 (2009) 1906–1918.
[290] S. Frank, U.A. Handge, S. Olliges, R. Spolenak, Acta Mater. 57 (2009) 1442–1453.
[291] B.A. Latella, G. Triani, P.J. Evans, Scr. Mater. 56 (2007) 493–496.
[292] A.A. Taylor, M.J. Cordill, L. Bowles, J. Schalko, G. Dehm, Thin Solid Films 531 (2013) 354–361.
[293] M.J. Cordill, V.M. Marx, Philos. Mag. Lett. 93 (2013) 618–624.
[294] C. Chambers, S.P. Lacour, S. Wagner, Z. Suo, J. Huang, Mater. Res. Symp. Proc. 769 (2003) 325–330.
[295] N. Lambricht, T. Pardoen, S. Yunus, Acta Mater. 61 (2013) 540–547.
[296] A. Favache, L. Libralesso, P.J. Jacques, J.-P. Raskin, C. Bailly, B. Nysten, T. Pardoen, Thin Solid Films 550 (2014) 464–471.
[297] J.W. Hutchinson, Z. Suo, Adv. Appl. Mech. 29 (1992) 63–191.
[298] Z. Suo, Fracture in Thin Films, in Encyclopedia of Materials: Science and Technology, Elsevier Science, Amsterdam, 2001, pp. 3290–3296.
[299] A.G. Evans, J.W. Hutchinson, Acta Metall. Mater. 43 (1995) 2507–2530.
[300] J.L. Beuth, Int. J. Solids Struct. 29 (1992) 2945–2952.
[301] R. Huang, J. Prévost, Z. Huang, Z. Suo, Eng. Fract. Mech. 70 (2003) 2513–2526.
[302] H. Mei, Y. Pang, R. Huang, Int. J. Fract. 148 (2007) 331–342.
[303] M.D. Thouless, Z. Li, N.J. Douville, S. Takayama, J. Mech. Phys. Solids 59 (2011) 1927–1937.
[304] T. Li, Z. Suo, Int. J. Solids Struct. 44 (2007) 1696–1705.
[305] T. Li, Z. Huang, Z. Suo, Appl. Phys. Lett. 85 (2004) 18.
[306] T. Li, Z. Suo, Int. J. Solids Struct. 43 (2006) 2351–2353.
[307] T. Tsuchiya, M. Hirata, N. Chiba, R. Udo, Y. Yoshitomi, T. Ando, K. Sato, K. Takashima, Y. Higo, Y. Saotome, H. Ogawa, K. Ozaki, J. Microelectromech. Syst. 14 (2005) 903.
[308] H.D. Espinosa, B.C. Prorok, B. Peng, J. Mech. Phys. Solids 52 (2004) 667–689.
[309] M.F. Ashby, Y. Bréchet, Acta Mater. 51 (2003) 5801–5821.
[310] W.T.S. Huck, N. Bowden, P. Onck, T. Pardoen, J.W. Hutchinson, G.M. Whitesides, Langmuir 16 (2000) 3497–3501.
[311] D.Y. Khang, H. Jiang, Y. Huang, J.A. Rogers, Science 311 (2006) 208–212.
[312] O. Graudejus, Z. Jia, T. Li, S. Wagner, Scr. Mater. 66 (2012) 919–922.
[313] N. Bowden, S. Brittain, A.G. Evans, J.W. Hutchinson, G.M. Whitesides, Nature 393 (1998) 146–149.
[314] T. Li, Z.Y. Huang, Z.C. Xi, S.P. Lacour, S. Wagner, Z. Suo, Mech. Mater. 37 (2005) 261–273.
[315] Y. Xiang, T. Li, Z. Suo, J. Vlassak, Appl. Phys. Lett. 67 (2005) 161910.
[316] N. Lu, Z. Suo, J.J. Vlassak, Acta Mater. 58 (2010) 1679.
[317] Z. Jia, T. Li, Int. J. Plast. 51 (2013) 65–79.
[318] W. Xu, J.S. Yang, T.J. Lu, Mater. Des. 32 (2011) 154–161.
[319] B.J. Jeon, S. Lee, J.K. Lee, Surf. Coat. Technol. 202 (2008) 1839–1846.
[320] D.R. Clarke, W. Pompe, Acta Mater. 47 (1999) 1749–1756.
[321] S.P. Lacour, D. Chan, S. Wagner, T. Li, Z. Suo, Appl. Phys. Lett. 88 (2006) 204103.
[322] S.P. Lacour, J. Jones, Z. Suo, S. Wagner, IEEE Electron. Dev. Lett. 25 (2004) 179–181.
[323] O. Kraft, R. Schwaiger, P. Wellner, Mater. Sci. Eng. A 319–321 (2001) 919.
[324] O. Kraft, P. Wellner, M. Hommel, R. Schwaiger, E. Arzt, Z. Metall. Mater. Res. Adv. Technol. 93 (2002) 392–400.
[325] R. Schwaiger, G. Dehm, O. Kraft, Philos. Mag. 51 (2003) 195.
[326] G.P. Zhang, C.A. Volkert, R. Schwaiger, P. Wellner, E. Arzt, O. Kraft, Acta Mater. 54 (2006) 3127–3139.
[327] R. Schwaiger, O. Kraft, Acta Mater. 51 (2003) 195–206.
[328] G.-D. Sim, Y. Hwangbo, H.-H. Kim, S.-B. Lee, J.J. Vlassak, Scr. Mater. 66 (2012) 915–918.
[329] O. Kolednik, J. Predan, F.D. Fisher, P. Fratzl, Adv. Funct. Mater. 21 (2011) 3634–3641.
[330] D. Gianola, C. Eberl, JOM 61 (2009) 24–35.
[331] K.J. Hemker, W.N. Sharpe Jr., Annu. Rev. Mater. Res. 37 (2007) 92.
[332] Y. Lu, J. Lou, JOM 63 (2011) 35–42.
[333] M.A. Haque, M.T.A. Saif, Exp. Mech. 43 (2003) 248–255.
[334] M.F. Pantano, H.D. Espinosa, L. Pagnotta, J. Mech. Sci. Technol. 26 (2012) 545–561.
[335] J.N. Florando, W.D. Nix, J. Mech. Phys. Solids 53 (2005) 619–638.
[336] W.N. Sharpe, B. Yuan, R.L. Edwards, J. Microelectromech. Syst. 6 (1997) 193–199.
[337] T. Tsuchiya, O. Tabata, J. Sakata, Y. Taga, Trans. IEEE J. Sens. Micromach. Soc. 116 (1996) 441.
[338] T. Tsuchiya, O. Tabata, J. Sakata, Y. Taga, J. Microelectromech. Syst. 7 (1998) 106–113.
[339] W.N. Sharpe, O. Jadaab, G.M. Beheim, G.D. Quinn, N.N. Nemeth, J. Microelectromech. Syst. 114 (2005) 903.
[340] J. Gaspar, M. Schmidt, J. Held, O. Paul, Mater. Res. Soc. Symp. Proc. 1052 (2008) 15.
[341] R.A. Meirom, T.E. Clark, C.L. Muhlstein, Acta Mater. 60 (2010) 1408–1417.
[342] R.A. Meirom, T.E. Clark, C.L. Muhlstein, Int. J. Fatigue 70 (2015) 258–269.
[343] M.T. Lin, C.J. Tong, K.S. Shiu, Exp. Mech. 50 (2010) 55–64.
[344] V. Prakash, P.B. Kaul, J. Park, M.F.P. Bifano, JOM 63 (2011) 49–56.
[345] B. Wu, A. Heidelberg, J.J. Boland, Nat. Mater. 4 (2005) 525–529.
[346] D. Jang, J.R. Greer, Scr. Mater. 64 (2011) 77–80.
[347] D. Kiener, W. Grosinger, G. Dehm, R. Pippan, Acta Mater. 56 (2008) 580–592.
[348] J.-H. Kim, A. Nizami, Y. Hwangbo, B. Jang, H.-J. Lee, C.-H. Woo, S. Hyun, T.-S. Kim, Nat. Commun. 4 (2013) 2520.
[349] W. Kang, M.T. Saif, J. Microelectromech. Syst. 19 (2010) 1309–1321.
[350] W. Kang, J.H. Han, M.T. Saif, J. Microelectromech. Syst. 19 (2010) 1322–1330.

[351] M.A. Haque, M.T.A. Saif, J. Microelectromech. Syst. 10 (2001) 146.
[352] M.A. Haque, M.T.A. Saif, Acta Mater. 51 (2003) 3053–3061.
[353] S. Kamiya, J.H. Kuypers, A. Trautmann, P. Ruther, O. Paul, J. Microelectromech. Syst. 16 (2007) 202.
[354] Y. Zhu, H.D. Espinosa, Proc. Natl. Acad. Sci. U.S.A. 102 (2005) 14503.
[355] H.D. Espinosa, Y. Zhu, N. Moldovan, J. Microelectromech. Syst. 16 (2007) 1219.
[356] E. Hosseinian, O.N. Pierron, Nanoscale 5 (2013) 12532–12541.
[357] P.O. Theillet, O.N. Pierron, Appl. Phys. Lett. 94 (2009) 181915.
[358] D. Fabrègue, N. André, M. Coulombier, J.P. Raskin, T. Pardoen, Micro. Nano-lett. 2 (2007) 13.
[359] S. Gravier, M. Coulombier, A. Safi, N. André, A. Boe, J.P. Raskin, T. Pardoen, J. Microelectromech. Syst. 18 (2009) 555–569.
[360] J.P. Raskin, F. Iker, N. André, B. Olbrechts, T. Pardoen, D. Flandre, Electrochim. Acta 52 (2007) 2850–2861.
[361] M. Coulombier, G. Guisbiers, M.S. Colla, J.P. Raskin, T. Pardoen, Rev. Sci. Instrum. 83 (2012) 105004.
[362] U. Bhaskar, V. Passi, S. Houri, E. Escobedo-Cousin, S.H. Olsen, T. Pardoen, J.P. Raskin, J. Mater. Res. 27 (2012) 571–579.
[363] C. Chisholm, H. Bei, M.B. Lowry, J. Oh, S.A. Syed Asif, O.L. Warren, Z.W. Shan, E.P. George, A.M. Minor, Acta Mater. 60 (2012) 2258–2264.
[364] H. Zheng, A. Cao, C.R. Weinberger, J.Y. Huang, K. Du, J. Wang, Y. Ma, Y. Xia, S.X. Mao, Nat. Commun. 1 (2010) 144.
[365] H. Zheng, J. Wang, J.Y. Huang, J. Wang, S.X. Mao, Nanoscale 6 (2014) 9574–9578.
[366] B. Peng, N. Pugno, H.D. Espinosa, Int. J. Solids Struct. 43 (2006) 3292–3305.
[367] E.I. Bromley, J.N. Randall, D.C. Flanders, R.W. Moutain, J. Vac. Sci. Technol. B 1 (1983) 1364.
[368] Y. Xiang, X. Chen, J.J. Vlassak, J. Mater. Res. 20 (2005) 2360.
[369] P.A. Gruber, J. Bohm, F. Onuseit, A. Wanner, R. Spolenak, E. Arzt, Acta Mater. 56 (2008) 2318–2335.
[370] Y. Xiang, J. McKinnel, W.M. Ang, J.J. Vlassak, Int. J. Fract. 144 (2007) 173–179.
[371] B. Merle, M. Goken, Acta Mater. 59 (2011) 1772–1779.
[372] D. Di Maio, S. Roberts, J. Mater. Res. 20 (2005) 299–302.
[373] C. Motz, R. Pippan, T. Schöberl, Acta Mater. 53 (2005) 4269–4279.
[374] D. Kupka, E.T. Lilleodden, Exp. Mech. 52 (2012) 649–658.
[375] D. Kupka, N. Huber, E.T. Lilleodden, J. Mech. Phys. Solids 64 (2014) 455–467.
[376] X. Li, B. Bhushan, Surf. Coat. Technol. 163–164 (2003) 521–526.
[377] S. Sundararajan, B. Bhushan, Sens. Actuators. 101 (2002) 338–351.
[378] D.S. Gianola, B.G. Mendis, X.M. Cheng, K.J. Hemker, Mater. Sci. Eng. A 483–484 (2008) 637–640.
[379] C.F. Niordson, P. Redanz, J. Mech. Phys. Solids 52 (2004) 2431–2454.
[380] C.F. Niordson, V. Tvergaard, Int. J. Solids Struct. 42 (2005) 2559–2573.
[381] M.P. de Boer, A.D. Corwin, P.G. Kotula, M.S. Baker, J.R. Michael, G. Subhash, M.J. Shaw, Acta Mater. 56 (2008) 3313–3326.
[382] P. Zhang, J.Y. Zhang, J. Li, G. Liu, K. Wu, Y.Q. Wang, W.J. Sun, Acta Mater. 76 (2014) 221–237.
[383] K. Kohama, K. Ito, T. Matsumoto, Y. Shirai, M. Murakami, Acta Mater. 60 (2012) 588–595.
[384] Y. Zhang, F. Wang, P. Zang, J. Wang, S. Mao, X. Zhang, J. Lu, Mater. Sci. Eng. A 618 (2014) 614–620.
[385] J. Inoue, Y. Fujii, T. Koseki, Acta Mater. 56 (2008) 4921–4931.
[386] M. Meyers, Traiviratana, V. Lubarda, D. Benson, E. Bringa, JOM 61 (2009) 35–41.
[387] K.N. Jonnalagadda, Failure and fracture of thin materials for MEMS (Ph. D. dissertation), University of Illinois at Urbana-Champaign, 2008.
[388] P.F. Thomason, Acta Metall. 33 (1985) 1079–1085.
[389] F.M. Beremin, Metall. Trans. A 12 (1981) 723–731.
[390] C.F. Niordson, Eur. J. Mech. A. Solids 27 (2008) 222–233.
[391] U. Borg, C.F. Niordson, J.W. Kysar, Int. J. Plast. 24 (2008) 688–701.
[392] X. Qiu, Y. Huang, Y. Wei, H. Gao, K.C. Hwang, Mech. Mater. 35 (2003) 245–258.
[393] J. Segurado, J. Llorca, Acta Mater. 57 (2009) 1427–1436.
[394] E.M. Bringa, S. Traiviratana, M.A. Meyers, Acta Mater. 58 (2010) 4458–4477.
[395] S.K. Yerra, G. Martin, M. Veron, Y. Brechet, J.D. Mithieux, L. Delannay, T. Pardoen, Eng. Fract. Mech. 102 (2013) 77–100.
[396] H. Klocker, V. Tvergaard, Int. J. Mech. Sci. 25 (2003) 1283–1308.
[397] D. Lassance, D. Fabregue, F. Delannay, T. Pardoen, Prog. Mater. Sci. 52 (2007) 62–129.
[398] S. Kumar, M.A. Haque, H. Gao, Appl. Phys. Lett. 94 (2009) 253104.
[399] S. Kumar, X. Li, M.A. Haque, H. Gao, Nano Lett. 11 (2011) 2510–2516.
[400] X.W. Gu, Z. Wu, Y.W. Zhang, D.J. Srolovitz, J.R. Greer, Nano Lett. 13 (2013) 5703–5709.
[401] H. Hirakata, O. Nishijima, N. Fukuhara, T. Kondo, A. Yonezu, K. Minoshima, Mater. Sci. Eng. A 528 (2011) 8120–8127.
[402] R.R. Keller, J.M. Phelps, D.T. Read, Mater. Sci. Eng. A 214 (1996) 42–52.
[403] H. Hosakawa, A.V. Desai, M.A. Haque, Thin Solid Films 516 (2008) 6444–6447.
[404] K. Hattar, J. Han, M.T.A. Saif, I.M. Robertson, J. Mater. Res. 20 (2005) 1869–1877.
[405] S.-W. Kim, X. Li, H. Gao, S. Kumar, Acta Mater. 60 (2012) 2959–2972.
[406] L. Liu, J. Wang, S.K. Gong, S.X. Mao, Sci. Rep. 4 (2014) 4397.
[407] S. Kumar, M.A. Haque, H. Gao, Int. J. Plast. 44 (2013) 121–128.
[408] H.-G. Kim, J.-W. Yi, S.-W. Kim, K.-S. Kim, K.S. Kumar, Acta Mater. 84 (2015) 95–109.
[409] S. Kumar, M.T. Alam, M.A. Haque, J. Microelectromech. Syst. 20 (2011) 53–58.
[410] R.A. Meirom, D.H. Alsem, A.L. Romasco, T. Clark, J.S. Polcawich, M. Dubey, R.O. Richie, C.L. Muhlstein, Acta Mater. 59 (2011) 1141–1149.